Quantifying Aquatic Microhabitat at the Riverscape

A Dissertation

Presented in Partial Fulfillment of the Requirements for the

Degree of Doctor of Philosophy

with a

Major in Water Resources

in the

College of Graduate Studies

University of Idaho

by

Jenna Duffin

Approved by:

Co-Major Professor: Daniele Tonina, Ph.D.

Co-Major Professor: Elowyn Yager, Ph.D.

Committee Members: Rohan Benjankar, Ph.D.; John Buffington, Ph.D.; Brian Kennedy, Ph.D.

Department Administrator: Timothy Link, Ph.D.

December 2021

Abstract

Analyzing morphologic, hydrologic, and biologic conditions that impact aquatic habitat conditions is vital for river management. With increasing anthropogenic pressures on natural systems, it has become more important to quantify the impacts of alterations to topography, water supply and biological characteristics such as temperature on riverine ecosystems. While most studies focus on reach-scale analyses of morphologic and habitat conditions, in this work we leverage high-resolution topobathymetric data to perform analyses along the entire length of rivers. This dissertation focuses on large-scale analysis of the morphology and aquatic habitat available in rivers with varying levels of human alterations. In the first research chapter, we used continuous wavelet analysis to identify scales of topographic variability present along three rivers. We found three wavelet scales of topographic variability: a small scale, representing the pools and riffles along the rivers; a mid-wavelet scale, detecting larger pools/bars and compound pools; and a large wavelet scale, linked to changes in reach morphology from valley-scale controls. Using the small wavelet scale, we developed a novel methodology to identify pools and riffles along entire lengths of rivers. We also found that redds (salmon nests) were not randomly located, but rather placed in areas of higher, small-scale, wavelet power showing the importance of well-developed pool-riffle morphology for spawning habitat selection. The second research chapter focuses on the effects of flow regulation on topography and physical habitat in two morphologically distinct reaches. We developed reach-scale morphodynamic models to address the impacts of regulated and unregulated flows on the morphology and resulting rearing and spawning habitat for salmonids. Our findings show that years of regulated flows have created subdued topography in the river, while unregulated flows can increase the frequency, area, depth, and volume of pools and bars in the meandering reaches of the river, but not in the highly-altered straightened reaches. Although changes to the topography between regulated and unregulated flows did not greatly affect the modeled habitat suitability for salmonids, the increase in pool characteristics greatly increased overwintering habitat for juvenile salmonids. In the final chapter, we use a bioenergetics model to quantify the juvenile salmonid carrying capacity along the entire length of a river. By varying the inputs of food availability, stream temperature, and juvenile fish size, we can address how juvenile carrying capacity varies throughout the river and the potential to increase or reduce carrying capacity. We found that increasing food and decreasing stream temperature generally increased the juvenile carrying capacity of the river, but the territorial nature of juvenile salmonids and the local hydraulics modulated how temperature, food and fish size affected carrying capacity. We also found that redd site selection was dependent, not only on spawning habitat

quality, but also on the presence of good juvenile habitat. These analyses efficiently provide information on existing morphology in rivers and potential changes to the morphology and aquatic habitat through hydrologic, topographic, and biological alterations. The analyses are completed using high-resolution topographic data and modeling, providing information at a scale relevant to a fish, but are completed, or can be extrapolated, to entire lengths of rivers, which provides an important riverscape view for managers.

Acknowledgments

I would like to thank my co-advisors Dr. Elowyn Yager and Dr. Daniele Tonina for their guidance and mentorship throughout this process. I would also like to thank my committee members for always being willing to offer their expertise and feedback. I really appreciate the co-authors on these papers who provided advice and data for these projects. This work would not have been possible without field work support from Richie Carmichael, Heidi Smith, Andrea Bertagnoli, and Brandon Hilliard. I would also like to acknowledge the support of a series of amazing office mates that always made my days brighter; thank you Courtney, Damon, Raine, Caitlin, Taylor, and Heidi.

I am grateful for the funding from the Idaho Governor's Office of Species Conservation, the Bonneville Power Administration, the U.S. Forest Service, and the University of Idaho Office of Research. I am also very thankful for funding from the National Science Foundation's Integrative Graduate Education and Research Traineeship (IGERT) program.

Dedication

This achievement is dedicated to my sister, Lea Duffin, and parents, Susie Vader and Dorian Duffin, for inspiring my curiosity of the natural world and for their unwavering encouragement and support.

Table of Contents

List of Tables

List of Figures

Statement of Contribution

I, Jenna Duffin, was the lead author of all chapters of this dissertation, but this work was completed in collaboration with my listed coauthors. Chapter 1 was a collaborative, interdisciplinary project with research development, analysis, and editing assisted by Richie Carmichael, MS. For all other chapters, the listed coauthors served in advisory roles and provided feedback on the text.

Chapter 1: Detecting multi-scale riverine topographic variability and its influence on Chinook salmon habitat selection

Authors: Jenna Duffin, Richard A. Carmichael, Elowyn M. Yager, Rohan Benjankar, Daniele Tonina

Duffin, J., Carmichael, R. A., Yager, E. M., Benjankar, R., & Tonina, D. (2021). Detecting multi-scale riverine topographic variability and its influence on Chinook salmon habitat selection. Earth Surface Processes and Landforms, 46(5), 1026-1040. https://doi.org/10.1002/esp.5077

Abstract

Quantifying geomorphic conditions that impact riverine ecosystems is critical in river management because of degraded riverine habitat, changing flow and thermal conditions, and increasing anthropogenic pressure. Geomorphic complexity at different scales directly impacts habitat heterogeneity and affects aquatic biodiversity resilience. Here we showed that the combination of continuous spatial survey at high resolution, topobathymetric LiDAR, and continuous wavelet analysis, can help identify and characterize that complexity. We used a continuous wavelet analysis on 1-m resolution topobathymetry in three rivers in the Salmon River Basin, Idaho (USA), to identify different scales of topographic variability and the potential effects of this variability on salmonid redd site selection. On each river, wavelet scales characterized the topographic variability by portraying repeating patterns in the longitudinal profile. We found three major representative spatial wavelet scales of topographic variability in each river: a small wavelet scale associated with local morphology such as pools and riffles, a mid-wavelet scale that identified larger pools/riffles, and a large wavelet scale related to valley-scale controls. The small wavelet scale was used to identify pools and riffles along the entire length of each river as well as areas with differing riffle-pool development. Areas along the rivers with high local topographic variability (high wavelet power) at all wavelet scales contained the largest features (i.e., deepest or longest pools) in the systems. By comparing the wavelet power for each wavelet scale to Chinook salmon redd locations, we found that higher small-scale wavelet power, which is related to pool-riffle topography, is important for redd site selection. The continuous wavelet methodology objectively identified scales of topographic variability present in these rivers, performed efficient channel-unit identification, and provided geomorphic assessment without laborious field surveys.

Introduction

Topographic variability, morphologic patterns, and aquatic habitat can be linked to species diversity (Jungwirth et al., 1993; Tews et al., 2004) and the spatial distribution of fish abundance (Torgersen et

al., 2004, 2006). Many spatial scales of river processes and characteristics influence fish habitat and abundance, from broad scale channel morphology, hyporheic flow, and temperature, to local scale substrate, depth, and velocities (Cram et al., 2017). The impact of river processes on fish habitat is not well understood at all spatial scales, and therefore a continuous view of rivers is needed (Fausch et al., 2002). The conceptual framework of nested hierarchical scales suggests that larger-scale controlling factors, such as geology, topography, and climate, influence geomorphic processes at intermediate scales, which then influence habitat at smaller scales (Frissell et al., 1986). Specifically, local habitat (length scale of ~10^{-1} bankfull channel widths, W_b) is influenced by multiple scales of processes including those at the reach-scale (~10s W_b, e.g., aggradation/degradation) and system-scale (e.g., topography, land use) (Frissell et al., 1986). The links between processes at different spatial scales and their impact on local habitat validate addressing habitat attributes, including topographic variability, at multiple scales (Newson & Newson, 2000).

Traditional methods for fluvial geomorphic analyses often focus either on intensively monitoring small discrete reaches or extensively monitoring larger segment or basin-scale areas, which may not capture the range and complexity of the geomorphology and physical habitat used by anadromous fish because of the lack of either spatial extent or fine resolution (Fonstad & Marcus, 2010). The ability to understand how species interact with geomorphology and habitat at multiple spatial scales has gained attention because of increased access to spatially-continuous, high-resolution, watershed-scale (100s km) imagery, elevation models (Marcus & Fonstad, 2008; Woodget et al., 2017), broad-scale bathymetric data (Dietrich, 2017; Tonina et al., 2019; Woodget et al., 2015), and spatially explicit biological data (Benjankar et al., 2016; Hatten et al., 2016). Although green LiDAR and drone technologies can collect continuous high resolution topographic and bathymetric data across entire river basins (Tamminga et al., 2015; Tonina et al., 2019), effective and efficient ways to utilize these data to characterize morphology and aquatic habitat are still in development.

Using high-resolution continuous bathymetric data, topographic variability can be measured at multiple scales in rivers. We define topographic variability as the spatial variation in 1D longitudinal bed elevations of a river channel over long stream segments. Topographic variability has been measured at the scale of morphologic units (Rayburg & Neave, 2008), sub-reaches (Lane et al., 2017), and reaches (Bartley & Rutherfurd, 2005; Brooks et al., 2006; Polvi et al., 2014), but few studies have measured multiple spatial scales of topographic variability continuously through a river. Exceptions include the use of continuous wavelet analysis to quantify variability of in-channel

bathymetry (McKean et al., 2008) and planform configuration like meandering (Zolezzi & Güneralp, 2015) at multiple scales along a river.

The continuous wavelet methodology analyzes patterns in the frequency domain by comparing a waveform to pieces of a signal (Torrence & Compo, 1998). For each location along the data set, the technique calculates a wavelet coefficient, the correlation between the measured signal and the wavelet, and this is completed for multiple wavelet lengths to assess all scales within the signal. The result is a matrix of wavelet coefficients for each combination of scale (frequency of the wavelet) and translation (the shift of the wavelet along the signal). This procedure has traditionally been applied to time series data to identify patterns in noisy signals, such as identifying the repeated temporal fluctuations in the El Niño Southern Oscillation (Torrence & Webster, 1999), but also to a variety of ecological topics including forest canopy structure (Bradshaw & Spies, 1992), landscape patterns (Csillag & Kabos, 2002), variability of river discharges (Labat, 2008), spatial distributions of cutthroat trout (Torgersen et al., 2004), LiDAR processing (Zhou et al., 2013), and only recently on stream morphology (Gutierrez et al., 2013; McKean et al., 2008; Zolezzi & Güneralp, 2015).

In this study, we use wavelet scale to differentiate between different length-scales of topographic variability identified by the continuous wavelet methodology; these wavelet scales represent repeating topographic patterns present along the length of each river. We will use the spatial variation in wavelet coefficients and power (the square of the wavelet coefficients) to quantify the amount of local topographic variability present within each of these wavelet length-scales. With large, continuous, topographic data sets, the continuous wavelet methodology can measure the patterns of local topographic variability (variation in wavelet coefficients or power) at countless wavelet length-scales throughout a topographic signal (McKean et al., 2008). McKean et al. (2008) found that a large wavelet scale (600 m) identified geomorphic domains (such as plane-bed sections) and was related to valley evolution. They also found that two smaller wavelet scales (310 m and 95 m) aligned with regularly spaced deep pools and riffle-pool topography, respectively. McKean et al. (2008) showed an association between the spatial pattern of wavelet coefficients at each of these wavelet scales and spatial patterns of salmon redd locations. Their wavelet analysis was performed on a 10 km long reach of Bear Valley Creek, Idaho; however, the method still needs to be tested along the entirety of multiple rivers.

We applied the wavelet analysis to the thalweg of river bathymetries along three rivers in the Salmon River watershed, Idaho: the Lemhi River, Upper Salmon River (defined as the Salmon River above Redfish Lake Creek), and Bear Valley Creek. The Salmon River basin provides important spawning

and rearing habitat, and migration corridors for many economically and culturally important fish species listed as threatened or endangered under the U.S. Endangered Species Act (NMFS, 2019). The drainage supports populations of Chinook salmon (*Oncorhynchus tshawytscha*), steelhead trout (*Oncorhynchus mykiss)*, sockeye salmon (*Oncorhynchus nerka*), bull trout (*Salvelinus confluentus)*, and coho salmon (*Oncorhynchus kisutch*); and a viable recreational fishery of cutthroat trout (*Oncorhynchus clarkii*) and resident rainbow trout.

We assessed the use of wavelets in different river settings, identified spatial scales of topographic variability (wavelet scales), and compared how these scales may differ between basins with different geomorphic characteristics (channel widths, slopes, channel morphologies) and varying levels of human impacts. With this analysis we aimed to address how the continuous wavelet methodology provides insight into river morphology in large-scale data sets. Specifically, we identified what each present wavelet scale represented in the morphology. We compared wavelet-identified pool-riffle features to field-identified channel units to validate a new tool for pool-riffle identification along rivers. We assessed whether wavelet power at the channel unit scale related to channel sinuosity, because we expected meanders to be associated with larger pools and riffles as they can play an important role in meander development (Knighton, 2014; Lofthouse & Robert, 2008; Thompson, 1986). Additionally, we addressed if wavelet power was related to Chinook salmon spawning site selection, an example of the application and utility of this type of analysis.

Methods

Topographic data

Airborne bathymetric LiDAR data were collected from three basins in the Salmon River drainage, Idaho, during low flows with high water clarity (Figure 1.1). A 1-meter resolution digital elevation model (DEM) for 14 km of Bear Valley Creek was produced with the Experimental Advanced Airborne Research LiDAR (EAARL) in October 2007 (McKean et al., 2009). A successor to the EARRL, the EAARL-B mapped the entire 106 km length of the Lemhi River in October 2013 from which a 1-m resolution DEM was derived (Tonina et al., 2019). An Upper Salmon River DEM was produced at 0.91 m (3 ft) resolution for 49 km using the Riegl VQ-880-G in April 2018 (Riegl, 2016). All three bathymetric LiDAR surveys had average in-water errors of ~10-15 cm, with larger errors in steep areas and deep pools (Tonina et al., 2019). These sites are all gravel-bedded rivers dominated by pool-riffle morphologies. Bear Valley Creek has a W_b of ~15 m and bed slopes that range between 0.002 to 0.006 (measured at 500-m long reaches). The Lemhi River has a W_b of ~15 m and bed slopes ranging from 0.001 to 0.01 that generally increase downstream. The first 24 km of the Upper Salmon

River study area has a W_b of ~15 m and bed slopes ranging from 0.002 to 0.01, and the last 25 km has a W_b of ~25 m with bed slopes ranging from 0.001 to 0.008.

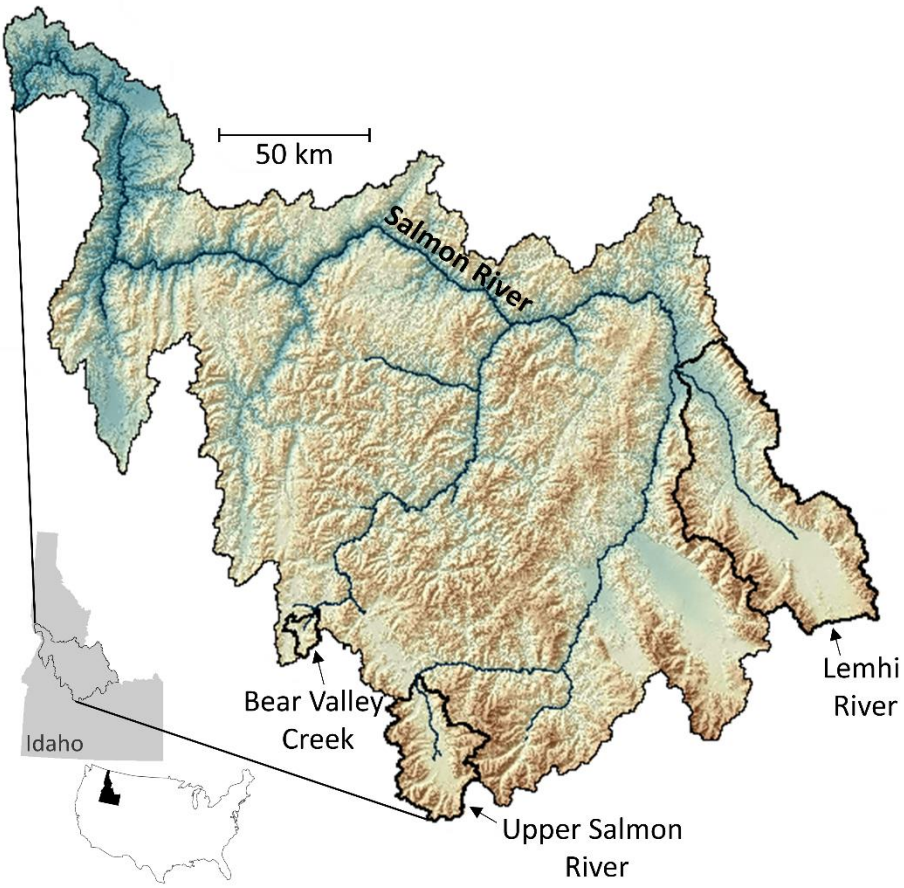

Figure 1.1: Site map showing the three study basins within the Salmon River Basin, Idaho, USA.

To focus on local variability in the river topography, we detrended each elevation model with geographic information systems (GIS) software by subtracting the valley slope surface, which was created from elevations along the top of the channel bank, from the bare-earth LiDAR surface. We then added 100 m to the detrended surface to create positive elevations, manually digitized river thalwegs (at ~5 m resolution) and extracted bathymetric data points along the thalwegs at the resolution of each detrended LiDAR surface.

Wavelet methodology

We used continuous wavelet analysis on the longitudinal detrended elevation profiles. This method analyzed spatial patterns along the thalweg at multiple wavelet length scales by comparing pieces of the elevation profile to a reference waveform and calculating a wavelet coefficient that quantified

how well the waveform aligned with the local profile. As the wavelet moves through the longitudinal profile, it will show high correlation with locations that best match its shape and size. Thus, small wavelets detect small concave (e.g., pools) or convex (e.g., riffle) features, whereas large wavelets will identify larger features and small undulations will not be detected. The range of wavelet scales allow for different-sized feature detection and feature presence or absence at a particular length scale and location. Wavelet analysis is analogous to, but more efficient than, a windowed Fourier analysis where a window of fixed size moves through the entire signal (Torrence & Compo, 1998).

For example, at the scale of individual riffles and pools, a negative wavelet coefficient resulted when the concavities of the wavelet shape aligned with a pool and the magnitude of the coefficient related to how well the wavelet, at a certain scale, lined up with the pool width and depth (Figure 1.2c,e, solid lines). As the convexities in the river signal and the wavelet shape aligned, a positive wavelet coefficient resulted, and the magnitude of the coefficients were correlated with how well the wavelet lined up with the shape of the convexity or riffle (Figure 1.2c,e, dashed lines). With this analysis, we assessed the scale (wavelet scale) and spatial distribution (locations of high wavelet power magnitudes) of pool-riffle formations and other geomorphic features on a continuous watershed scale. We performed this continuous wavelet analysis with the MATLAB Wavelet Analyzer toolbox (Misiti et al., 1997) on each thalweg profile for wavelet scales incrementally increasing wavelet length from 1 m to 500 m.

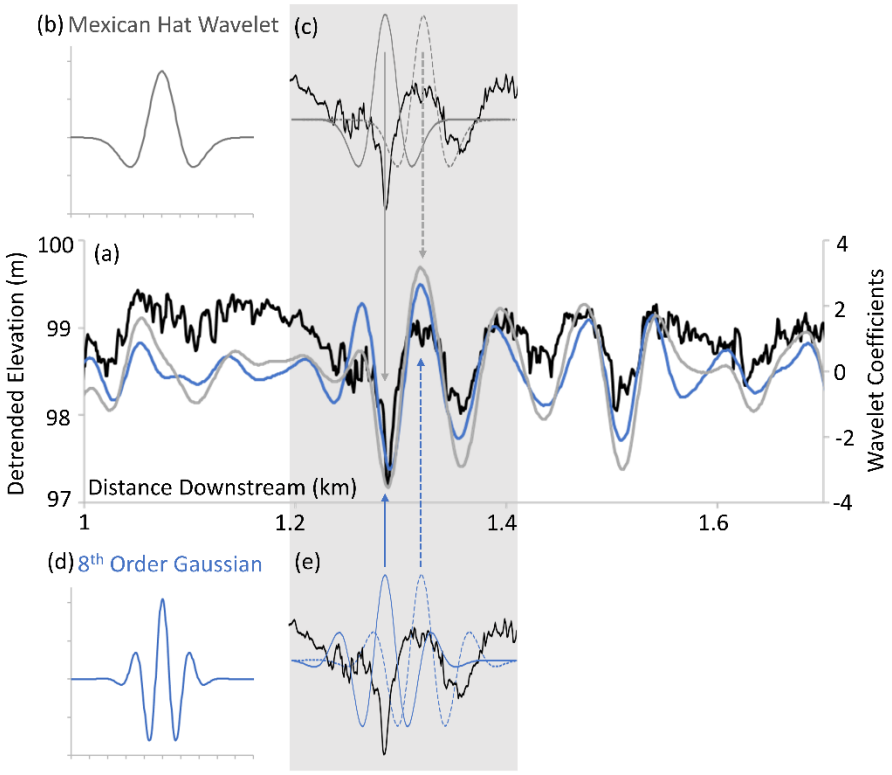

Figure 1.2: (a) Short 0.7 km reach of Bear Valley Creek showing the detrended topography (black line) and the wavelet coefficients of the 15 m Mexican hat wavelet (grey line) and the 35 m 8th order Gaussian wavelet (blue line). (b) Shows the Mexican hat wavelet form, and (c) shows how the Mexican hat wavelet, not to scale, may align with a pool (shown with solid line) or a riffle (shown in dashed line). (d) Shows the 8th order Gaussian wavelet, and (e) shows how the 8th order Gaussian wavelet, not to scale, may align with a pool (shown with solid line) or a riffle (shown in dashed line).

For continuous data sets, like ours, the nonorthogonal wavelets such as the Morlet or those based on a derivative of a Gaussian are typically used (Torrence & Compo, 1998). Although different wavelets will qualitatively provide similar results, the selection of the wavelet should be tailored to the signal of interest (Lane, 2007; Torrence & Compo, 1998). We selected a 2nd order Gaussian wavelet, known as the Mexican hat wavelet (Figure 1.2b), because its nonorthogonal smooth shape mimics natural pool-riffle transitions and its simple shape has been shown to perform better than more complex wavelets at detecting the locations of variations in signals such as convexities and concavities (Mi et al., 2005). We also tested using an 8th order Gaussian wavelet shape (Figure 1.2d), which was used by McKean et al. (2008) in a similar study. This wavelet is also smooth but has more positive and negative variations within the shape. Both curves produce similar results in coefficients, but at different scales, for example Figure 1.2a shows the wavelet coefficients from both the 15 m Mexican hat wavelet and the 35 m 8th order Gaussian wavelet and the curves generally follow the same pattern. In some areas, the extra variations in the 8th order Gaussian wavelet shape resulted in wavelet

coefficients that did not accurately represent the topography because the shape needed to align with not just one feature, but with multiple features in the topography (i.e. Figure 1.2a at ~1.575 km the 8th order Gaussian coefficient shows a concavity where there is not one in the topography). We therefore selected the Mexican hat wavelet shape for the rest of the analysis.

Using the Mexican hat wavelet, wavelet coefficients were calculated for all wavelet scales at all locations along each profile. We produced heat maps that show wavelet power (square of wavelet coefficient) along the thalweg profile for each wavelet scale. These maps highlighted how wavelet power changed between wavelet scales and along the river. Longitudinal locations with high wavelet power in a heat map (Figure 1.3b) show where wavelets had high correlation with the topography and at which wavelet scale that correlation ceased. For a given wavelet scale, the bright areas in the heat map highlight where the wavelet scale aligned well with the topography. Thus, the dark ridges highlight areas in the heat map where there was a shift in the dominant wavelet scales and therefore a change in the scale of identified streambed features. We identified the ranges of wavelet scales between dark ridges in the wavelet power patterns that were repeated throughout the length of each river (i.e., locations of brackets in Figure 1.3f, part III). We then found the wavelet scales within each region of possible wavelet scales where the wavelet coefficients visually best aligned with the detrended longitudinal profile (i.e., Figure 1.4b).

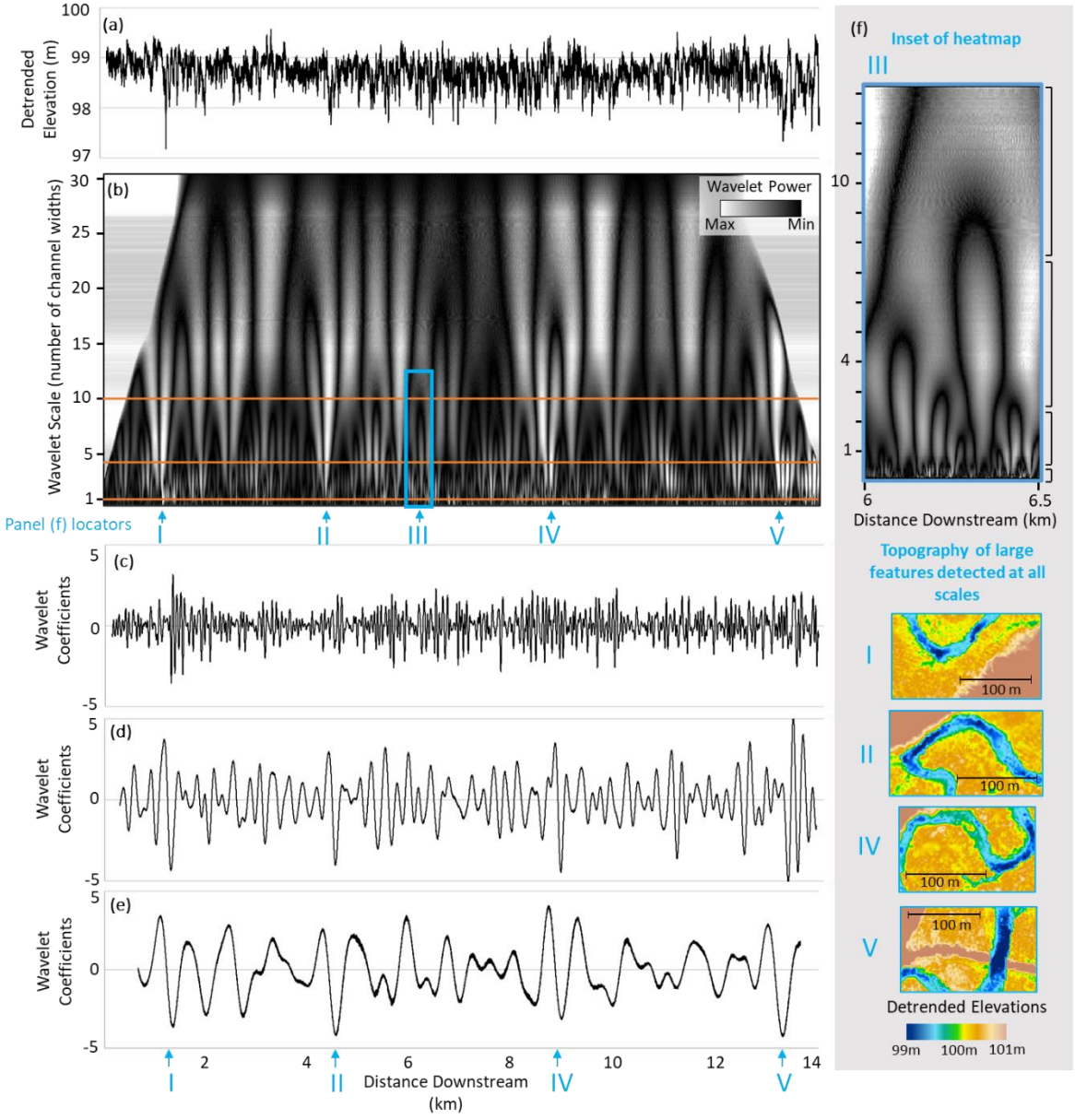

Figure 1.3: Wavelet analysis with the Mexican hat wavelet form for 14 km of Bear Valley Creek. (a) Detrended longitudinal thalweg profile, (b) heat map of all wavelet power with wavelet scales of interest shown with orange lines. The white areas along the figure sides are edge effects from the moving window that increase as the scale of analysis increases. (c) Small-scale variability (1 channel width, 15 m) wavelet coefficients, (d) mid-scale variability (4 channel widths, 60 m) wavelet coefficients, and (e) large-scale variability (10 channel widths, 150 m) wavelet coefficients. In panel (f) parts I, II, IV, and V show the topography of the four areas (locations shown on panel (b)) with large wavelet coefficients at all three wavelet scales. Panel (f) part III, shows an inset of the heatmap, highlighting the scales of interest identified from the wavelet and brackets along the right highlighting the regions of scales present.

For each river, we identified four longitudinally consistent regions where the dark ridges were present at a certain scale throughout the entire longitudinal profile (Figure 1.3f), with the smallest being related to the noise in the topographic signal, resulting in three major wavelet scales. The wavelet scales within these regions that best aligned with the topography were all consistently related to the

width of the channels. Therefore, the three major scales we identified were at one, four and ten channel widths (Figure 1.3f, part III). This resulted in analyzing the Upper Salmon River in two segments: the first segment with an average W_b of ~15 m, and second segment with average W_b of ~25 m. In Bear Valley Creek and the Lemhi River the W_b is on average ~15 m for the entire length of the study areas.

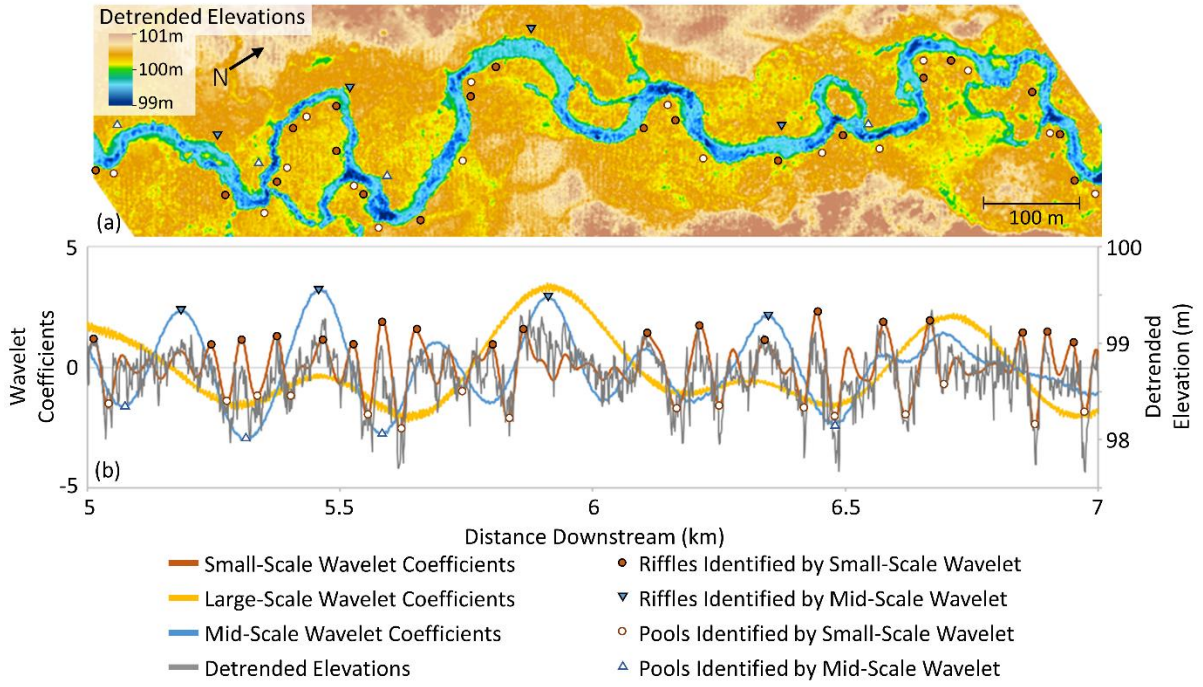

Figure 1.4: 2 km reach of Bear Valley Creek showing (a) the detrended digital elevation model created from the green LiDAR and (b) the detrended thalweg elevations along the same reach, overlaid with the small-scale (1 channel-width) wavelet coefficients, mid-scale (4 channel-widths) wavelet coefficients, and large-scale (10 channel-widths) wavelet coefficients. The riffles and pools identified using the wavelet method at both the small and mid-scales are shown by different colored circles and triangles, respectively.

New method for channel unit identification

The small wavelet scale, which we identified as a wavelength of one W_b for each river, was related to the bed undulations associated with the pools and riffles in each system, where the troughs and peaks in the wavelet coefficients represented pools and riffles, respectively. To differentiate pool-riffle features from small fluctuations in the bed or signal noise, we operatively defined a set of limits: troughs or peaks in the wavelet coefficients must be a distance of at least one W_b apart (wavelet troughs or peaks representing one channel unit may have multiple peaks within it, this avoids identifying one trough or peak as multiple units), and the peak or trough wavelet coefficient values must be greater than one standard deviation of all of the river's wavelet coefficients at the wavelet scale of interest. Tolerance values based on the standard deviation of bed elevations have been

suggested for other thalweg-based methods of channel unit identification (O'Neill & Abrahams, 1984). Pools identified by our method are limited to features of around at least one channel width in length and a residual pool depth, the difference in depth between a pool and downstream riffle crest, greater than roughly 40% of the channel's morphologic bankfull depth, D_b. The bankfull depth was identified by subtracting the thalweg elevation from the elevation where the channel started to overflow its banks in the detrended bathymetry, and we averaged those depths throughout a channel. To identify features of a different size, a different wavelet scale could be used.

Pool spacing, L_p, was quantified as the distance between two adjacent pool-identified wavelet coefficient troughs. The residual pool depth, D_p, was estimated by identifying the minimum detrended elevation within the wavelet trough for each pool and subtracting that elevation from the maximum elevation of the adjacent riffle, or if not directly adjacent to a riffle, we used the average maximum riffle elevation for the river. Bankfull width and depth have been used as scaling factors for comparing streams and reaches of different sizes (Buffington et al., 2002; Carling & Orr, 2000). We adopted these scaling factors and defined the dimensionless pool spacing, $L_p^* = L_p/W_b$, and a dimensionless pool depth, $D_p^* = D_p/D_b$, by normalizing the L_p and D_p by the bankfull width and depth, respectively. Rather than calculating distributions for riffles as well, we assume that the riffle spacing is similar to pool spacing, and riffle heights were used in the calculation of pool depth.

To assess the performance of this methodology to recognize pools and riffles, we compared the wavelet-identified pool and riffle locations to channel units delineated in three field surveyed reaches (each ~3-4 km long, two reaches on the Lemhi River and one on the Upper Salmon). These surveys were completed in the summer of 2018 by a highly trained crew using the Columbia Habitat Monitoring Program (CHaMP; Bouwes et al., 2011) protocols and all channel units were delineated utilizing a sub-meter, handheld Global Navigation Satellite System (GNSS) receiver and then digitized with GIS software. We also tested how another common longitudinal pool and riffle identification method, the bedform differencing technique, compared to the field methods. We followed the methodology outlined by O'Neill & Abrahams (1984) with pre-smoothed longitudinal profile data as suggested by Carling & Orr (2000) and a tolerance value above which a feature is identified of one standard deviation (σ) of the longitudinal bed differences instead of the suggested 0.75σ to avoid identifying minor topographic deviations as channel units.

To validate the wavelet method, we compared the observed field channel units to the predicted small-scale wavelet channel units based on true positives (TP, features identified by both methods), false positives (FP, features only identified by the wavelet), and false negatives (FN, features only

identified in the field). To address the accuracy of the wavelet method, we calculated the recall, precision and F-score based on the following equations (Mohan et al., 2017; Sokolova et al., 2006):

$$recall = \frac{TP}{TP+FN} \quad \text{Equation 1.1}$$

$$precision = \frac{TP}{TP+FP} \quad \text{Equation 1.2}$$

$$F - score = 2\left(\frac{recall \times precision}{recall+precision}\right) \quad \text{Equation 1.3}$$

Higher precision and recall result in higher F-scores, showing greater alignment between the two methods of feature identification (F-score of 1 representing a perfect alignment).

Redd analysis methods

Chinook salmon redd location data were compiled for each basin from a variety of data sources (The United States Forest Service, Idaho Department of Fish and Game, and University of Idaho) and sampling methods (ground-surveyed redd counts, and drone or helicopter identified redds). Each redd data set had varying levels of global positioning errors and variable location metadata. Therefore, we only included redds within 30 m of the thalweg. Those usable redd locations were snapped to the closest point on the thalweg line for analysis. We used 469 redds in Bear Valley Creek (surveyed in 1995 -2005), 1959 redds in the Lemhi River (1999 -2018), and 1599 redds in the Upper Salmon River (2010-2018).

To test if the redd locations were influenced by the topographic variability, we compared the wavelet power, at each of the three identified wavelet scales, between redd locations and random locations along the thalweg. Since redds were snapped to the thalweg, locations may not be accurate, for example, a redd located on land in the center of a meander bend may actually be located on either side of the meander, but we associated it with the closest side, potentially creating greater location uncertainty. To account for the spatial error in the redd locations, the wavelet power was averaged within a distance of ±50 m of each redd location (100 m total). For each basin, we randomly selected the same number of locations along the thalweg as the number of redds and averaged the wavelet power within ±50 m of these locations as well. Wavelet powers between redd and random locations were compared using the Kruskal-Wallis nonparametric statistical test (Kruskal & Wallis, 1952). For the Upper Salmon and Lemhi River, non-topographic variables of hatchery location and summer stream temperatures, respectively, were used to split the rivers into reaches for statistical testing (see results for further details). We obtained average August stream temperatures, modeled for 1-km reaches continuously along the basins, from the NorWeST database (Isaak et al., 2017) and, six point

location daily stream temperatures from instream Onset Hobo Tidbits deployed by CHaMP for the Lemhi River (Bouwes et al., 2011).

Results

Dominant wavelet scales

The wavelet analysis on the thalweg profiles revealed multiple scales of repeating topographic variability present on each river. The heatmaps of each river highlighted three longitudinally consistent wavelet scales representing the small, medium, and large-scale spatial topographic variability in the longitudinal bed elevations (Figure 1.3, see Appendix A for other basins) that scaled with channel width. The resulting wavelet coefficients from each of these three wavelet scales aligned with different features along the thalweg profile (Figure 1.4).

The first wavelet scale is one channel-width (1 W_b), which we call small-scale variability, representing the pool-riffle morphology in these systems. We used the small-scale wavelet coefficients to develop the channel unit identification method, which objectively identified morphologic units along the entire length of each river's thalweg (Figure 1.4). Average pool spacing along the whole length of each river was consistently 8-9 W_b with a median pool spacing of 6-7 W_b (Table 1.1).

Table 1.1: Mean, median, and standard deviation of dimensionless pool spacings (L_p*) and pool depths (D_p*) for small- and mid-scale wavelet-identified pools for each basin.

	Bear Valley Creek	**Lemhi River**	**Upper Salmon River**	**All Basins Combined**
Mean small-scale L_p*	8.5	8.9	8.5	8.8
Median small-scale L_p*	7	6.5	6.3	6.5
Standard deviation small-scale L_p*	4.9	7	6.5	6.7
Mean mid-scale L_p*	31.2	30.5	26.9	29.6
Median mid-scale L_p*	19.8	24.3	21.1	23.1
Standard deviation mid-scale L_p*	22.1	21.1	18.2	20.5
Mean small-scale D_p*	0.9	0.9	0.9	0.9
Median small-scale D_p*	0.9	0.9	0.9	0.9
Standard deviation small-scale D_p *	0.2	0.3	0.3	0.3
Mean mid-scale D_p *	1.2	1.2	1.3	1.2
Median mid-scale D_p *	1.1	1.2	1.2	1.2
Standard deviation mid-scale D_p *	0.3	0.3	0.3	0.3

The second wavelet scale of interest was found at four channel-widths (4 W_b), referred to as mid-scale variability, this represented a scale of larger morphology including larger pools and riffles. When using the same channel unit identification methodology as described for the small-scale wavelet, but with the threshold set as the standard deviation of the mid-scale wavelet coefficients, the mid-scale wavelet coefficients highlighted the longer and larger pools and riffles in the systems. This scale also identified a composite of some closely spaced features, which were individually identified by the small-scale wavelet (Figure 1.4). The pools or combinations of pools identified at this scale had an average spacing of 24-31 W_b and median spacings of 20-24 W_b (Table 1.1).

The dimensionless pool spacings and depths for both small and mid-scale wavelets showed wide distributions with long tails and positive skewness (Figure 1.5). The distributions were not statistically different among watersheds for both the small-scale and mid-scale identified pools (based on the Kruskal-Wallis non-parametric test, all p-values <0.05) and followed a lognormal distribution well. Thus, we combined all data for each wavelet scale and quantified the means and standard deviations for each composite distribution of L_p* and D_p* (Table 1.1).

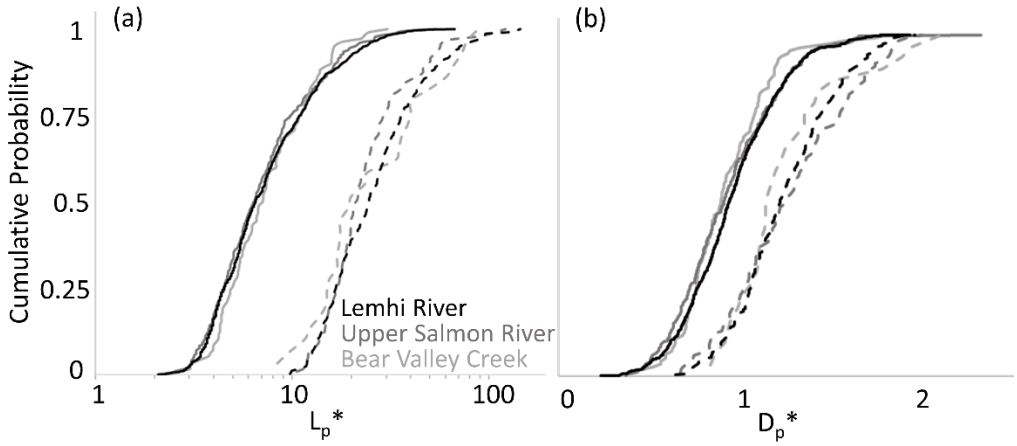

Figure 1.5: Cumulative frequency distributions for small-scale (solid lines) and mid-scale (dashed lines) identified (a) dimensionless pool spacing (L_p*) and (b) dimensionless pool depths (D_p*).

Validation of channel unit identification

We evaluated the accuracy of the wavelet channel unit identification by comparing the identified features to observed features from field channel unit identification in three reaches in the lower and upper Lemhi and Upper Salmon basins. Precision, recall, and F-scores were calculated for both pools and riffles (Table 1.2). In the lower Lemhi and Upper Salmon reaches, most of the features were identified by both the wavelet and field methods, but the F-scores were lower for pools and riffles in the upper Lemhi reach (Table 1.2). We visually attempted to locate each of the pools/riffles identified

by both methods in the LiDAR bathymetry. All features identified by the wavelet method were present in the LiDAR, but some of the field-identified features were not, potentially due to changes in the topography between the 2013 LiDAR collection and the 2018 field surveys, or because of uncertainty in the LiDAR surface. We therefore calculated the statistics for all features and just for features present in the LiDAR. In this upper Lemhi reach, of the features only identified in the field that were also present in the LiDAR, most were small features that did not meet the wavelet method identification requirements suggesting the field crews may have a different operative definition for pool-riffle identification than the wavelet method. To identify smaller features in the upper Lemhi reach, we found that decreasing the wavelet scale to 10 m (0.67 W_b), which decreased the minimum length of the pools to ~0.67 W_b, increased the F-scores to 0.82 for pools and to 0.74 for riffles. The wavelet method also performed better than the bedform differencing method of pool and riffle identification, which compared to the field identified features had F-scores between 0.44-0.74 for pools and 0.43-0.54 for riffles.

Table 1.2: Comparison between the wavelet pool identification method and field identification for three reaches in two of the study basins. Values are given for all features identified and for only features that are present in the LiDAR topography (values in parentheses).

	Upper Lemhi River	**Lower Lemhi River**	**Upper Salmon River**
Of the pools identified by the wavelet, the proportion that were also identified in the field (precision)	0.92 (0.92)	0.81 (0.81)	0.82 (0.82)
Of the pools identified in the field, the proportion that were also identified by the wavelet (recall)	0.51 (0.60)	0.89 (1.00)	1.00 (1.00)
Pools F-Score	0.66 (0.73)	0.85 (0.89)	0.90 (0.90)
Of the riffles identified by the wavelet, the proportion that were also identified in the field (precision)	0.75 (0.75)	0.87 (0.87)	0.80 (0.80)
Of the riffles identified in the field, the proportion that were also identified by the wavelet (recall)	0.47 (0.69)	0.80 (0.87)	0.89 (0.94)
Riffles F-Score	0.58 (0.72)	0.83 (0.87)	0.84 (0.86)

Small and mid-scale wavelet power variation with sinuosity

We hypothesized that wavelet power would be positively related to sinuosity because of the formation of forced pools which typically are deeper with smaller radius of curvature (increased sinuosity). Along the thalweg, we compared the reach-averaged small and mid-scale wavelet powers,

with reaches defined by changes in the sinuosity signal (calculated in 300 m reaches) along each river. We used wavelet power instead of wavelet coefficients because it is always positive, so both pools and riffles produce higher wavelet power. For all three rivers, no correlation existed between reach-averaged wavelet power and sinuosity (Figure 1.6). In the Lemhi basin, small-scale wavelet power generally increased in the downstream direction along with increased channel straightening, confinement, and overall decreased sinuosity (Figure 1.7).

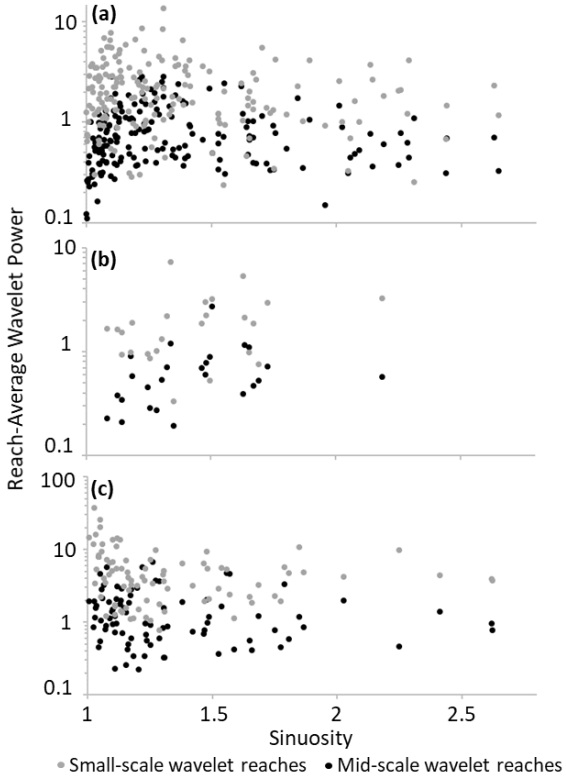

Figure 1.6: Reach sinuosity and reach-averaged small and mid-scale wavelet powers for (a) the Lemhi River, (b) Bear Valley Creek, and (c) the Upper Salmon River. Each data point represents a reach along the river.

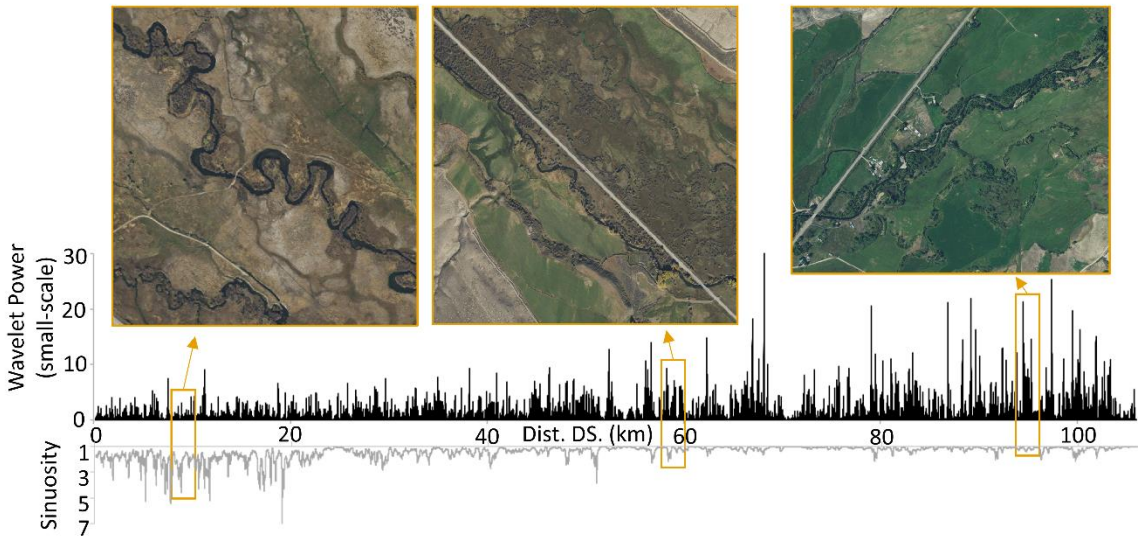

Figure 1.7: Small-scale wavelet power and sinuosity for 106 km of the Lemhi River with aerial imagery for three reaches highlighting the general landscape changes moving downstream.

The small and mid-scale wavelet powers can be analyzed in tandem to identify reaches with distinct morphologies. For example, we investigated reaches in the Lemhi River where small-scale and mid-scale wavelet powers were similar and different (Figure 1.8). One example reach with both low small- and mid-scale wavelet powers (Figure 1.8d) represented an area with little pool-riffle development; it only had 3 small-scale pools/km (compared to the whole-river average of 7.5 pools/km) and no mid-scale pools (compared to the whole-river average of 2.2 pools/km) despite having a higher sinuosity of 2.9. A reach with a lower sinuosity of 2 had high small- and mid-scale wavelet powers (Figure 1.8e), and well-developed pools/riffles among and superimposed on larger features with 9 pools/km (6 small-scale, 3 mid-scale pools). In reaches where the wavelet power of one scale was high and the other was low, the reaches were dominated by similar-sized features, such as a reach with high small-scale wavelet power, low mid-scale wavelet power, and a sinuosity of 2.1 that had 11 small-scale pools/km and no mid-scale pools (Figure 1.8c), whereas the reach with high mid-scale and low small-scale wavelet power had a higher sinuosity of 2.7, but only 4 small-scale and 4 mid-scale pools/km (Figure 1.8b). Wavelet analysis helped us highlight these unique spatial scale interactions and morphologies that occur regardless of the sinuosity.

The combination of all wavelet scales highlights the largest features in the system. Longitudinal locations on the heat map that have high wavelet power throughout all wavelet scales (identified by the white vertical areas in Figure 1.3b) represent the largest features throughout the system. These features were associated with the deepest pools in Bear Valley Creek at 1.3 km and 13.3 km, the

longest pool at 4.5 km, and the longest riffle, followed by one of the longest pools, located at 8.8 km (Figure 1.3f. parts I,II,IV, and V).

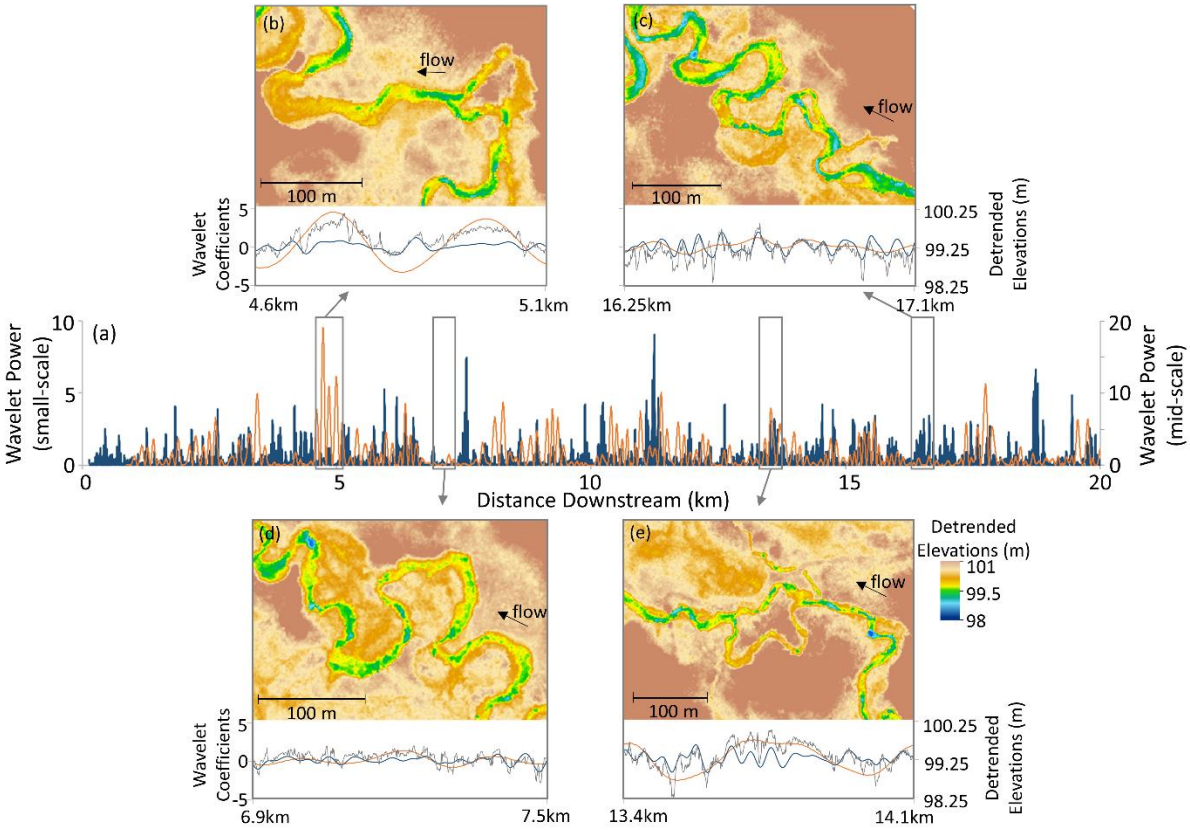

Figure 1.8: (a) Small-scale (blue line) and mid-scale (orange line) wavelet powers for the upstream-most 25 km of the Lemhi River. Inset panels show the LiDAR topography and wavelet coefficients for (b) low small-scale wavelet power and high mid-scale wavelet power, (c) high small-scale and low mid-scale wavelet power, (d) low small-scale wavelet power and mid-scale wavelet power, (e) high small and mid-scale wavelet power.

Large wavelet scale and controls

The largest wavelet scale that we identified was at ten channel widths; this large-scale topographic variability may be a result of valley-scale controls on the channel morphology. The large wavelet scale not only helped identify the largest features in the system, but also showed a relation with river confinement. Each river was divided into reaches based on natural breaks/changes in large-scale wavelet power identified using the *findchangepts* function in MATLAB. We then found what percentage of reaches with low large-scale wavelet power, identified as reaches with an average wavelet power < 2.5, were associated with areas visually identified as confined. In Bear Valley Creek, all of the low large-scale wavelet power reaches aligned with areas of channel confinement by terraces or roads running along the channel. In the Upper Salmon River, this relation was less consistent; 83% of the reaches with low large-scale wavelet power were associated with areas of

confinement, but some confined reaches had high large-scale wavelet power. The Lemhi River also did not show a consistent relation between low large-scale power and confinement (only 31% of low wavelet power reaches were associated with confinement), but the straight channelized reaches of the river running along the highway all had very low large-scale wavelet power (all with wavelet power <1). We also did not find any relations between the large-scale wavelet power and other large-scale watershed conditions that influence channels, such as bed slope changes, tributary inputs, and sinuosity.

Chinook redd locations and wavelet scales

To assess if local topographic variability, as measured by wavelet power, influences redd site selection, we compared the average wavelet power around redd locations to the average wavelet power at randomly selected sites in each river (see Appendix A.6-8 for distributions). Average small-scale wavelet power around actual redds was significantly ($p<0.05$) higher than that around the randomly selected locations (Table 1.3) for Bear Valley Creek and sections of the Upper Salmon River and Lemhi River, whereas the average mid-scale and large-scale wavelet powers around redds were not significantly different than those at random locations.

Table 1.3: P-values from the Kruskal-Wallis test, comparing average wavelet power around redds to average wavelet power around randomly selected locations.

	Bear Valley Creek	**Upper Salmon River (upstream of hatchery)**	**Lemhi River (above 18-mile creek)**
Small-scale power	0.02	2.79×10^{-7}	7.10×10^{-8}
Mid-scale power	0.54	0.40	0.95
Large-scale power	0.54	0.86	0.26

We had first tested the differences between the wavelet powers around the redd and random locations for each wavelet scale for the whole length of each river. For Bear Valley, the most natural and unaltered river in our study, the relation between small-scale wavelet power and redd locations held true for the whole study reach, whereas in the Lemhi and Upper Salmon, we did not see this expected relation. In the Lemhi, we hypothesized that high summer stream temperature during the spawning season may be a controlling factor for salmon spawning because of summer temperature concerns throughout the Pacific Northwest spawning habitat (Isaak et al., 2012, 2015). In the Lemhi River, predicted average August stream temperatures increased from ~10 ºC to ~16 ºC moving downstream through the river, increasing to stressful conditions for Chinook salmon (Figure 1.9), whereas predicted temperatures in the Upper Salmon River and Bear Valley Creek stayed within or near the recommended temperature range for Chinook salmon (see Appendix A). We split the Lemhi River at

the 18-Mile Creek tributary; downstream of which the average August temperatures began to increase outside of the recommended Chinook spawning water temperature range and redd density began to decrease (Figure 1.9). In the Upper Salmon, we hypothesized that the hatchery may be a controlling factor for salmon spawning because of the coincidence of the increase in redd density at the hatchery location (Figure 1.10). Therefore, we split these rivers into two sections to isolate areas with little influence from these non-topographic variables. The Upper Salmon River had a high density of redds around the hatchery; therefore, we tested the reach upstream of the hatchery, from 0 to 45 km, where the redd densities were generally lower (Figure 1.10). The small-scale wavelet power was significantly higher around redd locations than random locations for the Upper Salmon River and Lemhi River reaches above the hatchery and above 18-Mile Creek, respectively, whereas in the other reaches there was no significant relation for any wavelet scale.

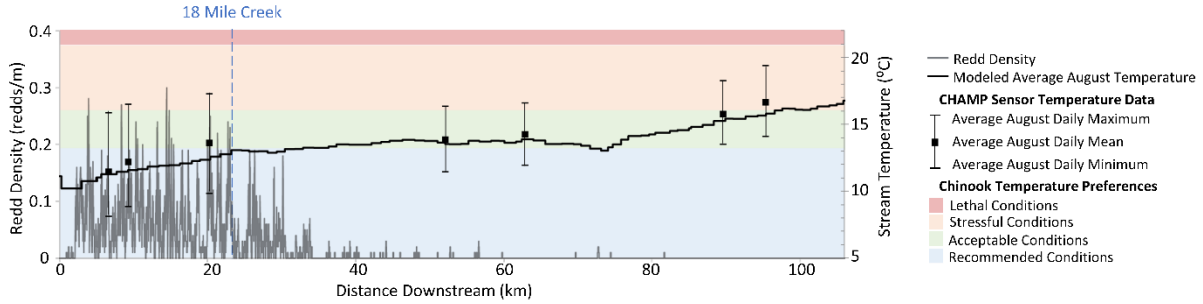

Figure 1.9: Redd density (grey line) variation with distance downstream on the Lemhi River. The modeled average daily August stream temperatures (from NorWeST, Isaak et al., 2017) are shown by the black line. Measured average August temperatures (representative of the highest water temperatures during the spawning season) from point-located CHaMP monitoring temperature sensors are shown as bracketed points (minimum, average, and maximum daily temperatures). The vertical dashed line shows the location of the 18 Mile Creek tributary, where temperature becomes a more important variable to redd site selection than wavelet power.

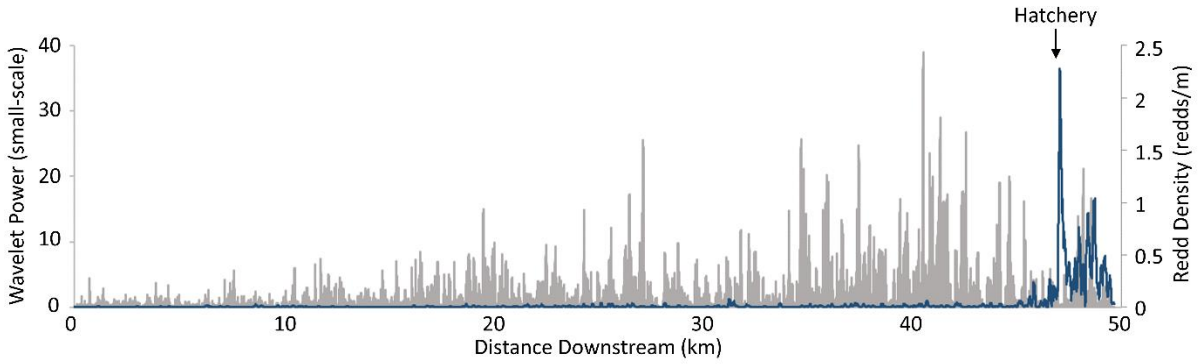

Figure 1.10: Redd density (shown in dark blue) for redds from 2010 to 2018 and small-scale wavelet power (shown in grey) for 49 km of the Upper Salmon River Basin, highlighting the location of the fish hatchery and its impact on redd densities.

Discussion

Wavelet scales and scales of topographic variability

Our results showed that wavelet analysis is an objective technique to extract multiple scales of topographic variability that are present in rivers. At all study sites, we found three representative scales of topographic variability that scaled with bankfull width (1, 4, and 10W_b). A range of wavelet scales around these three representative values aligned with the topography relatively well (see Appendix A). However, we found that W_b scaling of the wavelet scales remained similar among sites and provided transferable values among rivers. McKean et al. (2008) found longitudinal patterns in topographic variability similar to our results on Bear Valley Creek, but at different wavelet scales due to the use of an 8th order Gaussian wavelet shape, rather than the Mexican hat used in our analysis. When using the same wavelet shape for each analysis, the Mexican hat wavelet, we showed that the wavelet scales of interest are transferable among rivers with varying channel widths, discharges, and geomorphic histories.

The small and mid-wavelet scales clearly represented different scales of pools and riffles present along the rivers, whereas the large wavelet scale was representative of long low frequency variations in the bed topography, overlaid with small-scale and mid-scale wavelet scales of variability. This larger wavelet scale was likely governed by valley-scale controls. There was some alignment of low large-scale wavelet power and areas of channel confinement, but we did not see a clear association in all rivers. Further investigation is needed to fully understand what the large wavelet scale represents in these rivers.

Channel unit identification and features

The small wavelet scale (1 W_b), as with all the wavelet scales, was related to the shape and length of the features in the river and not the spacing of the repeating features. The wavelet identification method identified pool and riffles that were also delineated in the field, except for one test reach with many small features. Some field-delineated features were not present in the LiDAR data making it impossible for the wavelet method to identify them. This discrepancy could be because the LiDAR collection and field measurements were not conducted in the same year (e.g., Lemhi LiDAR collected in 2013; field units delineated in 2018), errors in the bathymetric LiDAR surface, which had an average root mean square error of 0.11 m and higher errors in areas with large elevation changes (Tonina et al., 2019), or subjective field identification. We found that by reducing the wavelet scale to 10 m, thereby reducing the lengths and depths for identified features, the smaller pools and riffles present in this reach could be identified. The wavelet analysis can be adjusted to identify the feature

size of interest, which would involve comparing a small section of the longitudinal profile to multiple scales of wavelet coefficients to visually identify the wavelet scale that best fits the features of interest, or by comparing the wavelet analysis to field data in a test reach and then applying the wavelet scale from this reach to a longer river profile.

The wavelet channel unit identification method offered many advantages to field identification—it is an objective, and repeatable method that does not require laborious field work and is independent of flow conditions. Channel units can be identified along entire lengths of rivers efficiently and the scale of the units of interest can be adjusted by using different wavelet scales. This method does not identify transitional units between pools and riffles, such as glides or runs. There are some drawbacks to using the thalweg to identify channel units, including that side-channel units will not be identified; the method is also limited by the errors in the LiDAR surface. When compared to another thalweg-based channel unit identification method, we found that the wavelet method more accurately identified pools and riffles in all reaches than the bedform differencing method (O'Neill & Abrahams, 1984). The bedform differencing method has difficulties when there are small variations in the bed profile that are not related to features or larger-scale undulations in the bed (Carling & Orr, 2000), but the wavelet methodology was able to separate these scales of deviations and only identified features at the scale of interest.

Larger geomorphic features were characterized by the mid-wavelet scale of four channel widths in length, which highlighted the larger pools and riffles in the systems as well as closely-spaced sequential pools and riffles. Given that this wavelet scale could be representative of multiple features or single large pools, further investigation is needed to fully understand what this wavelet scale represents. Gibson et al. (2019) also found two scales of pools present in larger rivers—a smaller pool sequence with a spacing of ~6 W_b and a larger scale of pools, forced by the river encountering a resistant bluff, with a spacing of ~40 W_b. In our three smaller rivers, we saw a similar pattern with two scales of pools: a spacing of small pools at ~9 W_b and larger (or combined multiple) pools at ~30 W_b.

The small- and mid-scale wavelets identified reaches with well-developed pool-riffle morphologies (areas of high wavelet power) versus reaches with more subdued morphologies (areas of low wavelet power). Spatially continuous information on topographic variability and feature locations can help fill the gap between microscale hydraulics and basin-wide management (Newson & Newson, 2000). This information on pool-riffle locations and reach morphology can be used to characterize the habitat availability and the existence of mesoscale habitat (Hanrahan, 2007).

Distributions of pool spacing and depths

For the small wavelet pool identification, the L_p* distributions calculated along the entire length of each river were similar to each other (Table 1.1). These lognormal distributions highlighted the positive skew of the pool spacings, similar to other known pool-spacing distributions (Keller & Melhorn, 1978; Thompson, 2001), but our data showed a much wider range in L_p* (Figure 1.5). Variability of L_p* has been shown to increase with decreases in the amount of pool-forming features such as large woody debris and boulders(Montgomery et al., 1995; Thompson, 2001). All three streams have been highly impacted by human activities, with the Lemhi River having the largest impacts and Bear Valley Creek and Upper Salmon River in recovery from past human disturbances. Even our least impacted stream, Bear Valley Creek, has limited wood and pool forming features. Thus, the potential long tail of the lognormal distributions of pool spacing identified by our analysis could be a result of anthropogenic activities, and a more natural system may have smaller standard deviations of pool spacing, while our median pool spacing for each river still falls within the range of consistently found pool spacings for a range of rivers (Leopold et al., 1964; Montgomery et al., 1995). Our pool data were also continuously collected and included many reaches within each river with more subdued morphology and no identified pool-riffle features. The ability to identify topographic features along continuous datasets allows for very long pool spacings that may have not been documented previously because of the limited study reach lengths. This suggests further research is needed using wavelet pool identification along the entire length of relatively unimpacted rivers to test the relative controls of pool-forming features versus continuous dataset on the tails of these distributions.

We found that pool depths along these rivers follow lognormal distributions, with wide ranges in D_p* (Figure 1.5). D_p* distributions were similar for all our basins despite the differences in human influences. In the Lemhi River, with many areas of channelization and flow alteration, the pool depths still followed the same distributions as the less altered rivers. Within the proposed dimensionless framework of D_p* and L_p*, all the basins have similar distributions, which suggests the features are in equilibrium with their current bankfull geometry. This may suggest that the Lemhi River, which has experienced reduced high and bankfull flows due to diversion dams, may be in equilibrium with the regulated flow regime and may have smaller pools than what a natural regime, with larger bankfull depths and widths, would generate.

Our data support the need to move beyond only addressing the central tendencies of channel unit morphological data (Carling & Orr, 2000). The L_p* and D_p* distributions based on entire lengths of

rivers show a wide variability in pool spacing and depths throughout rivers that could be used to inform restoration design to sustain more diverse aquatic systems. With information on bankfull characteristics from field, LiDAR, or regime equations (Raymond et al., 2012), these distributions provide a template for creating diverse geomorphology and habitat in restoration projects.

Variations in wavelet power

We initially hypothesized that pools and riffles, as represented by small-scale and mid-scale wavelet coefficients, would be highly correlated with topographic steering, specifically at channel bends where we expected the channel units to be associated with meanders (Knighton, 2014; Thompson, 1986). We found no direct positive relation between reach-averaged mid-scale and small-scale wavelet powers and sinuosity (Figure 1.6). Although pools and riffles can be present in both sinuous and straight channels (Keller & Melhorn, 1978; Montgomery et al., 1995), here we show that high sinuosity in these rivers was not always indicative of strong pool-riffle habitat and large pool refugia habitat.

Within the Lemhi River, we expected wavelet power to decrease downstream because of greater human impacts (straightening, decrease in floodplain connectivity, removal of side channels, bank armoring), but instead small-scale wavelet scale power increased with distance downstream (Figure 1.7). Although some increase in small-scale wavelet power could be due, in part, to increased stream flows as the river captures more drainage area, small-wavelet scale power in the Lemhi does not appear to be negatively impacted by low sinuosity and channel straightening. Pool-riffle sequences in these lower straightened reaches may be created and maintained through variations in channel width (Nelson et al., 2015; White et al., 2010), channel constrictions (Thompson et al., 1998), or alternate bar morphology (Colombini et al., 1987).

Chinook spawning habitat

We found that field-surveyed redds were more likely to be located in areas with higher small-scale wavelet power than randomly selected locations. Salmonid spawning has been shown to be associated with pool-riffle morphology and transitions between pools and riffles (Bjornn & Reiser, 1991; Fukushima, 2001; Hamann et al., 2014), and here we showed that Chinook salmon are favoring areas with more pool-riffle development, represented by higher small-scale wavelet power. We did not see a relation between mid-scale and large-scale wavelet power and redd locations, suggesting the local habitat dynamics are more important than broad scale variability, which agrees with previous studies showing the importance of local morphology and habitat for spawning salmonids (Benjankar et al., 2016; Hanrahan, 2007).

The relation of redd locations and higher small-scale wavelet power was only present in areas of our rivers not influenced by strong non-topographic habitat characteristics. In the Lemhi River, the high temperatures in the lower portion of the river were more important to redd site selection than wavelet power-identified topographic variability. Based on the average small-scale wavelet power around redd locations in the upper Lemhi River, there was enough small-scale wavelet power present throughout the entire length of the Lemhi River to support Chinook salmon spawning. Currently spawning in the lower Lemhi may be limited by stressful high summer water temperatures and not the quantity of small-scale wavelet power. Solely addressing high-water temperatures in the lower Lemhi River, through actions such as water management (Sinokrot & Gulliver, 2000) or riparian vegetation (Malcolm et al., 2004), could potentially open vast areas of seemingly suitable spawning habitat without extensive instream habitat improvements.

Similarly, the Upper Salmon River only showed a relation between redd location and small-scale wavelet power in the section upstream of the fish hatchery, where redd densities were generally much lower than around the hatchery. Because fish seem to congregate at and around the hatchery, the seemingly suitable spawning habitat upstream goes largely unused. In addition, any potential upstream juvenile rearing habitat will also likely go unseeded by salmon because of the short stopping of spawning adults, because juvenile salmonids typically rear downstream of their natal hatching locations (Copeland et al., 2014). Our analysis identified potentially underutilized spawning habitat that may be suitable for adult out-planting or supplementation programs. This could include moving fish upstream to spawn and utilize existing suitable habitat rather than constructing new habitat through restoration and could result in an increase in juvenile rearing capacity downstream of the unused, suitable spawning areas.

Conclusion

With increased access to high-resolution and continuous bathymetric data from drone and green LiDAR platforms, wavelet analysis can be used to detect multiple scales of topographic variability present in riverine thalweg profiles. Our analysis identified three main wavelet scales of topographic variability present along each river based on the Mexican hat wavelet form. These wavelet scales were linked to channel dimensions of one, four, and ten bankfull widths. Using the small-scale wavelet coefficients, the analysis also served as a technique to efficiently and objectively classify morphological units, such as pools and riffles, along segments and entire lengths of rivers. Mid-scale wavelet coefficients mapped the larger pools and riffles in the system or closely-spaced series of pools or riffles following the same method.

This approach allowed us to characterize the entire distribution of pool spacing and depth at different spatial scales. We generalized our findings by scaling pool depth, D_p, and spacing, L_p, by bankfull depth and channel width, respectively, to define, D_p* and L_p*. Their cumulative frequency distributions were not statistically different among the three river systems and follow lognormal distributions for each scale of wavelet analysis. We suggest that these distributions quantify the morphological variability of pool-riffle bedforms in meadow systems and can be used to predict the local distribution once the bankfull characteristics, depth and width, are known. We also show no relation between small-scale and mid-scale wavelet power and sinuosity, suggesting very sinuous and less sinuous reaches can have similar pool characteristics in these meadow systems. Large-scale wavelet power highlighted reaches within the basins with long low-frequency variations in the longitudinal profile, which were possibly related to river confinement.

This study not only introduced a valuable technique to quantify and assess local topographic variability, through wavelet coefficients and power, it also provided valuable conservation analysis to aid in the recovery of Endangered Species Act listed aquatic species. We demonstrated the importance of higher small-scale wavelet power on Chinook salmon redd site selection. Although small-scale wavelet power is abundant throughout our study rivers, we found that non-topographic variables, such as high summer stream temperatures and fish hatchery locations, can be more important habitat influencers than small-scale wavelet power and should therefore be considered in future restoration and habitat analyses in the basins. As we continue to recognize how spatial morphologic patterns and topographic variability impact aquatic habitat quality and quantity, wavelet analysis provides a way to quantify topographic variability, through wavelet coefficients and power, across all scales of interest.

Chapter 2: Impact of flow regulation on stream morphology and aquatic habitat quality distribution

Authors: Jenna Duffin, Elowyn M. Yager, Carter Borden, John M. Buffington, Rohan Benjankar, Daniele Tonina

Abstract

The importance of interactions among stream hydrology, morphology, and biology is well recognized for stream ecosystems. However, when quantifying the impacts of altered flow on aquatic habitat, the consequent changes in channel hydraulics and morphology are typically convolved or channel topography is treated as static. Here, we address the impacts of altered flow and topography separately and we hypothesize that regulated hydrographs have a larger detrimental impact on aquatic habitat quality when the channel topography is allowed to respond to the flow regime, rather than remain static. In particular, regulated hydrographs, through altered sediment transport, are expected to result in subdued morphologies and decreased habitat diversity. We address this hypothesis by quantifying spawning and juvenile rearing habitat distributions for Chinook salmon (*Oncorhynchus tshawytscha*) using a set of quasi-three-dimensional hydromorphodynamic models for two morphologically distinct reaches along the Lemhi River, Idaho (USA): an engineered, straightened, plane-bed reach and a meandering pool-riffle reach. Sediment transport was modeled with both real hydrographs and cycled, synthetic, representative hydrographs for 60 years of regulated and unregulated flows. The real and synthetic hydrographs produced similar morphologic results, which implies that flow variation and hydrograph order did not have a strong effect on the modeled topography. Unregulated hydrographs enhanced the frequency, area, volume, and depth/height of pools and bars in the meandering reach compared to regulated flows. These morphological changes did not increase the modeled habitat suitability index in the unregulated scenario, but the large growth of pools greatly improved fall and winter refugia for juvenile salmonids. In the straight reach, both regulated and unregulated scenarios resulted in a plane-bed morphology with similar habitat, suggesting that flow restoration in highly altered reaches is not sufficient to improve ecological function of the stream. Addressing both hydraulic and morphologic changes can better inform water management decisions to benefit habitat in regulated systems.

Introduction

Human alterations of rivers have led to worldwide concern over degradation of aquatic ecosystems and the need for stream habitat enhancement (Geist & Hawkins, 2016). To aid in restoration design

and site selection, quantifying aquatic habitat and the processes of habitat loss are critical to identify potential impacts of restoration (Beechie et al., 2008; Roni et al., 2008). The natural flow regime, which represents the flow quantity, timing, and variability, is a primary driver for physical habitat and ecological integrity in river ecosystems (Poff et al., 1997; Richter et al., 2003) and interruptions to functional flows can reduce physical and biological diversity (Wohl, 2012). Flow regulation has been linked to an overall reduction in geomorphic complexity, decreases in channel area, and losses in longitudinal and lateral connectivity of the river (Brandt, 2000; Graf, 2006; Williams & Wolman, 1984). Reduction in flows can also decrease the number and area of high bars, increase channel stability and river straightening, and reduce competent flows for sediment transport (Church, 1995; Grant et al., 2003; Ligon et al., 1995). All of these geomorphic effects, coupled with reduced flows, are partially responsible for a decrease in fish abundance and habitat (Bunn & Arthington, 2002; García et al., 2011; Poff & Zimmermann, 2010). Therefore, in rivers with modified hydrographs, considering how the morphology may adjust as the flow regime changes is important (Yarnell et al., 2015) because physical habitat, specifically depth, velocity, and bedforms, results from the interaction between the hydrologic regime, the channel morphology, and the hydraulics (Brierley & Fryirs, 2000; Pasternack & Brown, 2013).

Although the importance of river morphology to physical habitat, and specifically to salmonid habitat, is known (Cram et al., 2017; Geist & Dauble, 1998; Hanrahan, 2007; Montgomery et al., 1999), flow-driven changes in habitat are often modeled assuming a static topography (e.g., Bovee et al., 1998) or changes in topography and flow are convolved (e.g., García et al., 2011). As topographic data and morphodynamic modeling become more accessible, some studies have treated the topography as dynamic. Using repeat topographic surveys, Wheaton et al. (2009) monitored a restoration project after a spring flood event and found that areas of scour were associated with reductions in salmon spawning habitat, while areas of deposition led to improved spawning habitat. Another study used hydraulic modeling and a sediment transport model to identify unregulated flow conditions needed to scour fines and expose coarse spawning substrate for white sturgeon (*Acipenser transmontanus*) (McDonald et al., 2010). However, additional studies are needed that consider the long-term morphodynamics of river systems and their influence on habitat (Kail et al., 2015), as well as separation of the relative impacts of altered flow regime and morphologic changes on habitat conditions.

Prior studies of the effects of altered flow regime on topography using numerical models and laboratory flumes have used either variable hydrographs (i.e. Hassan et al., 2006), depicting the full

variability of a system, or have used representative simplified repeated/cyclic hydrographs to simplify calculations and to better constrain the impacts of specific hydrograph characteristics (i.e. Parker et al., 2003). Flume experiments have shown that increases in discharge variability, represented by multiple high-flow hydrographs, may increase channel width (Vargas-Luna et al., 2019), whereas variation in the order of hydrographs could affect bedform morphology (Nelson et al., 2011). The duration and frequency of individual hydrographs can affect channel slope and topographic variability (Plumb et al., 2020), but conversely the shape and duration of repeated hydrographs may have little effect on channel characteristics such as slope and sediment transport rates (Nelson & Morgan, 2018; Wong & Parker, 2006). The effects of hydrograph characteristics vary in the literature and research directly comparing the morphologic impact of variable and cycled simplified hydrographs is limited (Huthoff et al., 2010). Thus, work is needed to quantify differences between actual and synthetic hydrograph inputs on modeled geomorphic responses and the consequent effects aquatic habitat.

Beyond addressing how hydrograph differences may affect morphologic response, altering flows in rivers may have different topographic effects depending on the existing morphology, which mediates the effectiveness of flow reintroduction strategies (Meitzen et al., 2013), and the current morphologic condition of rivers should be considered when studying the potential effects of deregulated flows. Habitat in river reaches with more physical diversity, such as those with pools and riffles, is more resilient to changes in flows than habitat in plane-bed rivers (Hauer et al., 2012). Furthermore, restoration of natural flow regimes may not be successful in confined, human-impacted rivers because of alterations in river processes (Wohl et al., 2015; Yarnell et al., 2015). Therefore, when assessing the potential effects of changing flow regimes, it is necessary to consider the range of existing morphologic conditions and how they may mediate the potential resulting topography.

In this study, to address the potential changes in physical habitat from both alterations in flow and morphology, we developed a set of morphodynamic models for two morphologically distinct reaches, a straight highly-altered reach, and a meandering more natural reach, on the Lemhi River (central Idaho, USA). The Lemhi River is an ideal study area because flows have been regulated for decades through irrigation diversion throughout the system and the river supports endangered anadromous fish species listed under the U.S. Endangered Species Act (NMFS, 2019). Our goal was to model topographic changes under potential unregulated flow scenarios to separately understand the effects of altered hydraulics and morphology on salmonid habitat. We hypothesized that the current regulated riverbed morphology is subdued and that unregulated flows will increase the complexity of channel topography, thereby improving the available of high-quality spawning and juvenile overwintering

habitat suitability. We also tested the hypothesis that interannual hydrologic variability would affect channel morphology and consequent aquatic habitat. To explore this issue, we modeled regulated and unregulated flows using both actual hydrographs (representing natural variability) and cycled synthetic hydrographs (representing no interannual variability). Improved understanding of geomorphic and hydraulic changes from flow deregulation, and the impact of these changes on salmonid habitat, could be used to help meet restoration goals in controlled rivers through water management.

Methods

Study Area

The Lemhi River is a 100 km-long gravel-bedded river draining a 3300 km^2 basin before flowing into the Salmon River in Idaho, USA (Figure 2.1). Like many streams in the western USA, it has a history of hydrologic regulation due to agricultural irrigation diversions that affect the magnitude and timing of flows throughout the year, but primarily cause reduced spring and summer flows. The historic, unregulated flow regime was characterized by larger peak flows, longer duration spring flows, and larger summer flows. The entire river and its floodplain were mapped at 1 m resolution with the airborne topobathymetric LiDAR EAARL-B system in October 2013 during low-flow and clear-water conditions (Tonina et al., 2019).

We selected two morphologically distinct reaches to encompass the degree of human alteration at the study site: an engineered straightened reach and a less-altered, more natural, meandering reach (Figure 2.1). The 350 m-long straight reach is channelized along a highway, with an average bankfull channel width of 14 m and a channel slope of 0.006 m/m. A surface median grain size (D_{50}) of 46 mm was measured in the reach in 2020 with a Wolman (1954) pebble count. The 650 m-long meandering reach, located ~20 km upstream from the straight reach, flows through a narrowed floodplain area that is confined by agriculture. This reach had a sinuosity of 2.8, average bankfull width of 15 m, and channel slope of 0.003 m/m. Due to limited access, a grain-size distribution could not be measured for this reach; instead, we used a D_{50} of 36 mm, which was measured with a Wolman pebble count in 2020 in a naturally meandering reach with a similar bankfull width, depth, and slope that was located 10 km downstream of our reach, with no tributary inputs between the two reaches.

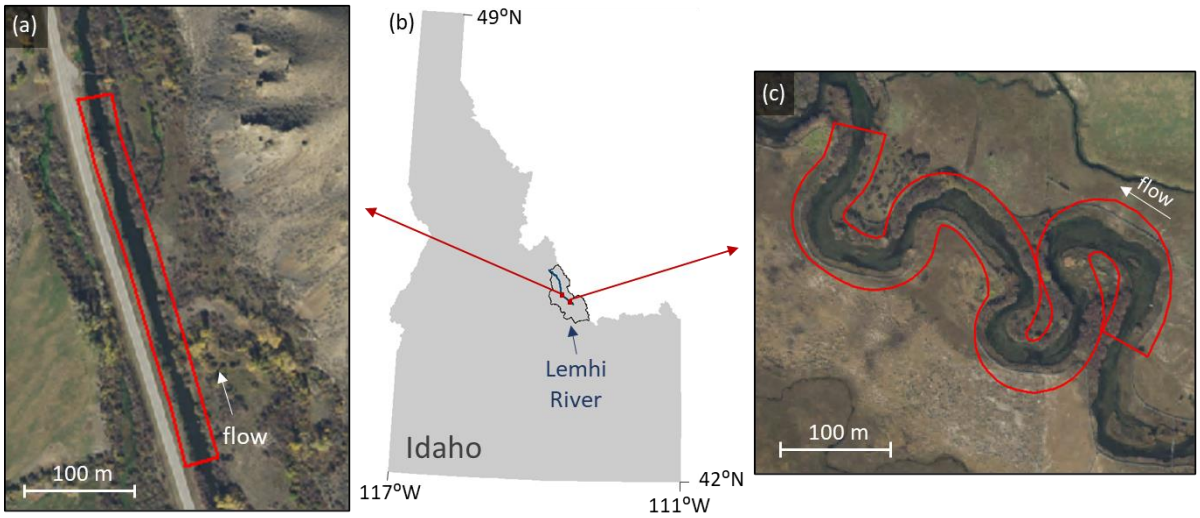

Figure 2.1: Aerial photographs of (a) the straight reach and (c) the meandering reach within (b) the Lemhi watershed in Idaho (USA). Red polygons indicate the model domain for each site.

Hydraulic Modeling

We developed two reach-scale morphodynamic models using the Flow and Sediment Transport with Morphological Evolution of Channels (FaSTMECH) software developed by the U.S. Geological Survey (USGS) and hosted by the International River Interface Cooperative (iRIC) (Nelson et al., 2003, 2016). FaSTMECH is a quasi-steady, quasi-3D solver that simulates sediment transport and channel bed evolution and efficiently handles long time scales. We input the 1 m-resolution LiDAR point elevations into FaSTMECH and used template mapping, a curvilinear inverse distance interpolator, to interpolate the stream and floodplain topography. We selected model grid sizes for each reach based on preliminary testing for a resolution that created the most stable model. For the straight and meandering reaches, we used a 1 m by 0.4 m (downstream by cross-stream direction) and a 1.5 m by 1 m averaged cell size, respectively, for the curvilinear grid. To create a stable downstream boundary in each model, we used a 10 m grid extension and forced no recirculation at the boundary. The upstream and downstream boundary conditions were set by the flow discharge and stage.

FaSTMECH requires specification of the lateral eddy viscosity and a roughness value quantified by a drag coefficient that remains constant for all discharges. The lateral eddy viscosity was determined as $0.01uh$, where u and h are the reach-averaged flow velocity and water depth, respectively (Tonina & Jorde, 2013). The drag coefficient was selected to minimize the mean and standard deviation of the residuals between the measured and predicted water-surface elevations and velocities. In the straight reach, 15 measurements of depth and depth-averaged velocity were collected with an acoustic

Doppler velocimeter (ADV) along the channel centerline during low-flow conditions (~2.3 m^3/s). In the meandering reach, field measurements were limited; therefore, the drag coefficient was selected by comparing FaSTMECH hydraulics with 30 depths and velocities (at 1.5 m^3/s) extracted along the reach centerline from a larger whole-Lemhi River 2D hydraulic model (Tonina et al., 2020). The whole-river model was calibrated with widely spaced depth and velocity field measurements, three of which were in our meandering reach and were used to validate the selection of the drag coefficient in our meandering-reach model. In the straight reach, we selected a drag coefficient of 0.01, which resulted in mean errors of 0.01 m and 0.13 m/s and standard deviations of 0.05 m and 0.22 m/s for water-surface elevation and velocity, respectively. In the meandering reach, we selected a drag coefficient of 0.015, which resulted in a water-surface elevation mean error of -0.02 m and a standard deviation of 0.08 m, and a velocity mean error of 0.03 m/s and standard deviation of 0.10 m/s.

Morphodynamic Modeling

To simulate bedload sediment transport, we selected the Yalin (1963) single grain-size bedload transport equation based on D_{50}, similar to Nelson et al., (2015) who found that the Yalin equation produced similar bars compared to a mixed grain-size equation in FaSTMECH. For each model, we allowed the flow to fully develop before calculating sediment transport by setting sediment transport to begin 60 m (about 4 bankfull channel widths) downstream of the upstream model boundary. Due to a lack of bedload transport data for the reaches because sediment was immobile at wadable flows, we assumed that the sediment input to the reach was equal to the transport capacity calculated at the 60 m cross section (e.g., Nelson et al., 2015). As the streambed evolved, the local flow depth changed not only as a function of discharge but also from erosion and depositional processes. These changes affect the numerical stability of the model if they occur too suddenly. Thus, we ran the models with an initial time step of 8,640 seconds (1/10 of a day) that was adjusted by the automatic time-stepping option to limit changes in water depth for each cell to 2% of the previous time step.

After preliminary model runs, we found that shear stresses on the bed were likely being overpredicted because they resulted in sediment transport at low flows when no transport had been visually observed in the field and they created instabilities in the models at high flows. FaSTMECH provides an option for shear-stress partitioning that accounts for roughness caused by dune-like bedforms, which we used to reduce the bed stress empirically to produce initial pool depths similar to those observed in the reaches for regulated flow and to improve model stability at high flows. In contrast to how stress-partitioning is typically done, we do not predict the bed stress based on actual topographic roughness, but rather use fictitious topography that produces a minimum reduction in shear stress

needed for proper model behavior compared to observed field conditions. The stress partitioning equation used for the dune-like bedforms (Bennett, 1995; Nelson et al., 1993; Smith & McLean, 1977) was,

$$\frac{\tau'_0}{\tau_b} = \frac{1}{1+\frac{C_d \Delta}{2k^2\lambda}\left(ln\left(\frac{0.368\Delta}{z_0}\right)\right)^2}, \quad \text{Equation 2.1}$$

where C_d is the bedform drag coefficient with a value of 0.2 for separated flow, *k* is von Karman's constant with a value of 0.4, Δ is the height of the bedform, λ is the bedform wavelength, and z_0 is the grain roughness height calculated as $0.2D_{50}$. We found that a fictitious bedform height of 0.1 m and wavelength of 0.8 m produced the minimum reduction in shear stress (~13% reduction in the straight reach and ~17% in the meandering reach) needed for proper model behavior. The partitioning likely accounted for bank roughness and for small-scale topographic variations in the bed that were smaller than the topographical variations captured by the LiDAR survey and discretized by the numerical mesh.

Hydrology

We represented the hydrology with regulated and unregulated flow scenarios from a basin-wide hydrologic model, the Lemhi River Basin Model (LRBM), which was developed to evaluate diversion operations and tributary reconnections in the Lemhi River basin (DHI, 2003, 2006). The LRBM simulates the daily water allocation and in-stream discharge in the system from October 1, 2007 to September 30, 2017, by accounting for catchment inflows, routing of water in the stream network, and diversion operation, consumption, and return flows for irrigation. The LRBM was built with the Danish Hydraulic Institute's (DHI) MIKE BASIN software and included lumped conceptual rainfall-runoff models (Nedbør-Afrstrømnings-Model) to predict inflow to the system, and a water allocation model to route water in the stream network and account for agricultural water use. The LRBM was constructed using a stream network determined from the USGS National Hydrography Dataset and delineation of catchments from a USGS 30 m digital elevation model (DEM) (DHI, 2006). The agricultural irrigation network, represented by 322 water-user nodes, was constructed from known points of diversion, places of use, aerial photography, and consultation with local water authorities and stakeholders. Historic diversion records or full water rights were used for water demand, and consumptive rates were determined by crop coefficients and reference evapotranspiration records reported by ETidaho (Allen & Robison, 2017). For more information on the development of LRBM, see DHI (2006).

We ran each reach-scale morphodynamic model for 60 years to ensure the models had sufficient time to reach dynamic equilibrium (defined as the balance between aggradation and degradation within the reach) and to model the long-term effects of the flow scenarios. To create our 60-year hydrograph inputs for the morphodynamic models, we used 10 years of LRBM-simulated flows and repeated this sequence of flows six times for the regulated and unregulated flow scenarios (Figures 2.2a and c). Accurate hydrographs were available for the straight reach, but not for the meandering reach, which was approximated with data from the downstream reference reach used to quantify the D_{50}. No significant tributary inputs occurred between the two meandering reaches; therefore, we used the available reference meandering reach hydrographs as a proxy for our reach even though some differences may exist due to diversions.

We also created cycled, synthetic, regulated and unregulated hydrographs for the models (Figure 2.2). The actual hydrographs were used to represent the natural annual variability of flows, while the synthetic hydrographs used an annually-constant shape, representing the probability of flows that occurred within the 10 years of LRBM simulated hydrographs (further explained below). We used the synthetic hydrographs to understand if the annual variability and hydrograph sequencing affected the resulting topography. To create the synthetic hydrographs, we calculated the probability of all 10 years of daily flows predicted by the LRBM and then subsampled the probabilities, selecting a low flow at 97.5% probability, then flows representing every 5% of the probability distribution from the 95% to 10% exceedance probability, and finally sampled the high flows with increasing frequency to accurately capture high-flow events down to the smallest probability of 0.027%, which represents 0.1 day, the timestep of our model (for values see Appendix B). To recreate the shape of the regulated and unregulated hydrographs, we created a 10-year time-averaged hydrograph for each of the actual regulated and unregulated scenarios. We shifted each of the 10 actual hydrographs in the series such that each annual peak flow occurred on the same day of the water year and then calculated the average daily flow over the 10 years. We used the shape of the averaged hydrograph for each scenario to create the synthetic hydrographs by arranging the subsampled flows into the same order of flows as the average hydrograph (see Appendix B). Rather than applying an average hydrograph, our approach faithfully includes all flows in proportion to their duration. Although the synthetic hydrograph includes the highest flows of the 10-year series, their annual application is mediated by the probability distribution and the associated duration of each of these high flows. Consequently, annual application of high flows is not expected to cause undue work compared to the 10-year series of flows. For each reach, a synthetic hydrograph was created for the regulated and unregulated

hydrographs and each synthetic hydrograph was repeated 60 times to create the full synthetic hydrograph time series.

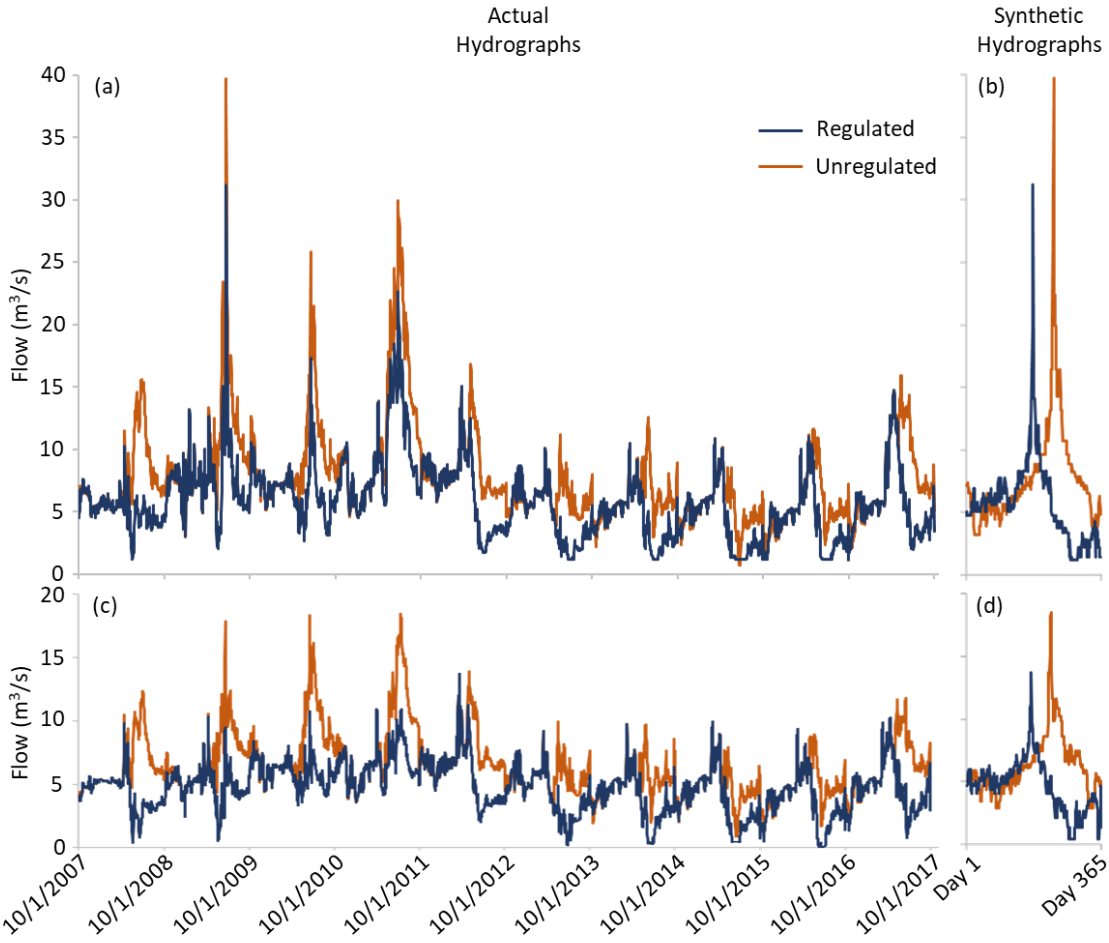

Figure 2.2: Hydrograph scenarios used for the morphodynamic models. Hydrographs for the straight reach: (a) 10 years of actual regulated and unregulated hydrographs (repeated six times for the model), and (b) the synthetic hydrograph for the regulated and unregulated water year (repeated 60 times for the model). Hydrographs for the meandering reach: (c) 10 years of actual regulated and unregulated hydrographs (repeated six times for the model), and (d) the synthetic hydrograph for the regulated and unregulated water year (repeated 60 times for the model).

Topographic Analysis

For each reach, the models were run for 60 years of regulated and unregulated scenarios with both the actual and synthetic hydrographs for a total of four scenarios per reach. At the end of each modelled year, we calculated the difference in topography between successive years to determine annual volumes of reach aggradation and degradation for each scenario. We compared the final topography after 60 years among the scenarios by creating DEMs of difference (DOD). To visualize all of the topographic data, we detrended the bed elevations by removing the reach slope from the topography and vertically translated the data by 100 m to create only positive detrended elevations.

We also extracted thalweg profiles through the final, 60-year topography of each model scenario. From these thalwegs, we calculated residual pool depth as the difference between the deepest point in the pool and the downstream high point at the pool tail; identification of pools was limited to features having residual depths larger than 40% of the reach-averaged bankfull depth (defined by the 1.5-year flow for each scenario) (Duffin et al., 2021). A similar approach was used to identify bars from longitudinal profiles of the streambed "divide" (a profile connecting the highest point within each grid cross section after deleting points within a meter of the channel edge to reduce the effects of steep banks on the analysis); bar height was determined as the difference between the highest point on the bar and the subsequent downstream low point of the profile, with features limited to heights larger than 40% of the reach-averaged bankfull depth. For each identified pool and bar, area and volumes were calculated by delineating the feature within the final topographic surface based on the elevation of the high point of pool tail for the pools or the elevation of the downstream low point for the bars.

Habitat Analysis

Discharges for the fall spawning season of Chinook salmon (August and September) and juvenile overwintering (December and January) were determined for the regulated and unregulated flow regimes based on the median discharges in each reach during each time frame (Table 2.1). Using the hydraulic models for each reach and scenario, depths and velocities for each of these seasons were modeled on the final regulated and unregulated topographies. To assess the relative impacts of flow versus topography on aquatic habitat, we considered four cases: regulated flow on the final regulated topography (fully regulated); unregulated flow on the unregulated topography (fully unregulated); regulated flow on the unregulated topography; and unregulated flow on the regulated topography. For each reach, the four scenarios for habitat modeling included fully regulated and fully unregulated scenarios, and scenarios for regulated flows on unregulated topography and unregulated flows on regulated topography. Habitat was assessed using only the actual hydrographs, justification for which is provided in the Results. For each reach and discharge, habitat quality was calculated for each model cell using suitability index curves, for depth and velocity, for Chinook salmon that were created for the Upper Salmon basin (Maret et al., 2005) (see Appendix B for curves).

Table 2.1: Seasonal habitat discharges based on median flows for each season for the regulated and unregulated flow scenarios in each reach.

Reach	**Season**	**Regulated Scenario (m^3/s)**	**Unregulated Scenario (m^3/s)**
Straight	Fall	3.5	7
Straight	Winter	5.5	5.5
Meandering	Fall	3.5	6
Meandering	Winter	5	5

For each scenario, a suitability index was quantified for each cell of the model based on the geometric mean of suitability scores for depth and velocity (each ranging from 0-1). Resultant values of the cell suitability index (CSI) were divided into the following categories of habitat quality: 0 to 0.2 - no habitat, 0.2 to 0.4 - low quality, 0.4 to 0.6- moderate quality, 0.6 to 0.8 - high quality, and 0.8 to 1 - excellent quality habitat. We calculated the reach total available habitat by calculating the weighted usable area (WUA) and hydraulic habitat suitability (HHS)

$$WUA = \sum_{i=1}^{n} A_i \cdot CSI_i, \quad \text{Equation 2.2}$$

$$\text{HHS} = \frac{\text{WUA}}{\sum_{\text{i=1}}^{\text{n}} \text{A}_\text{i}}\ , \quad \text{Equation 2.3}$$

where A_i is the horizontal area of each model cell.

Overwintering juvenile salmonids may have different habitat needs than during other seasons because of low temperatures and ice (Brown et al., 2011; Huusko et al., 2007). Habitat suitability curves used to quantify juvenile habitat also may not fully account for juvenile winter habitat needs, such as access to low velocities and deep-water refugia (Favrot et al., 2018; Huusko et al., 2007). Therefore, we also assessed winter juvenile habitat in terms of specific habitat features, such as pool depths and volumes.

Results

Topographic Change Model Validation

All the model scenarios for the straight and meandering reaches reached dynamic equilibrium by the third decade for the unregulated flows, and after two decades for the regulated flows, shown by net zero sediment volume change each year, indicating a balance between aggradation and degradation (Figure 2.3). Only very small topographic changes (<10 cm) were predicted for the regulated scenarios after attainment of dynamic equilibrium. Repeat surveys in the straight reach and a similar meandering reach between 2011 and 2013 showed no in-channel elevation changes greater than 10 cm. This confirms the model predictions for the current regulated conditions. Similarly, D_{50} is rarely mobile in the regulated scenarios, matching field observations of a mostly stationary streambed.

Actual versus Synthetic Hydrographs

Before the models reached dynamic equilibrium, sediment transport was predicted at lower discharges. After dynamic equilibrium, the morphodynamic models only predicted reach-scale (i.e.,

in more than just a few cells of the model) movement of the D_{50} at the highest flows present in each reach; specifically, for flows above ~23 m^3/s (for which only 0.94% of unregulated flows and 0.10% of regulated flows are greater) in the straight reach and above ~17 m^3/s (for which only 0.21% of the unregulated flows are greater) in the meandering reach. Sediment movement occurred mainly during high flows and resulted in smooth increases in the annual, cumulative, reach aggradation/degradation for the synthetic hydrographs, but caused a stepped increase in aggradation/degradation for the actual hydrographs (Figure 2.3). For the actual hydrographs, these high flows occurred during three consecutive years each decade, whereas in the synthetic hydrographs high flows occurred every year, resulting in differing shapes for the annual cumulative aggradation/degradation curves.

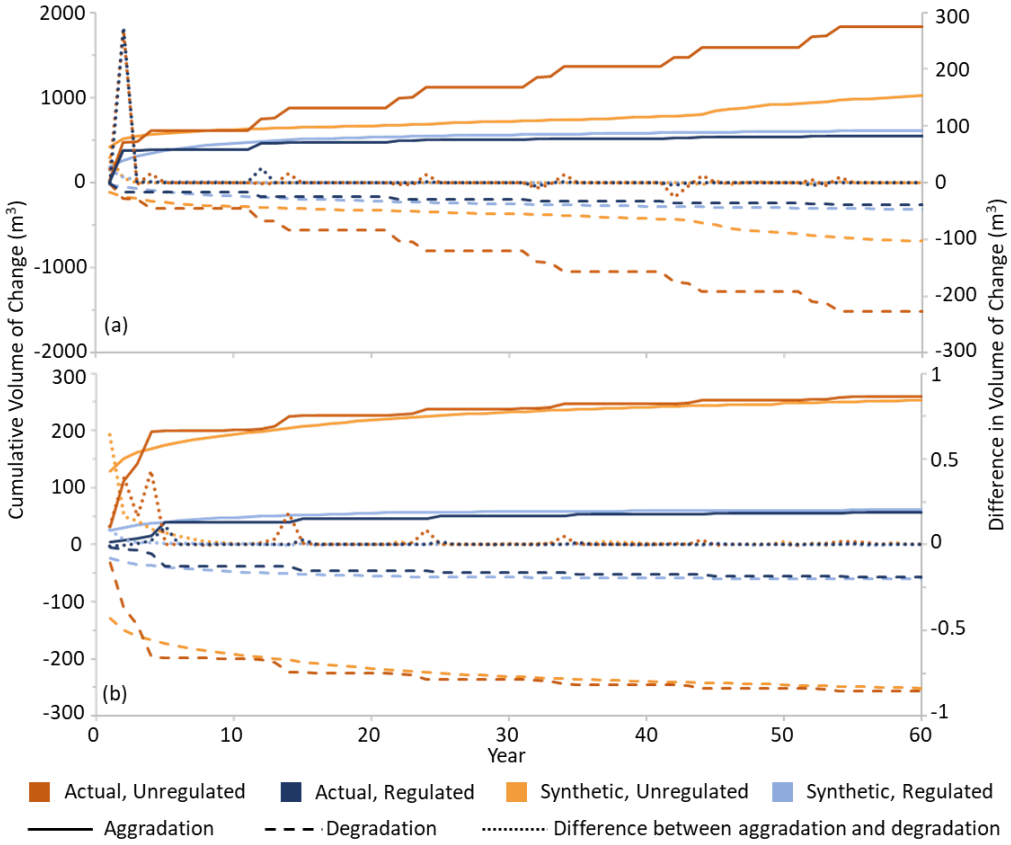

Figure 2.3: Annual total aggradation and degradation over time for (a) the straight reach and (b) the meandering reach. Each hydrograph scenario is represented by a different color, cumulative aggradation over time is shown by the solid lines, cumulative degradation is shown by the dashed lines, and the annual difference between the aggradation and degradation is shown by the dotted lines.

In the straight reach, the actual and synthetic scenarios for regulated flow produced similar volumes of aggradation/degradation (Figure 2.3a), a similar plane-bed topography (Figure 2.4h), and similar thalweg profiles (Figure 2.5a). In contrast, for the unregulated scenarios in the straight reach, the actual hydrographs resulted in larger overall volumes of aggradation and degradation than occurred

for the synthetic hydrographs (Figure 2.3a). In the unregulated actual scenario, after the first decade of model adjustment, the first high flow of each decade washed out a series of subdued bedforms (possible incipient bars and pools) and topographic undulations, which were subsequently rebuilt during the second and third high flows of each decade, but this pattern of washing out and rebuilding of subdued bedforms did not occur for the unregulated synthetic hydrographs, which resulted in less overall aggradation and degradation over time. Nevertheless, there was little difference in the final plane-bed topography (Figure 2.4g). Although more change was predicted for the unregulated flows, the regulated and unregulated scenarios produced similar morphologies, i.e., plane-bed topographies with less than ± 0.1 m difference in elevation between actual and synthetic hydrographs for 82% and 97% of the bed for unregulated and regulated flows, respectively (Figures 2.4g-h). In the unregulated scenarios, several larger differences in topography between synthetic and actual hydrographs resulted from location differences in the pattern of the final topography, rather than the development of different overall morphology. This is highlighted by the thalweg profile, where a subdued pool-like bedform was produced by the actual hydrograph at 200 m but was shifted downstream to 240 m by the synthetic hydrograph (Figure 2.5), causing larger DOD values due to a phase shift in otherwise similar topography.

In the meandering reach, for both regulated and unregulated scenarios, the actual and synthetic hydrographs produced similar final volumes of change (Figure 2.3b) and final topographies (Figures 2.6g-h). In this reach, the differences in elevations produced by the actual and synthetic hydrographs were mainly small (mostly cell differences of ± ~0.1 m for both the regulated and unregulated flows) because aggradation and degradation were localized to areas of forced pools and bars. In the unregulated scenario, the 0.2% of cells that had larger elevation changes (± ~0.5 to 1 m) between the actual and synthetic hydrograph topographies resulted from a shift in the location of the pools or bars, as well as some shallower pools for the regulated flow (Figure 2.5b). However, for both the regulated and unregulated scenarios, the scale and pattern of the morphology formed by the actual and synthetic hydrographs were overall similar. These results suggest that for our models, the interannual variability and sequence of hydrographs did not greatly affect the resulting topography and that both synthetic and actual hydrographs can be used to represent the hydrology for these reaches when modeling morphology. As such, to streamline the presentation, hereafter the results will be based on the topography produced by the actual hydrographs, without presentation of otherwise similar findings for the synthetic hydrograph.

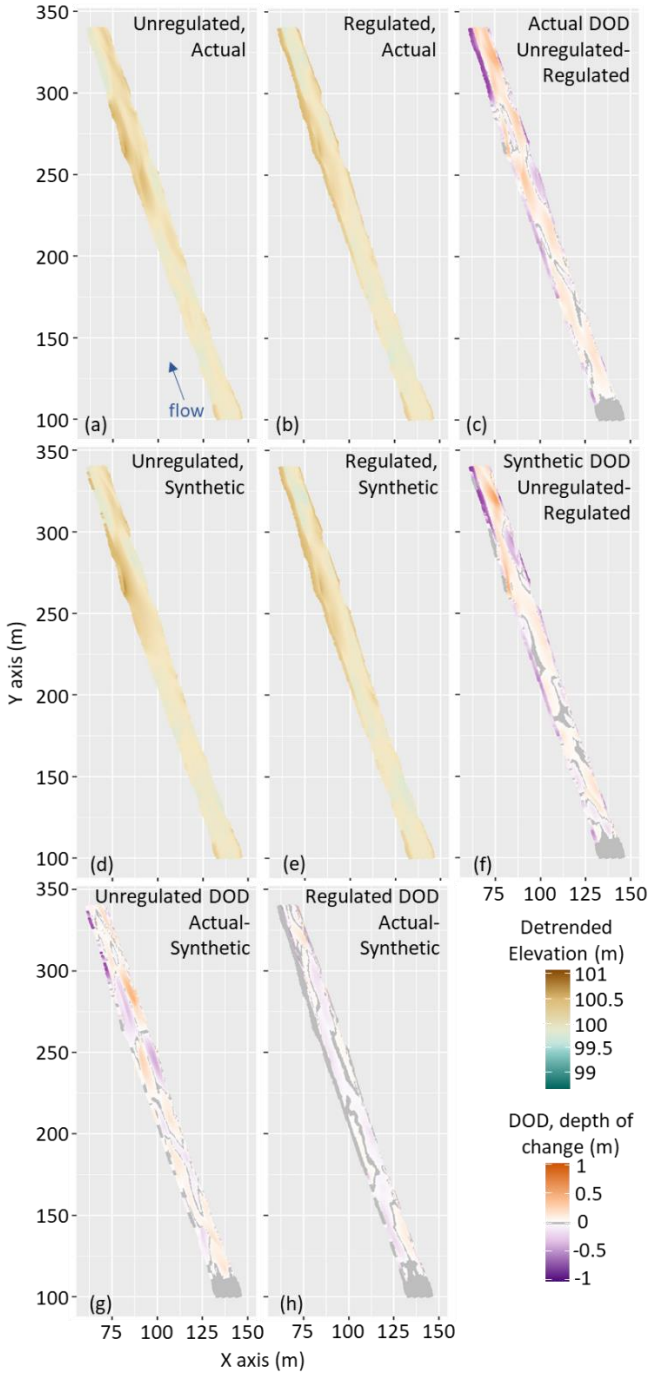

Figure 2.4: The final, 60-year, modeled straight reach topography for each hydrograph scenario: (a) the unregulated, actual hydrographs, (b) the regulated, actual hydrographs, (d) the unregulated, synthetic hydrographs, and (e) the regulated synthetic hydrographs. The digital elevation model (DEMs) of Difference (DODs) between the different final topographies are shown for (c) the unregulated minus the regulated actual scenarios, (f) the unregulated minus the regulated synthetic scenarios, (g) the actual minus the synthetic unregulated scenarios and (h) the actual minus the synthetic regulated scenarios. Note that the detrended elevations and DOD maps are shown on the same scale as the meandering reach in Figure 2.6, which has a wider range of elevations and magnitudes of change.

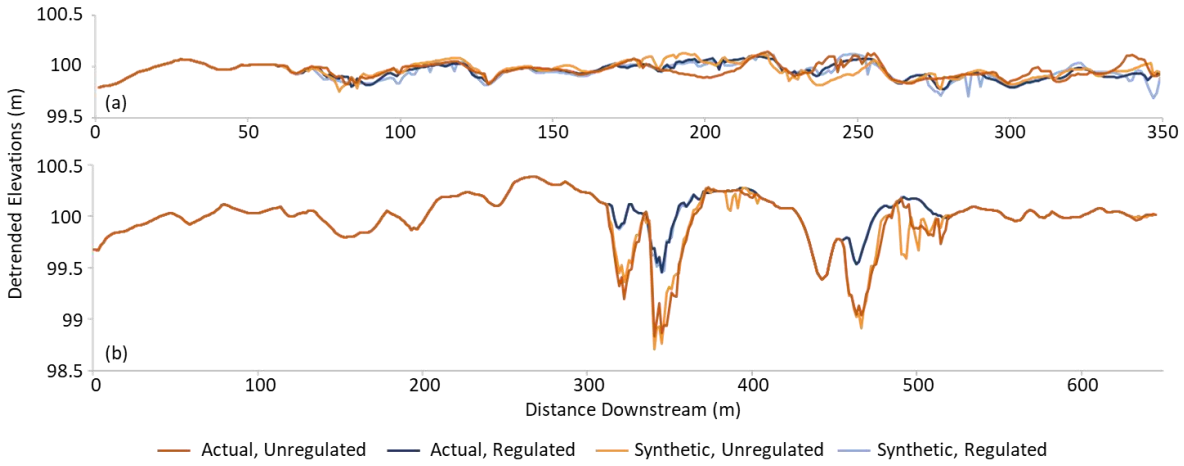

Figure 2.5: Detrended thalweg profiles for the final topography for (a) the straight reach and (b) the meandering reach. The profiles for each hydrograph scenario are shown in different colors, with some lines not visible due to overlap with others.

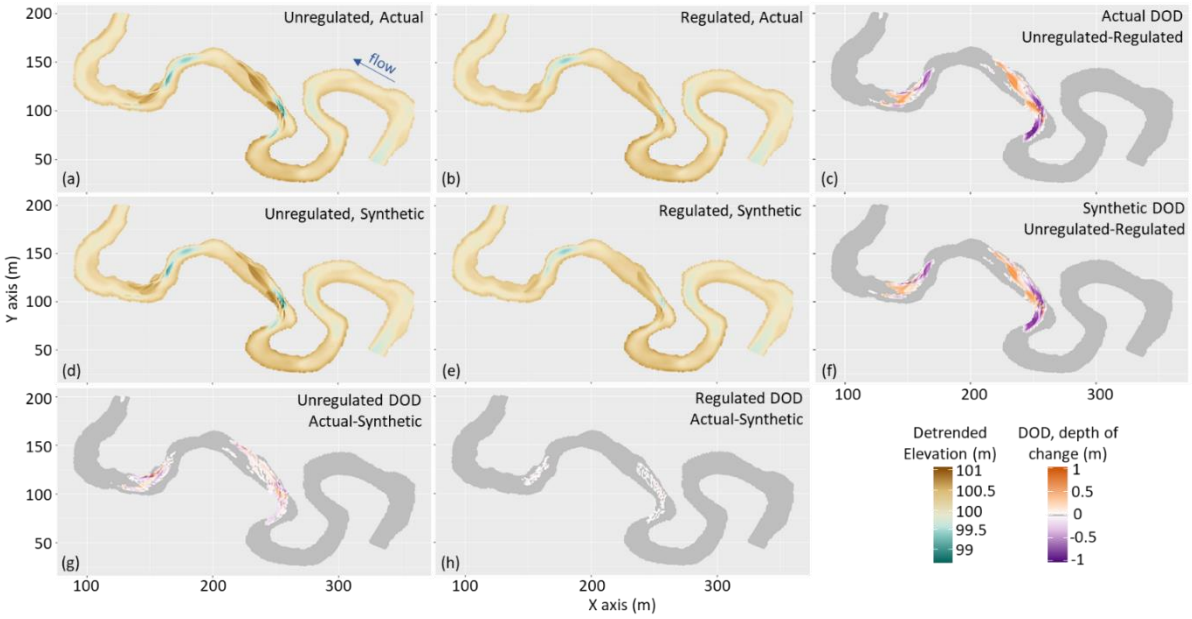

Figure 2.6: The final, 60-year, modeled meandering reach topography for each hydrograph scenario: (a) the unregulated, actual hydrographs, (b) the regulated, actual hydrographs, (d) the unregulated, synthetic hydrographs, and (e) the regulated synthetic hydrographs. The digital elevation model (DEMs) of Difference (DODs) between the different final topographies are shown for (c) the unregulated minus the regulated actual scenarios, (f) the unregulated minus the regulated synthetic scenarios, (g) the actual minus the synthetic unregulated scenarios and (h) the actual minus the synthetic regulated scenarios.

Regulated versus Unregulated Flows: Morphological Differences

In the straight reach, we identified no pool or bar features in the final bed topographies for the regulated and unregulated flows, and the morphology remained plane-bed. For all scenarios in the straight reach, the final detrended thalweg elevations show 0.35 m of vertical range, with a standard deviation of 0.07 m (Figure 2.5a). The comparison between the final unregulated and regulated topographies showed mostly small differences in elevations; 66% of the model cells had less than ±

0.1 m of difference in elevation (Figure 2.4c), with some larger differences (never larger than 0.6 m) due to slight shifts in the topographic patterns or due to boundary effects at the downstream end of the reach.

In the meandering reach, the regulated conditions formed subdued morphology compared to the unregulated conditions. Between the regulated and unregulated hydrographs, the variability in the detrended thalweg elevations increased from a vertical range of 1.00 m to 1.55 m and the standard deviation in elevations increased from 0.18 m to 0.27 m (Figure 2.5b). The unregulated flows scoured pools deeper than the regulated scenario and the scoured sediment built larger downstream bars, resulting in 8.6% of the cells having differences in elevation greater than ± 0.1 m between the regulated and unregulated topography at pool and bar locations (Figure 2.6), with many of those cells having larger differences (up to ±1.15 m). The area, volume, and maximum depth/height of pools and bars generally increased from the regulated to the unregulated conditions (Figure 2.7), and a new pool formed for the unregulated scenario (Pool 2), resulting in a 33% increase in pool frequency. Total pool volume increased by 92% and total bar volume increased by 43% between the regulated and unregulated scenarios. The pool and bar characteristics increased largely during the first high flow, and with maximum area, volumes, and depths generally attained after three high-flow years.

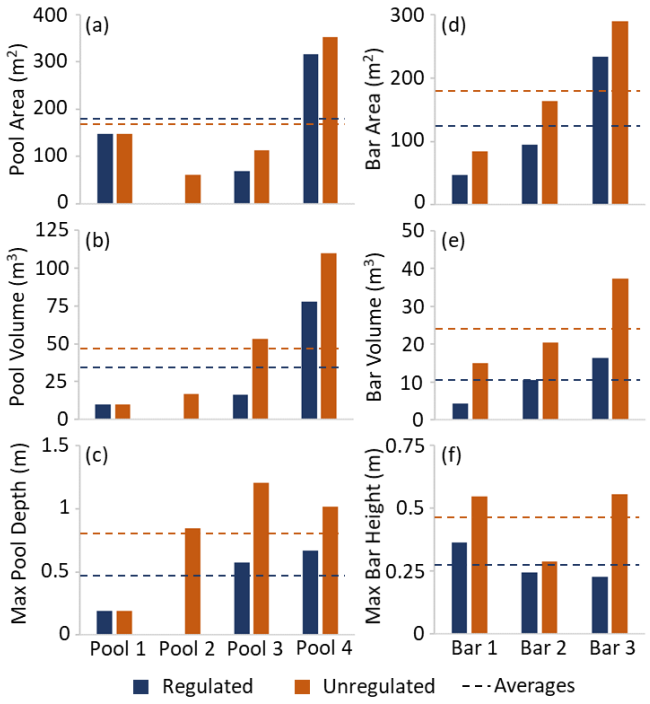

Figure 2.7: Predicted values of (a) pool area, (b) pool volume, (c) maximum pool depth, (d) bar area, (e) bar volume, and (f) maximum bar height for each pool and bar in the meandering reach, with reach averages shown as dashed lines, for the regulated and unregulated actual hydrograph scenarios.

For both the regulated and unregulated conditions, the meandering reach showed more topographic variability and complexity than the straight reach, which is highlighted by the final thalweg profiles (Figure 2.5, total detrended elevation range of 1.05 m and 2.32 m for the straight and meandering reaches respectively) and by comparing the final reach topographies (Figures 2.4 and 2.6). The straight reach maintained a plane-bed morphology in all scenarios, whereas in the meandering reach, the regulated conditions resulted in subdued pools and bars, while the unregulated conditions greatly increased the topographic variability through pool scour and concurrent downstream bar deposition.

Regulated versus Unregulated Flows: Habitat Differences

The fully regulated condition (i.e., regulated flows on regulated topography) produced a greater extent of fall spawning habitat that was higher quality (HHS= 0.41) than the fully unregulated condition (HHS = 0.15) in the straight reach (Figures 2.8a-c). This result was driven by the fact that the unregulated flows had larger velocities that more frequently exceeded the suitability criteria than regulated flows (Figure 2.10b). Similar results occurred for regulated flows on the final unregulated topography and for unregulated flows on the regulated topography, demonstrating that results are dominated by the flow regime, with minimal topographic effects. Despite improved spawning habitat by the regulated fall flows, there was little to no winter juvenile habitat (HHS = 0.01) predicted for either the regulated or unregulated flows (Figures 2.9a-c). The overwintering juvenile habitat in this reach was limited by high velocities, which were almost entirely outside of the suitable range (Figure 2.10d).

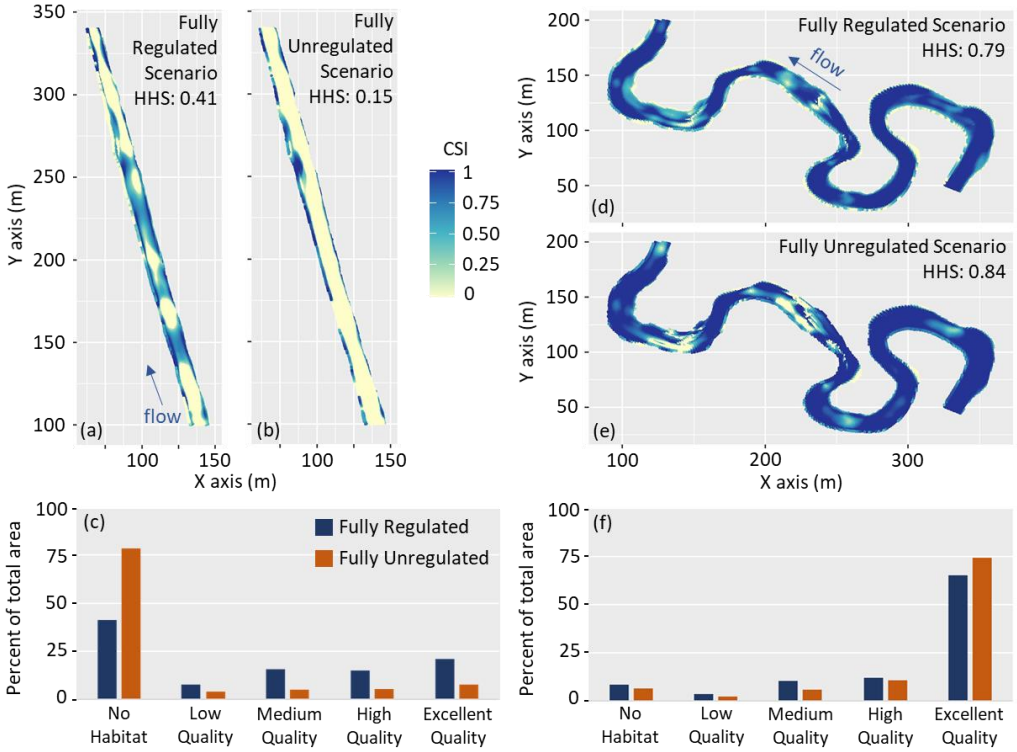

Figure 2.8: Fall spawning habitat suitability maps for Chinook salmon in the straight reach for (a) regulated topography and regulated fall flow (3.5 m^3/s) (fully regulated), (b) unregulated topography and unregulated fall flow (7 m^3/s) (fully unregulated), and (c) habitat availability by quality for the fully regulated and unregulated conditions. Right panels show fall spawning habitat in the meandering reach for (d) the regulated topography and regulated fall flow (3.5 m^3/s), (e) the unregulated topography and unregulated fall flow (6 m^3/s), and (f) the habitat availability by quality for the fully regulated and unregulated conditions.

In the meandering reach, excellent and high-quality fall spawning habitat quality was abundant for all scenarios, but habitat suitability was slightly higher for the fully unregulated case (HHS= 0.84) than for fully regulated conditions (HHS = 0.79) (Figures 2.8d-f). This increase in modeled habitat suitability was not due to the change in final topographies (regulated vs. unregulated), but directly to the change in hydrology. The unregulated high flows in the fall increased habitat on both topographies (both HHS = 0.84), whereas the regulated flows resulted in a slightly lower HHS values (0.79) for both topographies. Although the HHS values for the regulated and unregulated flows on the unregulated topography were similar, the unregulated topography resulted in a 2-5% increase (depending on flow condition) in excellent quality spawning habitat compared to the regulated topography (Figure 2.8f).

Winter juvenile habitat availability remained similar between the fully regulated (HHS = 0.09) and fully unregulated (HHS = 0.10) conditions in the meandering reach (Figures 2.9d-f). The regulated and unregulated winter flows were the same; therefore, the small differences in HHS were entirely

attributable to changes in the topography. The high-quality winter juvenile habitat was mainly on the margins of the channel, where the velocities were low. In most of the meandering reach, winter velocities were higher than suitable for both the regulated and unregulated topographies (Figure 2.10h).

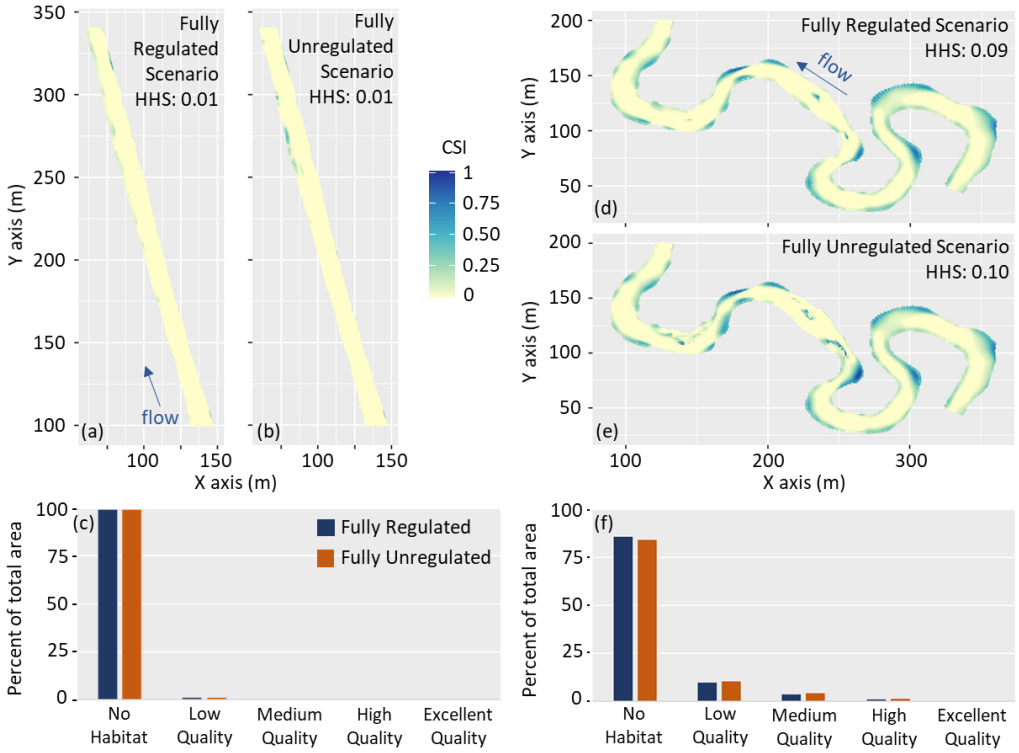

Figure 2.9: Overwintering habitat suitability maps for juvenile Chinook salmon in the straight reach for (a) regulated topography and regulated winter flow (5.5 m^3/s) (fully regulated), (b) unregulated topography and unregulated winter flow (5.5 m^3/s) (fully unregulated), and (c) habitat availability by quality for the fully regulated and unregulated conditions. Right panels show overwintering habitat in the meandering reach for (d) the regulated topography and regulated winter flow (5 m^3/s), (e) the unregulated topography and unregulated winter flow (5 m^3/s), and (f) the habitat availability by quality for the fully regulated and unregulated conditions.

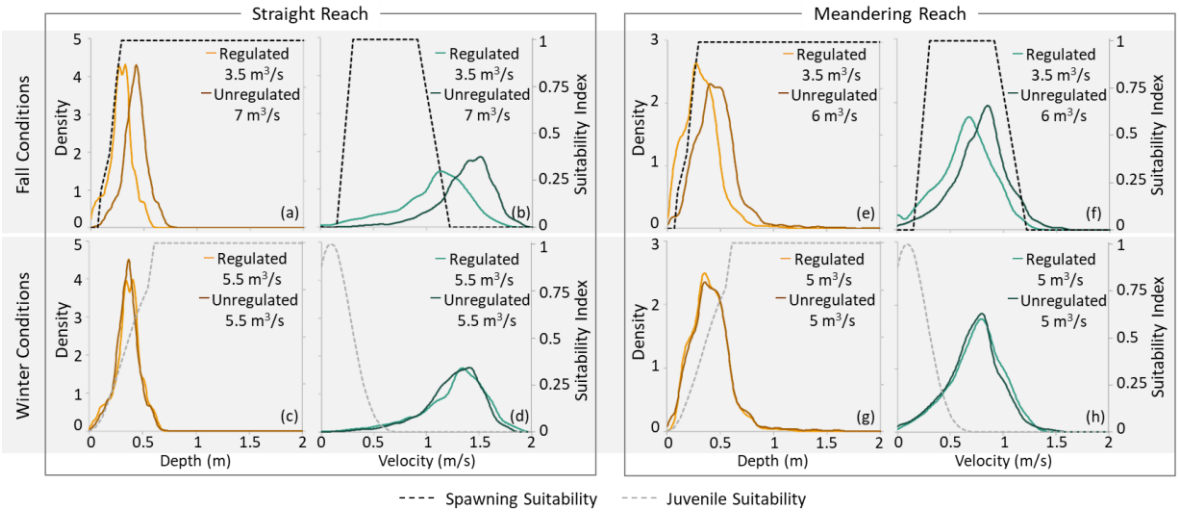

Figure 2.10: Depth and velocity distributions for the fully regulated and fully unregulated conditions for fall and winter flows in (a-d) the straight reach and (e-h) the meandering reach. Probability density distributions for depth and velocity (solid lines) are shown on the primary y-axis and overlaid with the suitability curves for Chinook spawning and juvenile rearing (dashed lines) on the secondary y-axis.

Discussion

Actual Versus Synthetic Hydrographs

Our results show that both the actual hydrographs, representative of the natural variability of flows, and the synthetic hydrographs, a single cycled representative hydrograph, produced similar morphologic patterns in each of our study reaches. Flume studies assessing the impact of cycled hydrograph shape and duration have found varying results; sometimes having little influence on bedform and channel characteristics (i.e. slope) (Nelson & Morgan, 2018; Wong & Parker, 2006), whereas other studies have found that hydrograph shape and duration had an impact on bed load flux (Mao, 2012; Redolfi et al., 2018) and channel morphology (Waters & Curran, 2015; Zhang et al., 2020). Another study addressed the effect of flow order and found that changing the location of a uniform high-flow period within low flows resulted in similar bedform geometry (Nelson et al., 2011). A morphodynamic modeling study looking at the effects of cycled hydrographs found that using a single, repeated, representative hydrograph produced aggradation and degradation volumes outside of the range produced by hydrographs representing variability in discharge (Huthoff et al., 2010), but suggested the representative hydrograph may have been oversimplified by not including the full range of flows. Phillips et al. (2018) showed that, with a uniform grain size distribution, bed load flux from a variety of hydrograph shapes scaled with transport capacity, suggesting that maintaining transport capacity between hydrograph comparisons may provide more similar morphologic results. Many of these studies, also with uniform grainsize distributions, did not hold

transport capacity constant between their compared hydrographs, which may explain the variation in results. Therefore, the design of representative hydrographs should preserve physical properties of the hydrology, such as the peak discharge, transport capacity, and hydrograph shape that accurately represents the full probability of flows (Serinaldi & Grimaldi, 2011). There is likely complex feedback between transport capacity, grain size distributions, and bed morphology, which is not always considered in studies; here we used a single grain size, which may reduce the differences in morphology between our actual and synthetic hydrographs. The synthetic hydrographs presented in this paper accurately represented the full probability of flows present in the actual hydrographs and maintained the hydrograph shape, therefore producing similar final bed elevations and topographic features. Fully and accurately representing the high flows in this system was important because after equilibrium conditions the D_{50} only moved at the highest flows, which is similar to what has been observed in other meadow systems (Andrews, 1994; Maturana et al., 2014; McKean & Tonina, 2013).

Regulated Versus Unregulated Flows: Morphological Differences

The meandering reach model showed that regulated flows resulted in subdued topography, whereas unregulated flows formed pools that were larger in area, depth, volume, and frequency than the regulated scenarios. The current channel topography has adjusted to years of flow regulation with reduced magnitudes and durations of high flows that are needed to maintain pools and bars (MacWilliams et al., 2006; Sawyer et al., 2010). Our model results indicate that the river may have had more topographic variability, with deep pools and more pronounced bars prior to flow regulation. Increasing the occurrence of high flows in regulated rivers will not only improve topographic variability, but also has important ecological effects. The unregulated high flows help to create an active river bed, which can remove fines and clean spawning gravels (Milhous, 1998; Reiser et al., 1989) and can break up armor layers (Parker & Klingeman, 1982; Ryan et al., 2005; Vericat et al., 2006; Yager et al., 2015).

Topographic differences between unregulated and regulated flows were more pronounced in the meandering reach, where pools and bars were already present, than in the straight reach. The occurrence of topographic steering (Whiting & Dietrich, 1991), flow convergence (MacWilliams et al., 2006; Thompson & Wohl, 2009), or a combination of such effects (Brown & Pasternack, 2014) likely helped to develop pools and bars in the meandering reach. Furthermore, restoration of flows may not regenerate and improve the morphology of highly altered reaches (Wohl et al., 2015) like the straight reach, where the existing channel conditions, such as channel width and variability in the topography, was not supportive of pool and bar development.

Regulated Versus Unregulated Flows: Habitat Differences

Both regulated and unregulated models produced abundant spawning habitat for most scenarios, and changes in topography between the regulated and unregulated model outputs had very little effect on the availability of spawning habitat. The increased fall flows under the unregulated scenario had competing effects on the suitability of spawning habitat in the two channel types; spawning habitat was reduced in the straight reach and was increased in the meandering reach. However, the potential topographic induced changes in spawning habitat for regulated versus unregulated flows are relatively minimal and not as consequential as potential changes in juvenile overwintering habitat.

Previous studies have shown that juvenile habitat, specifically overwintering habitat, is a limiting factor in the Lemhi River (Carmichael et al., 2020; Copeland et al., 2014). Contrary to our expectations of an increase in juvenile habitat quality due to changes in morphology caused by unregulated flows, in the meandering reach we only saw a 1% increase in overall habitat suitability between the fully regulated and fully unregulated scenarios. For all scenarios, the depth-averaged velocities were generally unsuitable for overwintering of juvenile Chinook salmon (Figure 2.10); therefore, no large increase in calculated habitat occurred. The 33% increase in pool frequency, 36% expansion in pool area, 92% growth in pool volume, and 54% increase in the maximum residual pool depths between the regulated and unregulated scenarios (Figure 2.7) did not affect the modeled habitat suitability in the meandering reach, but are nonetheless important habitat features, especially for juvenile salmonids. Diverse habitat with deep pools act as refugia from high velocities, create stable conditions during discharge changes, and increase the probability of overwintering survival for juvenile salmonids (Brown et al., 2011). Although juvenile fish can benefit from the lower velocities at the bottoms of these deeper pools (Favrot et al., 2018), this advantage is not recognized by the HHS scores due to their reliance on depth-averaged velocities. A study of microhabitat use in a similar stream found that Chinook parr disproportionally occupied the deepest water available during fall and winter rearing, specifically deep water areas greater than 1.15 m (Favrot et al., 2018). In the meandering reach, the streambed area with depths greater than 1.15 m increased from 1.7 m^2 to 104.2 m^2 (6029% increase) between the regulated and unregulated topographies for the regulated fall flows (3.5 m^3/s), and from 30.9 m^2 to 145 m^2 (372% increase) for the unregulated fall flows (6 m^3/s), highlighting the relative importance of changes in topography versus flow. For regulated and unregulated winter flows (5 m^3/s), the streambed area with depths greater than 1.15 m increased from 13.0 m^2 to 130.5 m^2 (902% increase), resulting in a substantial increase in deep-water juvenile refugia from the regulated to unregulated topography, respectively.

Model Limitations

Results from modeling studies like this have limitations based on the imposed modeling conditions. For example, our model does not allow for lateral migration, which is an important process for river evolution. We also used a median grain size-based sediment transport model, ignoring the potential effects of grain-size interactions, such as particle hiding and size-selective transport, that could result in errors in bedload predictions (Durafour et al., 2014). Using a full grain size distribution versus a single grain-size could have morphological effects due to spatial differences in critical shear stress, but our results based on a single grain-size should generally hold true. When modeling channel evolution with a full grain-size distribution and a single grain size Nelson et al., (2015) found minimal differences, but using a spatially constant roughness created bars with shorter wavelength and higher amplitude. However, accounting for a full grain-size distribution with smaller sediment may reduce the modeled depths and volumes of pools due to low-flow sand deposition in pools (Thompson et al., 1996). Including channel unit-based (e.g., riffle versus pool) grain-size information is also important in accurately predicting sediment transport, but may not be as important as the spatial variability in flow and shear stress (Monsalve et al., 2016), which was included in our models.

However, our simulations also do not consider history-dependent critical shear stress values, which can impact subsequent bedload transport rates (Milhous, 1973; Reid et al., 1985; Turowski et al., 2011). Without large flow events that mobilize the bed and break up granular resistance, channel stabilization can occur as the critical shear stress increases due to a preponderance of low and moderate flows (An et al., 2021; Masteller et al., 2019) that move grains into more stable positions or increase bed packing. Changes in bed structure can explain critical shear stress variations over time, which is not accounted for in our model. Inclusion of the dependence of critical shear stress on flow history might alter the results of our modelling. In particular, we could see larger differences between the regulated and unregulated results due to the larger, more frequent, peak flows in the unregulated hydrographs reducing the critical shear stresses and potentially resulting in more morphological changes over time. The interannual variability in flows in the actual hydrographs could also affect the critical shear stress and the order of the flows could be more important than we showed. Similarly, the synthetic hydrographs, with repeated annual high flows, might maintain a temporally constant critical shear stress, similar to what is assumed in our modelling. Furthermore, our estimation of sediment fluxes and predicted morphology may be inaccurate with respect to field conditions because of our use of a simplified model (i.e. using a single grain size for modeling changes to channel morphology

and the assumption of a temporally constant critical shear stress), but our results highlighting the main potential morphologic differences between regulated and unregulated flow.

Management Implications

Our results show that unregulated flows could create more complex habitat through scouring of larger pools and increased pool frequency than regulated flows. Instream restoration goals often include adding stream complexity by manually creating deep-pool habitat and bars. However, in regulated rivers, reintroduction of the highest flows may be an effective way to facilitate widespread restoration of subdued topography with minimal instream disturbance (Groll, 2017). We found that only the highest flows present in our reaches mobilized the D_{50} and resulted in meaningful morphologic changes. In the meandering reach, for the unregulated scenario, our models demonstrated that pools developed quickly, with much of the scour occurring during the first high flow, and with maximum pool depths attained after three high-flow years. Each of these high flows (larger than 17 m^3/s) lasted only about one day each year. The actual timescale for morphological changes at other sites may differ from our modeled values, depending on local channel conditions, such as bed armoring, sediment supply, and the degree of size-selective transport. Although caveats exist, the results showing rapid development of deep large pools are promising for water management.

Large disturbance events have the potential to produce large shifts in habitat (Reich & Lake, 2015). Consequently, keeping high flows from being diverted for human use during high-water years may be enough to improve juvenile habitat quality. However, full restoration of unregulated flows may not be necessary or beneficial for improving habitat. For example, Carmichael et al., (2020) modeled the bioenergetics of juvenile salmonids in multiple reaches of the Lemhi River and found that regulated flows produced more favorable conditions for juvenile growth than unregulated flows; although their work did not account for flow-related changes in topography, their study highlights the importance of slow water refugia during higher flow conditions. We also show that the impact of flow restoration on instream morphology is not enough to reduce high flow velocities during the winter period, which highlights the importance of lateral habitat reconnection and the potential addition of large wood to aid in velocity reduction if diversions were removed for extended periods of time.

We assessed potential effects of unregulated flows on two reaches along the Lemhi River, but the effects of flow restoration would likely upscale to the entire river. As we showed, the effect of flow magnitude on habitat quality was limited, but the indirect effects of unregulated flows, such as the increase in pool characteristics, could have a large effect on juvenile habitat. Our results showed that channelized, highly-altered reaches may not improve with flow restoration but that less altered

reaches, like the meandering reach, have the potential to improve morphologically. To identify how much of the Lemhi River could exhibit improved habitat from restoration of unregulated flows, we calculated what portion of the river has similar topographic variability to the meandering reach. A previous study on the Lemhi River found that the small-scale wavelet power, depicting the topographic variability of the river thalweg, was representative of the pools and riffles along the river (Duffin et al., 2021). Based on the small-scale wavelet power of the meandering reach, we found that 93% of the Lemhi River has similar or higher existing reach topographic variability. Those portions of the river represent areas with existing pools that are subdued from decades of flow regulation, while the remaining 7% of the river is composed of highly-altered reaches without existing pools. Although 93% of the river has similar topographic variability to the meandering reach, only 65% of the Lemhi River is meandering (sinuosity >1.2). Therefore, due to forced pools being associated with smaller radius of curvature (Lofthouse & Robert, 2008), those sinuous reaches may have a stronger morphologic response, similar to our meandering study reach, than the less sinuous reaches. The potential to improve juvenile overwintering habitat through temporary flow deregulation along this river by increasing channel complexity and increasing pool depths, area, volume, and frequency is likely much larger than the potential effects of local large instream habitat improvement projects (e.g., woody debris placement or channel realignment) because of the considerably larger extent of the river that can be affected by flow deregulation. Increases in deep-pool habitat could also improve the resiliency of the river to potential climate change stresses, such as reduced flows (Walters et al., 2013), by providing consistent hydraulic and thermal refugia (Justice et al., 2017). This analysis highlights the possibility and benefits of a passive restoration approach, which leverages functional flows in restoring aquatic habitat not just at the reach scale but at the river segment and even higher scale. Many streams not only in the Pacific Northwest of the United State have similar characteristics of the Lemhi River such that our results could provide potential trends in similar system worldwide.

Conclusion

Hydromorphodynamic models can help to assess the effects of water management strategies on both stream hydraulics and morphology. Our analysis revealed the differences in reach topography, hydraulics, and habitat between regulated and unregulated flows applied over 60-year scenarios for an engineered, straightened, plane-bed reach and a more natural meandering reach. We tested a series of actual hydrographs that represent the natural annual variability of flow versus cycled (annually constant), representative, synthetic hydrographs. The actual and synthetic hydrographs after 60 years resulted in similar final modeled topographies for both reaches. The D_{50} was only mobile at the highest flows present in these reaches, and both the actual and synthetic hydrographs have the same

probability of high flows occurring for our flow scenarios. For these models, the sequence and annual variability of flows was not as important as the occurrence of the high flows. Consequently, both hydrograph types produced similar topographic results.

For the straight reach, we found that the plane-bed topography persisted for both regulated and unregulated flow scenarios. Spawning habitat quality in this reach did not improve from the negligible topographic changes but was negatively affected by higher fall flows for the unregulated conditions. Overwintering habitat for juvenile salmonids in the straight reach was essentially non-existent for both the regulated and unregulated scenarios.

The unregulated scenario in the meandering reach resulted in more spatially variable topography than occurred in the regulated flows, with a notable increase in pool depth, volume, and frequency. However, the change in the topography between the regulated and unregulated scenarios did not greatly affect the amount of available spawning habitat. Nor were there significant changes in the quality of overwintering habitat for juvenile salmonid but increases in pool depth and area from the unregulated flows likely had additional habitat benefits, including improved availability of fall and winter refugia for juvenile Chinook salmon.

Increases the frequency and magnitude of high flows in regulated rivers, it may have the potential to scour subdued pools and build larger bars in regulated rivers. Temporarily restoring unregulated high flows may improve in-channel morphology where pools and bars are present but have limited effect in engineered straightened sections, which may need more intervention than hydrologic restoration alone. Restoration of selected functional flows that can mobilize the median grain size may provide effective benefits for a passive stream restoration approach, where the high flows can restore subdued topography. Our modeling shows that pool and bar restoration can occur quickly within days and the process may occur at spatial scales much larger than the typical single reach scale of most active river restoration projects. This suggests that short period of high flows, for instance during a wet year, may have noticeable ecological benefits.

Rivers exhibit complex responses between hydrology, topography, and habitat. Consequently, the use of morphodynamic models (which capture linked changes in hydraulics, sediment transport, and channel morphology) can be a powerful tool to help water managers make informed decisions for the greatest benefit to the ecological function of rivers.

Chapter 3: Mapping salmon rearing carrying capacity at the riverscape: The role of fish size, multi-life stage interaction, and fish behavior

Authors: Jenna Duffin, Daniele Tonina, Elowyn M. Yager, Brian Kennedy, Rohan Benjankar, Ernest Keeley

Abstract

Most ecohydraulic modeling combines biological criteria of habitat suitability, bioenergetics, or individual based modeling) with stream hydraulics at the reach scales, providing partial and limited information to understand habitat use of highly mobile organisms such as fish. This limited spatial scale constrains our understanding of habitat quality and selection, which are spatially and temporally variable due to flow, temperature, food, and bathymetric variations. In this study, we develop a riverscape ecohydraulic model, by linking a two-dimensional hydraulic model with a bioenergetic model, and a habitat suitability index (HSI) based model to quantify spawning and rearing habitat quality for Chinook salmon (*Oncorhynchus tshawytscha*) along 106 km-long segment of the Lemhi River (Idaho, USA). We determine the spatial variations in energy dependent juvenile carrying capacity, when constrained by fish space requirements and growth potential, at the microscale across an entire river length. We found that when accounting for fish territorial behavior, increasing food availability from the field-observed average availability had negligible effect on carrying capacity, but decreasing food negatively affected the carrying capacity. Habitat quality for each juvenile life stages varies along the river and often increases with fish size as they can access habitat with faster flows, but this positive effect is mitigated when accounting for territory size. We show that stream temperature was inversely related to carrying capacity, but temperature, food, and fish size effects were all modulated by local flow hydraulics. We also found that spawning redd locations were related to, not only on spawning habitat quality, but also the presence of good juvenile habitat. Our results at the riverscape highlight the role of drift concentration, temperature, fish size, fish behavior, and multi-life-stage effects, when interpreting habitat quality and carrying capacity.

Introduction

As human demands for water resources increase, anadromous fish populations are at continued risk of decline and extirpation (Gustafson et al., 2007; Honea et al., 2016). Habitat alteration and fragmentation are considered some of the key reasons for reductions in salmonid populations (Gregory & Bisson, 1997), highlighting the importance of freshwater habitat quantification and restoration to limit the pressure on populations. Although the value of accessible high-quality habitat

is understood, the combination of stream characteristics that affects habitat quality remains an area of active research. Measures of salmonid habitat quality are often linked to physical characteristics of rivers, such as depth and velocity (Bovee, 1982), substrate (Kondolf & Wolman, 1993), water-surface slope (Benjankar et al., 2016), morphology (Hanrahan, 2007), habitat patch size (Carnie et al., 2016) and connectivity between patches (Isaak et al., 2007). Although habitat quality is often characterized by local features such as depth, width, velocity, and cover, some studies have found those metrics to be of minor importance in habitat selection (Isaak et al., 2007). Complementary habitats have also been shown to be important, with studies finding a relation between the proximity of feeding, resting, and spawning areas to redd locations (Le Pichon et al., 2006; 2009), or higher juvenile densities in locations with shorter distances to spawning habitat (Flitcroft et al., 2012). These studies highlight a need to consider the value of a compilation of multiple, well-connected habitat types to overall measures of habitat quality. However, habitat quality is most often quantified through habitat suitability curves created through correlative statistics that connect variables such as depth, velocity, and substrate to observed habitat use (Bovee, 1982; Shirvell, 1989). Such metrics of habitat suitability have been criticized for assuming habitat use is an indicator of preference, while also sometimes only assessing a limited range of conditions present in rivers (Roloff & Kernohan, 1999). The development of habitat suitability curves also assumes that habitat preference is related to increased fitness across sometimes broad size ranges (Garshelis, 2000) and, based on these limitations, lacks clear ecological interpretation (Hayes et al., 2016).

Alternatively, process-based models that incorporate more biological criteria such as behavior-based individual-based modeling (Railsback, 2016), statistical growth models (Crozier et al., 2010), and energy profitability modeling through bioenergetics (e.g., foraging models, Jenkins & Keeley, 2010; Naman et al., 2020; Urabe et al., 2010) resolve some of these issues. Drift-feeding bioenergetics models are based on the assumption that invertebrate drift foraging fish select habitat to maximize energy gain and growth and are based on estimating net energy intake (NEI), or the balance between minimizing energy expenditure of factors such as metabolic and swimming costs, while maximizing energy gains from food intake. These models can account for spatial variations in food or drift, which is often considered a limiting factor for fish in rivers (Chapman, 1966; Poff & Huryn, 1998), and differences in drift can have large effects on NEI and growth predictions (Chipps & Wahl, 2008; Dodrill et al., 2016). Stream temperatures are included in bioenergetic modeling to account for temperature-driven variations in energy expenditures, food intake, and growth rates (Benjamin et al., 2012; Myrvold & Kennedy, 2018; Reeder et al., 2021). Habitat suitability defined by bioenergetics modeling better predicts fish growth and density than habitat suitability curves (Naman et al., 2019),

although more model validation linking habitat quality to fish use is needed (Hayes et al., 2016). Bioenergetics models can provide important information on the suitability of habitat by accounting for foraging, but do not account for density-dependent processes, such as juvenile growth and recruitment, that are included in more complex individual-based models (Harvey & Railsback, 2013).

Large-scale application of fish habitat models depend on accurate morphologic and hydraulic information to assess habitat at a scale relevant to fish (Escobar-Arias & Pasternack, 2010; Kammel et al., 2016). The models rely on coupled high-resolution bathymetric data and hydraulic modeling data. Consequently, access to large-scale high-resolution data often limits the scope of these models to the reach scale (Booker et al., 2004; Hayes et al., 2007). However, to understand the spatial dynamics of habitat quality for highly mobile animal populations such as salmon and trout, a continuous riverscape view of habitat is needed (Fausch et al., 2002). Recent advancements in remote sensing have increased access to broad-scale bathymetric topography (Dietrich, 2017; Tonina et al., 2019) that can be coupled with numerical flow modeling to allow for broader scale studies of habitat availability.

Analyzing the spatial distribution of habitat characteristics over tens of kilometers of river would advance our understanding of the interaction among habitat types, habitat quality, and how fish use the available habitat. This also allows for the quantification of the potential carrying capacity and identification of habitat bottlenecks that is especially important when evaluating human disturbances and addressing the potential outcomes of river restoration projects. Based on NEI values from bioenergetics modeling, carrying capacity estimates better predict fish densities than habitat suitability (Wall et al., 2016). Within the bioenergetic framework, habitat quality and fish carrying capacity depend on flow hydraulics, food availability, water temperature, fish size, and potential fish growth, whose effects have not been well constrained at the riverscape. Thus, our goal is to understand the role of stream water temperature, juvenile fish size, food availability, and fish behavior on carrying capacity. Following the works of Jenkins and Keeley (2010) and Carmichael et al., (2020), we propose a juvenile size-dependent definition of stream carrying capacity based on available net energy and the energy required for growth.

In this study, we develop two habitat models at the riverscape by coupling two-dimensional surface hydraulics either with a bioenergetic model or with an HSI-based model. We apply the models to quantify Chinook salmon (*Oncorhynchus tshawytscha*) juvenile carrying capacity and habitat quality throughout the entire 106 km-long Lemhi River in central Idaho, USA. In addition to a bioenergetic estimate of habitat quality we also apply estimates of space requirements for juvenile salmonids to

account for aggressive or territorial defense of space by rearing Chinook salmon. In doing so, we define an effective carrying capacity which is constrained by the territory size needed for fish of a given size (Grant & Kramer, 1990). We vary the inputs of drift concentration, temperature, and fish size to address their effects on carrying capcity throughout the study system. To build on our current understanding of habitat quality and the relations between spawning and juvenile habitat, we also examine the role of spawning and juvenile habitat quality on redd site selection.

Methods

Study Area

Our study focuses on a 106 km-long segment of the gravel-bedded Lemhi River, in east-central Idaho, USA, that drains a 3300 km^2 basin before flowing into the Salmon River (Figure 3.1). It has an average bankfull width of ~15 m and bed slopes ranging from 0.001 to 0.01 m/m. Like many rivers in the western United States, the Lemhi River has a history of human alterations, mainly through channel simplification, channelization, and floodplain narrowing from agriculture, roads, and other human infrastructure. Currently the first 52 km of the river, the upper section, generally meanders through agricultural and ranching lands and the lower section is more channelized with less sinuosity, less lateral connectivity, and fewer side channels. This basin provides important spawning and rearing habitat for culturally and ecologically important endangered fish species including Chinook salmon (NMFS, 2019).

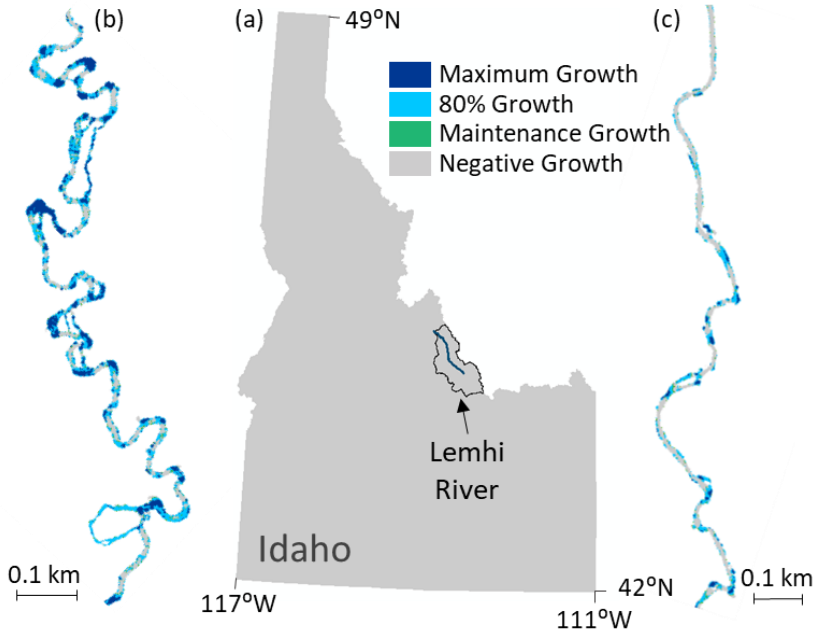

Figure 3.1: Site map (a) showing the location of the Lemhi River in central Idaho, USA. Examples of reaches from the (b) upper Lemhi River and (c) lower Lemhi River are also shown overlaid with the areas that have the potential to provide 100% and 80% of maximum ration, and 0% growth or maintenance ration for median-size juvenile Chinook salmon with average drift concentration, average August temperatures and fall base-flow conditions.

Topographic and Hydraulic Data

Airborne bathymetric LiDAR was collected at low flow, with high water clarity conditions along the Lemhi River in October 2013 (McKean et al., 2009) and a 1-m resolution digital elevation model (DEM) was produced, representing the channel bed and the surrounding floodplain and valley. Using the LiDAR DEM, a multi-reach, 1-m resolution, 2D hydraulic model was created in MIKE 21 for the whole mainstem Lemhi River (Tonina et al., 2020). The model was calibrated to reduce the error between modeled and measured water-surface elevations and flow velocities with a spatially constant roughness value (Manning's n = 0.025 $s/m^{1/3}$) and lateral eddy viscosity (0.15 m^2/s). Depths and flow velocities were calculated with the calibrated model for several different discharge scenarios. The 2D hydraulic model was split into eight reaches based on differences in discharges along the river due to discharge increases from tributary inputs and decrease from irrigation withdrawals. To represent the base-flow and fall spawning flows, we used modeled flow depths and velocities during August and September in 1 km reaches. (Figure 3.2).

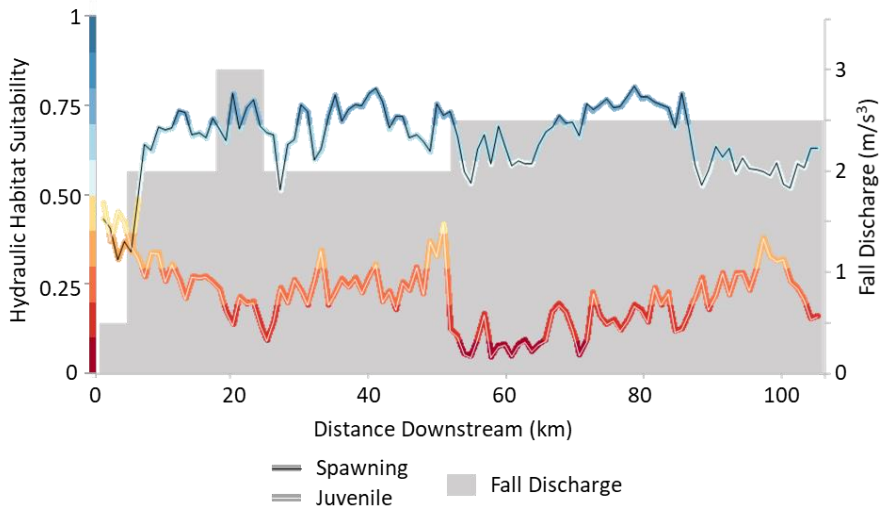

Figure 3.2: Chinook salmon spawning and juvenile hydraulic habitat suitability summarized in 1km reaches along the Lemhi River for a fall/ base-flow discharge scenario shown by the grey area.

Habitat Analysis: Suitability Indices

To quantify Chinook salmon spawning and juvenile rearing habitat along the Lemhi River, we calculated the suitability of each model cell using Chinook salmon habitat suitability curves for flow depth and velocity developed for the Upper Salmon Basin (Maret et al., 2005) (see Appendix C for curves). For spawning and juvenile life stages, the cell suitability index (CSI), based on the geometric mean of the depth and velocity suitability, was calculated for each 1-m model cell for the fall flows. For each 1 km reach of the river, we then calculated reach-based hydraulic habitat suitability (HHS) as

$$\text{HHS} = \frac{\sum_{i=1}^{n} A_i \cdot CSI_i}{\sum_{i=1}^{n} A_i} \qquad \text{Equation 3.1}$$

where A_i is the area of each cell (1 m^2) for each life stage.

Habitat Analysis: Bioenergetics Modeling

Juvenile habitat along the Lemhi River was also assessed through energy profitability using bioenergetics modeling. To determine energy profitability in terms of the net rate of energy intake (NREI), we used the BioenergeticHSC software to quantify the available energy for juvenile Chinook growth (Naman et al., 2020). The software calculates a cell-based NREI for drift-feeding juvenile fish independently from the adjacent cells, because the dimension of each cell is larger than the fish prey detection radius. The in-cell information, such as food abundance, water temperature, flow depth, and flow velocity fully characterize the feeding environment as homogenous for each feeding position. The drift-foraging bioenergetics model uses these stream conditions to calculate a cell-based NREI for drift feeding juvenile fish of different sizes. NREI is calculated based on the balance between

energy acquired from feeding and energy expended from swimming and maneuvering to capture prey and digesting it. For all model runs, we used a swimming cost model for Chinook salmon (Trudel & Welch, 2005) that accounted for fish size, nose velocity (at the cell scale), and temperature, as well as, increased energy expenditure of unsteady swimming through turbulence adjustment (Enders et al., 2003). We selected a constant energy assimilation of 0.7 to account for energy losses from digestive metabolic processes (Elliott, 1982). We selected a constant energy assimilation rate instead of a more complex model that varies with fish size, temperature, and consumption (Stewart & Lbarra, 1991). The complex models include a consumption cap based on maximum daily ration for single fish and we were interested in the total amount of energy available for multiple fish. For each run, we input the fork length and mass of the juvenile fish of interest, drift concentration data, and water temperature (see following sections for details). Using the batch processing function, we ran the model for depth and velocities for each 1 m^2 cell for the entire mainstem Lemhi River. We ran the model multiple times to assess the effects of fish size, drift concentration, and temperature.

For each cell, the model quantifies NREI in J/s. Therefore, to account for the energy intake of a fish over a day, we converted NREI to daily net energy intake, DNEI (J/day). By assuming that fish may forage for on average 8 hours a day, we calculated DNEI = NREI (J/s) •3600 (s/hr) • 8 (hr). We leveraged the empirically derived equations of Elliott (1976), modified by Jenkins and Keeley (2010), to approximate the energy needed to support 100% (maximum ration), 80%, and 0% (maintenance ration) growth through growth rations, GR (J/day):

$$GR = 0.58 \times 18.58 \times aM_{fish}{}^{b_1} e^{b_2 \times T} \qquad \text{Equation 3.2}$$

where 18.58 is a constant that converts mass to joules, 0.58 is the energy assimilation fraction (Elliott, 1976), M_{fish} is the fish mass (g), T is the stream water temperature (°C), and a, b_1, and b_2 are constants depending on growth ration (see Appendix C for constant values). The growth rations quantify the amount of energy needed to support juvenile fish growth for a fish of a given size, with maintenance growth ration representing the minimum energy needed to support a fish without growth and maximum growth ration representing the energy needed to provide the highest growth potential for a fish at a given temperature. Similar to Carmichael et al., (2020), we then calculated the available energy ratio (AE), defined as the ratio of DNEI to GR, to represent the energy available for each growth ration for each modeled cell. An AE = 1 represented a cell with enough energy to support 1 fish at that growth ration, while values <1 represented reduced growth potential, and values >1 provided more energy than needed by one fish at the specified growth ration.

We quantified carrying capacity for each 1 km reach by summing all AE values ≥1 in the reach and dividing by the reach area, resulting in a total carrying capacity (TCC) in fish/m^2. We also considered the territorial behavior of Chinook salmon and calculated an effective carrying capacity (ECC) by capping the number of individual fish a cell could support. The territorial area is a function of fish size; thus, a larger fish requires a larger stream area than smaller fish. We use the equation from Grant and Kramer (1990) to calculate space requirement based on territory size of juvenile salmon:

$$\log_{10} T_s = 2.61 \log_{10} F_l - 2.83, \quad \text{Equation 3.3}$$

where T_s is the territory size (m^2), and F_l is the fish fork length (cm).

In addition to estimating juvenile rearing capacity, we also estimated number of emergent fry, based on the average annual number of redds in the Lemhi River, we calculated the potential number of emergent fry and parr or pre-smolts we could expect annually in this stream. To quantify the number of theoretical juveniles, we multiplied the average number of redds/year/km by an estimated 5400 eggs (Quinn, 2018). We then multiplied by either an estimated egg-to-fry survival rate of 0.6 (McMichael et al., 2005; Roni et al., 2008) or an egg-to-parr/pre-smolt survival rate of 0.04 (Bradford, 1995; Reeder et al., 2021; Zimmerman et al., 2015). Our proposed ECC definition also allowed us to predict the maximum number of juvenile fish of a given size that the system can support at a specific growth ration and from that we can calculate the number of redds the system can support by back calculating the number of eggs and redds needed to produce the maximum number of juveniles. Comparing the number juveniles the current habitat can support to the number of theoretic juveniles present, allowed us to determine if the system is mainly limited by returning spawners or by available juvenile habitat.

Juvenile Fork Length and Mass

We used fish size data, the fork length (F_l) and mass (M_{fish}), for juvenile Chinook salmon throughout the Lemhi River summarized from the Integrated Status Effectiveness Monitoring Program (ISEMP) and originally gathered by Carmichael et al. (2020). These data, collected from rotary screw traps and electrofishing mark-recapture studies, were comprised of length and mass for juvenile parr and pre-smolts before overwintering and spring migration. From these data, a regression model (modified from Carmichael et al., 2020) was created to quantify the relation between fork length and mass,

$$\log_{10} M_{fish} = 3.18 \times \log_{10} F_l - 5.24\,, \quad \text{Equation 3.4}$$

where M_{fish}, is in grams, and F_l is in mm (see Appendix C). Based on the ISEMP data, we selected three fork lengths, which represent three stages for sub-yearling or potentially yearling Chinook

salmon: a fry of 40 mm length, an averaged parr of 75 mm length and a large parr or presmolt of 102 mm, for the bioenergetics model. The 75 mm and 102 mm sizes represent the 50th and 90th percentile of measured fork length, respectively. Each of these fork lengths were modeled with average drift concentration and average August temperatures along the Lemhi River.

Temperature

We obtained average August stream temperatures for 1 km reaches along the Lemhi River from the NorWeST database (Isaak et al., 2017). For the Lemhi River, the average August temperatures vary from 10.21 °C in the upper reaches of the Lemhi River to 16.58 °C at the confluence with the Salmon River. We used the bioenergetics model to calculate carrying capacity values based on four temperature scenarios: a variable scenario where temperature varied downstream based on the NorWeST data, and three constant scenarios, 10.21 °C, 13 °C, and 16.58 °C, representing the minimum average August temperature, an intermediate recommended temperature for Chinook salmon rearing (Richter & Kolmes, 2005), and the maximum average August temperature, respectively. Each temperature scenario was assessed with the average drift concentration for the median fork-length juvenile salmonid.

Drift Concentration

Food availability for juvenile salmon was quantified from drifting invertebrate count data collected from 12 sites on the Lemhi River by the Columbia Habitat Monitoring Program (CHaMP, 2014). A total of 18 samples were collected from 2011 to 2015 distributed along the entire length of the Lemhi River. Each sample consisted of counts and lengths of drifting invertebrates captured over two hours by two nets placed near the thalweg of the river along with the average measured flow velocity at the sample site. For each sample, we binned the invertebrate count data by lengths into 3 mm length bins and calculated the drift concentration (DC) within each bin as the number of invertebrates (N_p) divided by the volume of water. Water volume passing through the net was calculated by multiplying the area of the net opening (A_n) by the average flow velocity (v) and the sampling time (Δt), that the nets were filtering water during sampling ($DC=N_p/(A_n\, v\, \Delta t)$).

To test the effect that total drift concentration had on carrying capacity, we ran the model for multiple DC scenarios. We used the size class concentrations from the sample with the lowest total DC and highest total DC (based on the DC used in Carmichael et al., 2020), and an average of all samples (averaged for each invertebrate size class) (Table 3.1). Some studies show that drift concentration is related to flow velocity (Kennedy et al., 2014; Stark et al., 2002) and, based on the 18 samples, we found a negative relation between total DC (sum of all size classes within sample) and flow velocity

(Figure 3.3). There is scatter and uncertainty around this relation (R^2=0.49) but based on this general trend, we used the regression to calculate the total DC for six velocity ranges. We then calculated the drift concentration for each size-class bin based on the average proportion of drift in each bin (Table 3.1). Therefore, we ran a bioenergetics model where DC spatially varied with flow velocity within the range of discharges when drift was collected. The effects of the differences in drift concentration were modeled for the median juvenile fish size and average August temperature along the river.

Table 3.1: Drift Concentration (DC, number of prey/m^3) by prey class bins for four drift concentration scenarios (low, average, high, and variable by the velocity bins shown) used as inputs in the bioenergetics model.

Size Class	Low DC	Average DC	High DC	Variable DC					
				0-0.25	0.25-0.35	0.35-0.45	0.45-0.55	0.55-0.65	>0.65
0 to 3 mm	0.2421	0.6984	2.004	1.3896	1.2512	0.9743	0.6974	0.4206	0.2268
3 to 6 mm	0.1688	0.4918	0.9442	0.9786	0.8811	0.6861	0.4912	0.2962	0.1597
6 to 9 mm	0.0216	0.0513	0.0856	0.1022	0.0920	0.0716	0.0513	0.0309	0.0167
9 to 12 mm	0.0027	0.0089	0.0054	0.0177	0.0159	0.0124	0.0089	0.0053	0.0029
12 to 15 mm	0.0016	0.0011	0.0000	0.0023	0.0021	0.0016	0.0011	0.0007	0.0004

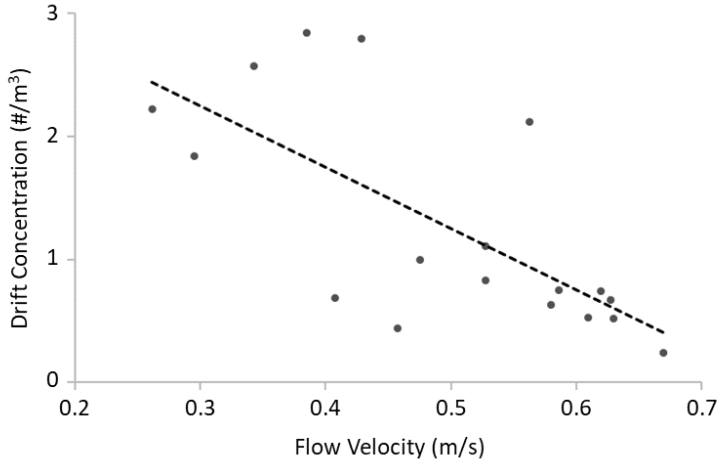

Figure 3.3: Total drift concentration compared to average velocity at the sample site, fit with a linear regression: drift concentration = -4.96 * velocity + 3.73, with an R^2 = 0.49 and p-value < 0.01.

Redd Analysis

Chinook salmon spawning sites or redd locations were compiled from ground and aerial surveys (collected by the United States Forest Service and Idaho Department of Fish and Game) between 1999 and 2018. The georeferenced coordinates of redd locations had large uncertainty, from few to tens of meters. Thus, redd locations with uncertainty less than 30 m were snapped to the closest

location along the channel centerline, and redd locations with larger global position errors were deleted, leaving 1959 viable redd locations.

To test if habitat suitability or estimated juvenile carrying capacity influenced redd locations, we compared the habitat metrics between redd locations and the same number of randomly selected locations along the river centerline. For spawning and juvenile HHS and 100% and 0% growth TCC and ECC for 40 mm juvenile fish (with average drift concentration and variable temperature), we calculated each habitat metric for 100 m reaches around each redd location (50 m upstream and 50 m downstream) and for 100 m reaches around randomly selected locations. This 100 m buffer (+/- 50 m) around each location accounted for the uncertainty in the original redd location along the river centerline. Distributions of each habitat metric were compared between the redd locations and random locations using a two-sample Kolmogorov–Smirnov nonparametric statistical test (α=0.05). We ran these tests for three sections of the river: the whole river, the upper 52 km section of the river, and the upper 23 km of the river to account for other variables leading to habitat avoidance (almost no redds were present below 52 km, thus other differences in the upstream and downstream areas (e.g., human influence, temperature) might affect the results). The high-quality juvenile habitat and the majority of the redds were above 23 km. Therefore, running this test in just this area allowed us to determine the strength of this spatial relation when the juvenile habitat is abundant.

Results

Hydraulic Habitat Suitability Modeling

Based on habitat suitability indexes for depth and velocity, Chinook salmon spawning habitat for fall flows was generally abundant throughout the Lemhi River (Figure 3.2). The spawning habitat quality in the uppermost 5 km was more limited, but the average reach-scale spawning suitability for the entire Lemhi River was still high (HHS = 0.65). The Lemhi River was more limited by availability and quality of juvenile habitat, with an average reach-scale fall juvenile HHS of 0.22 (Figure 3.2). The HHS values were based on the local hydraulics (depth and flow velocity), highlighting areas with non-suitable hydraulics for spawning and juvenile rearing.

Hydraulic Effects on Juvenile Habitat

The downstream trend of decreasing juvenile HSI was similar to that of the bioenergetics-based carrying capacity. Generally, juvenile carrying capacity was highest in the upper reaches of the Lemhi River, lowest in the middle reaches, and moderate in the lower section of the Lemhi River. For juvenile HHS and carrying capacity, the upper 50 km of the river had generally more suitable hydraulics than the lower reaches of the river, and the middle reaches from around 50 to 70 km were

very limited by the hydraulics, where the river was straightened and confined. Due to the limiting nature of inadequate hydraulics (specifically velocity) juvenile HSI and carrying capacity results show similar longitudinal trends, but the bioenergetics accounted for variables affecting the energy profitability of the stream for juvenile fish and therefore better constrained the habitat quality for juvenile salmonids.

Bioenergetics Modeling: Effects of Drift Concentration

The bioenergetic-based total carrying capacity, TCC, varied greatly depending on the amount of food available (Figure 3.4). The effect of drift concentration was largest in the upper Lemhi River, which had the highest potential habitat, and lowest in the reaches that had limited carrying capacity. When drift concentration was low, there was less variation in TCC throughout the river; for this case, drift became the limiting factor for juvenile growth and other variables controlling TCC (e.g., hydraulics and temperature) became less important. As drift values increased, TCC became more variable throughout the river, and no longer the limiting habitat factor, reflecting the importance of other variables controlling TCC.

When we accounted for space requirement based on territory size (density dependent behavior) of juvenile Chinook was considered, the effects of drift concentration decreased for 0% (maintenance ration) and 80% growth (80% of the maximum ration); the ECC for high, average, and variable drift concentration provided similar ECC values, closer to the low-drift concentration ECC. For many model cells, the TCC calculated from all drift densities were higher than the number of median-size juvenile fish that could be present based on territory size limits and capping the carrying capacity to the total number of fish based on territory size (e.g., 3.52 fish/m^2, for median-size fish, 75 mm) reduced the carrying capacity. Therefore, when accounting for territory size, if food availability was above the field-measured low, drift concentration did not limit the ECC for 0% and 80% growth rations. Maximum, 100%, growth TCC and ECC were more limited in the system in general and when drift concentration was low, 100% growth potential was essentially nonexistent throughout most of the Lemhi River. For all drift concentration scenarios, capping the 100% growth carrying capacity based on territory size did not greatly affect ECC because the TCC in most cells was lower than the maximum number of fish per cell. For the 75mm fish size class, a maintenance ration predicting 0% growth, the average difference, across the entire river, between the TCC for high and low drift concentration was 4.73 fish/m^2 and between the ECC was 0.66 fish/m^2; whereas for 100% growth, the average difference between the high and low drift concentration was 0.31 fish/m^2 for both

TCC and ECC. Increasing food availability would increase the 100% growth potential of juvenile salmonids until the TCC exceeds the territory size for Chinook salmon.

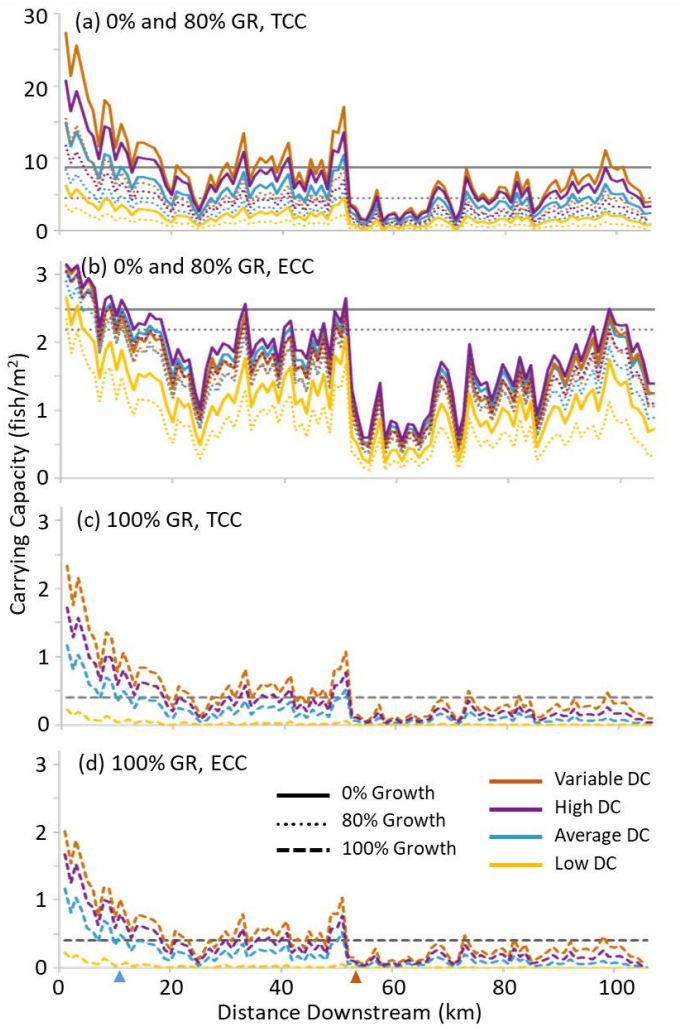

Figure 3.4: Carrying capacity for median-size fork length (75 mm) with variable average August temperature for four drift concentration (DC) scenarios: variable by velocity, high, average, and low drift. The carrying capacity by drift concentration are shown for (a) 0% and 80% growth rations for total carrying capacity, (b) 0% and 80% growth rations for effective carrying capacity accounting for territory size, (c) 100% growth for total carrying capacity, and (d) 100% growth effective carrying capacity. Each plot also shows, in grey lines, the average total and effective carrying capacity of a less impacted river, Bear Valley Creek, ID, U.S.A., for the different growth rations (see discussion for more details). Locations of example reaches 11 (blue) and 55 (orange) are shown on the x-axis (see Figure 3.8).

The low and high drift concentrations provided a general range of potential TCC and ECC when drift was held constant throughout the river. Spatial and temporal variability in food availability would affect the local carrying capacity. Therefore, we also tested the effect of the flow-dependent variable drift concentration, which in our case decreased with higher flow velocity, on carrying capacity. These carrying capacity results were similar to and higher than those for our high drift concentration. The amount of energy or food received by a feeding fish is a function of both DC and local *v*, such

that the drift flux is F_{DC}=DC *v*. Our variable drift concentration scenario showed DC decreases with velocity, which may penalize TCC in cells with high velocities, as those locations also require more energy to swim, while stream areas with low velocities may see similar F_{DC} as the higher velocity areas because the lower velocities are compensated by high DC.

Bioenergetics Modeling: Temperature Effects

Temperatures varied widely along the length of the Lemhi River, and the carrying capacity results from the multiple constant temperature runs demonstrated the importance of temperature on habitat (Figure 3.5). The average difference in TCC, for 75 mm fork length fish, between the minimum average August stream temperature and the maximum average August stream temperature was 3.42 fish/m^2 for 0% growth and 0.43 fish/m^2 for 100% growth. The 0% ECC values for all temperature scenarios were similar and the average difference in ECC between the average minimum temperature and maximum temperature was 0.23 fish/m^2, whereas for 100% growth the average difference in ECC was 0.42 fish/m^2. When space requirements limited carrying capacity, the 0% growth ECC was similar for all temperatures, whereas 100% and 80% growth habitat still varied throughout the Lemhi River because the TCC values were generally below the threshold for territory size. Hence, when accounting for fish behavior, temperature had less influence on the amount of 0% growth ECC, but still had large effects on the ECC of 100% and 80% growth potential. Overall, temperature effects were strongest in the upper reaches of the river where the habitat is currently generally good, and lowest in the middle reaches between 50 and 65 km downstream, where the habitat was poor because the river was more channelized and highly confined producing higher unsuitable velocities. The average August temperatures were variable throughout the river, and the general decrease in TCC moving downstream is due to the increase in stream temperatures moving downstream and changes in hydraulics.

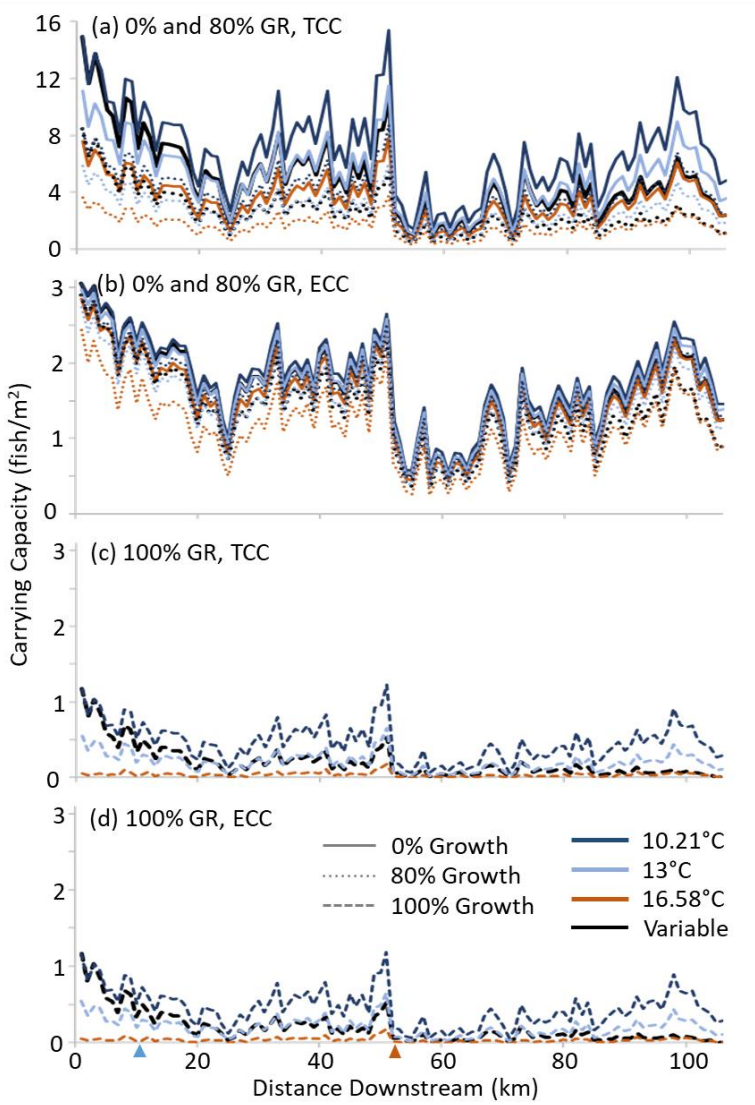

Figure 3.5: Carrying capacity for median size fork length (7.5cm) with average drift concentration for four temperature scenarios: variable temperature by 1 km reach, constant maximum average August temperature (16.58°), constant 13°, and constant minimum average August temperature (10.21°). The carrying capacity values for different temperature are shown for (a) 0% and 80% growth ration for total carrying capacity, (b) 0% and 80% growth ration for effective carrying capacity accounting for territory size, (c) 100% growth for total carrying capacity, and (d) 100% growth effective carrying capacity. Locations of example reaches 11 (blue) and 55 (orange) are shown on the x-axis (see Figure 3.8).

Bioenergetics Modeling: Juvenile Size Effects

For 0% and 80% growth potential, TCC was highest for the largest size-class juvenile and lowest for the smallest size-class because of increased swimming ability of larger fish at higher current velocities and the ability to consume larger drift sizes. However, when fish behavior was accounted for through territory size, this relation flipped and there was higher ECC for smaller than larger fish in the upper Lemhi River (Figure 3.6). As territory size is a function of body size, there is a larger decrease in effective carrying capacity for larger fish than for smaller fish. The average difference

between the 0% growth for 102 mm and 40 mm fork lengths was 6.26 fish/m^2 for TCC and -0.81 fish/m^2 for ECC. The uppermost reaches could support more small fish and fewer large fish when space requirements of each juvenile size were accounted for (Figure 3.6). This relation was only present in the upper Lemhi River where there was more abundant juvenile habitat and most of the lower Lemhi River had limited ECC for all fork lengths. For 40 mm fork lengths, 100% growth TCC and ECC were only non-zero in the upper Lemhi River, but habitat throughout the lower reaches of the Lemhi River would be available for 100% growth once the fish increased in size. For all fish sizes throughout the river, 100% growth ECC was similar to TCC because the cell based carrying capacity rarely exceeded the territory cap on carrying capacity. The average difference between 100% growth for 102 mm and 40 mm fork lengths was 0.41 fish/m^2 for TCC and 0.31 fish/m^2 for ECC.

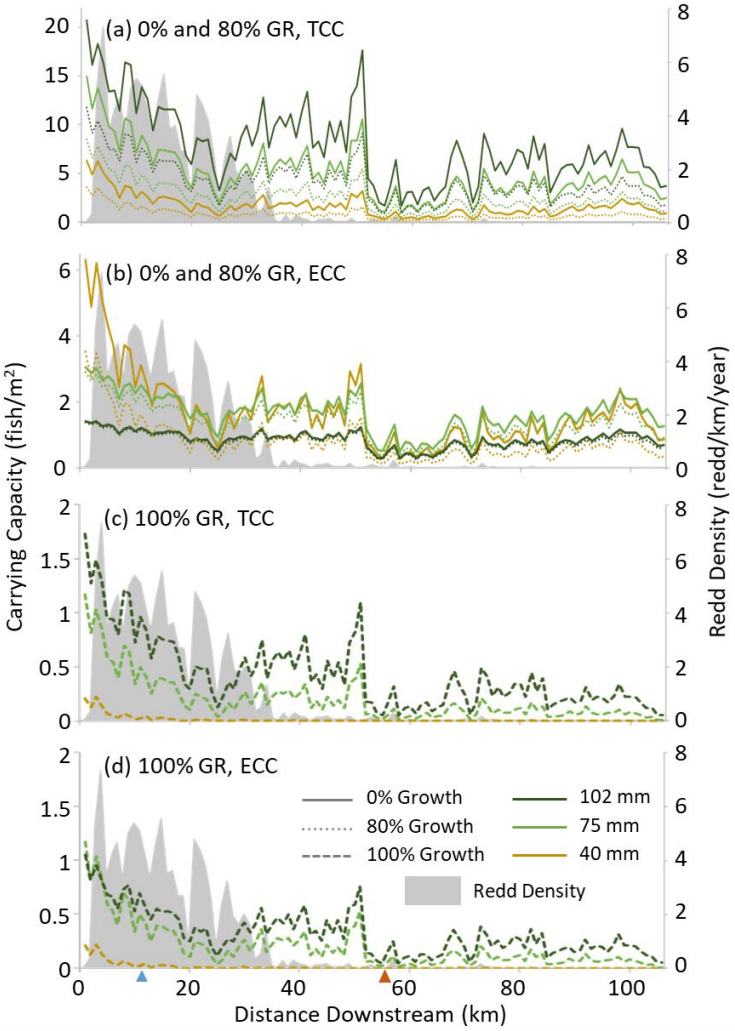

Figure 3.6: Estimated carrying capacity of juvenile Chinook salmon based on average drift concentration with variable average August temperature for three fish sizes: 40 mm, 75 mm, and 102 mm. The carrying capacities by fork length are

shown for (a) 0% and 80% growth for potential total carrying capacity (TCC), (b) 0% and 80% growth for effective carrying capacity (ECC) accounting for territory size, (c) 100% growth for total carrying capacity, and (d) 100% growth effective carrying capacity. Plots are also overlaid with average annual redd density by kilometer. Locations of example reaches 11 (blue) and 55 (orange) are shown on the x-axis (see Figure 3.8).

In the upper reaches of the Lemhi River, more potential area for growth for all fish sizes was available, and we also saw the highest densities of redds (Figure 3.6). Redds were clustered in the upper reaches with access to high growth potential habitat for emergent fry, as well as habitat for further life stages. All habitat downstream of the redds was available to fry, whereas habitat upstream of redds would not be accessible to small fish who cannot swim against current. This limited the access to the highest quality, 100% growth, habitat to the fry hatched within the first few kilometers of the river. Redds, and their subsequent fry, located downstream of this 40 mm fork-length 100% growth habitat, will only have access to habitat of 80% or lower growth potential.

To assess the availability of existing juvenile habitat, we compared the potential number of emergent fry and parr from the known redds to the cumulative effective carrying capacity in total fish/km (Figure 3.7). We found that the system can currently support the potential annual population of emergent fry (352,440 fry) at a growth ration of 80%, but not at 100% growth (could only support 10,570 fry), whereas the system could support the potential parr/pre-smolt population (23,496 parr/pre-smolt) at all growth rations throughout the river. The juvenile habitat with the highest growth potential is clustered in the upper Lemhi River, and the redds must also be located in these areas for emergent fry to have access to high quality habitat. The cumulative ECC lines with magnitudes higher than the potential fry and parr values (Figure 3.7 b and c) showed the prospective number of juvenile salmonids that the river could support, for example at 80% growth ration, the current river could support ~920,000 fry, ~1,650,000 parr or ~960,000 pre-smolts.

Bioenergetics Modeling: Reach Comparison

Carrying capacity varied along the length of the river, with the upper sections of the river having the highest overall TCC and ECC, a middle section with overall lowest TCC and ECC, and the lower reaches having moderate TCC and ECC values. By comparing two reaches, reach 11 and 55, along the river we addressed the differences in carrying capacity values (Figure 3.8). Reach 11, a natural upstream reach, had a sinuosity of 2.2, slope of 0.004 and average stream velocity of 0.44 m/s; whereas reach 55, in the middle confined and highly altered section, had a sinuosity of 1.1, slope of 0.008, and average stream velocity of 0.98 m/s. In all scenarios, reach 11 had higher 0% and 100% growth TCC and ECC values than reach 55. Reach 11 also had larger ranges of carrying capacity between 0% and 100% growth than reach 55, showing more space for potential moderate growth

habitat between these growth rates. Between the different drift concentration, temperature, and fork-length scenarios, reach 11 has larger variability in TCC and ECC than reach 55.

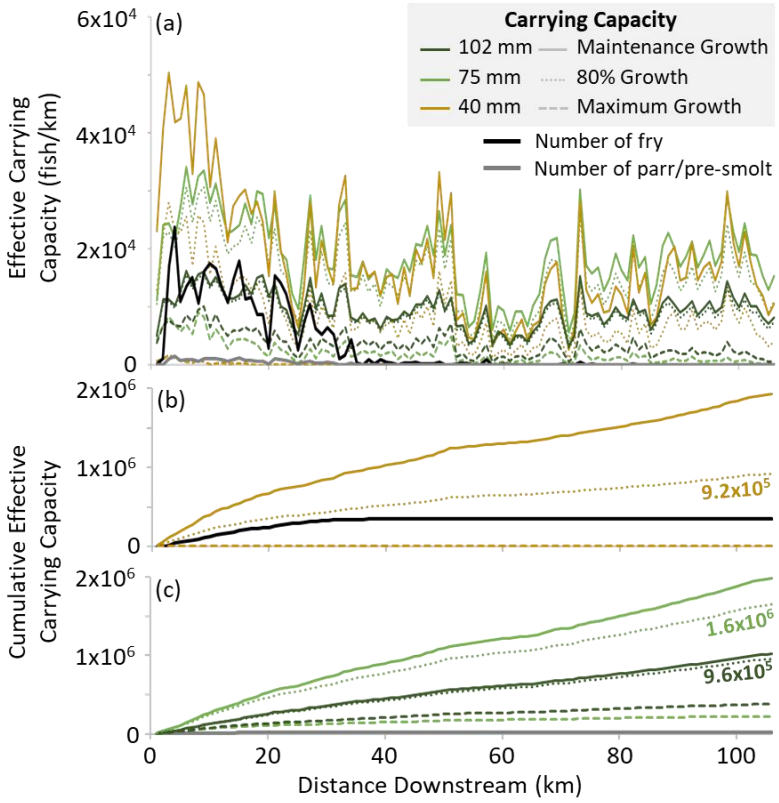

Figure 3.7: Effective carrying capacity per km for average drift concentration with variable average August temperature for three fork lengths: 40 mm, 75 mm, and 102 mm. The effective carrying capacity for each 1-km reach by fork length is shown for (a) 0%, 80%, and 100% growth, along with the annual potential number of fry and parr/pre-smolt calculated based on redd data. Cumulative effective carrying capacity downstream is shown for (b) 40 mm fork length juveniles with the potential number of fry (based on a 0.04 egg-to-fry survival rate) and (c) 75 mm and 102 mm juveniles with the potential number of parr or pre-smolts (based on a 0.60 egg-to-parr survival rate). The total effective cumulative carrying capacity values for 80% growth are shown on b and c.

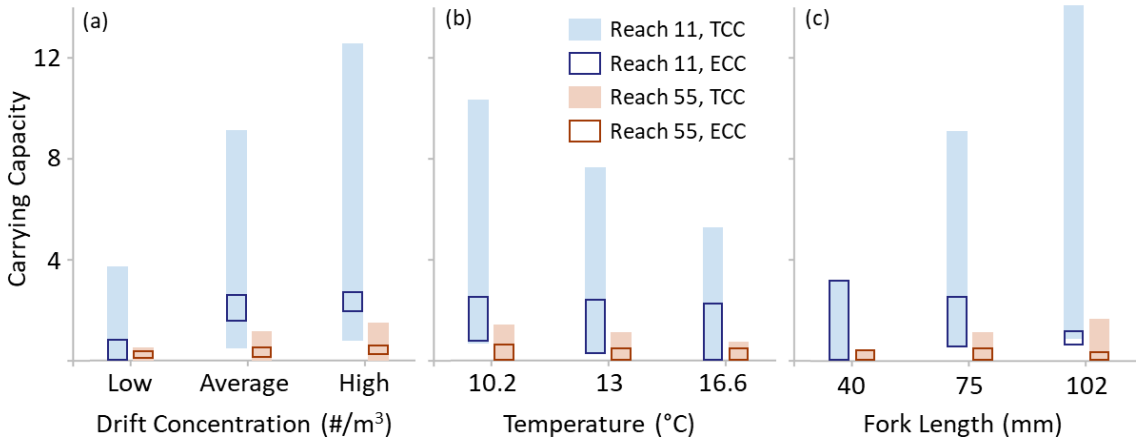

Figure 3.8: Comparison of total carrying capacity and effective carrying capacity for between the difference scenarios for (a) drift concentration, (b) temperature, and (c) fork length. Each bar represents the range of carrying capacity between the lower extent of the bar, corresponding to the 100% growth carrying capacity of the reach, and the upper extent of the bar, corresponding to the 0% growth carrying capacity of the reach.

Redd Site Selection

We found that at the 1-km reach scale, TCC and ECC for all fork lengths were related to redd density (Figure 3.9). The reaches with higher redd densities had higher TCC and ECC, but there were reaches with high carrying capacity with few to no redds. To better understand local redd site selection, we tested if redds were more likely than random site selection to be in locations of better spawning or juvenile habitat. We found that spawning HHS was not higher around redds than around random locations, but random locations had higher spawning HHS than did redd locations ($p<0.001$), suggesting that although high quality spawning habitat was necessary for redds, it was not sufficient for site selection. Areas around redds had higher juvenile HHS than did random locations ($p<0.001$). We also tested if redds were more likely than random site selection to be in locations of higher juvenile TCC and ECC for the life stage directly after gravel emergence from around the redds. For the 40 mm fork length, the first drift-feeding life-stage, we found that redds were more likely than random site selection to be in locations of higher 0% and 100% TCC and ECC ($p<0.001$). The relations between redd location and juvenile HHS, TCC, and ECC held true for tests of the entire Lemhi River, the upper 52 km, and just the upper 23 km, which were tested to account for potential issues of spawning avoidance in the lower sections of the Lemhi River. These results indicated that spawning Chinook salmon were possibly selecting redd locations based on juvenile habitat characteristics, even if better spawning habitat quality was available.

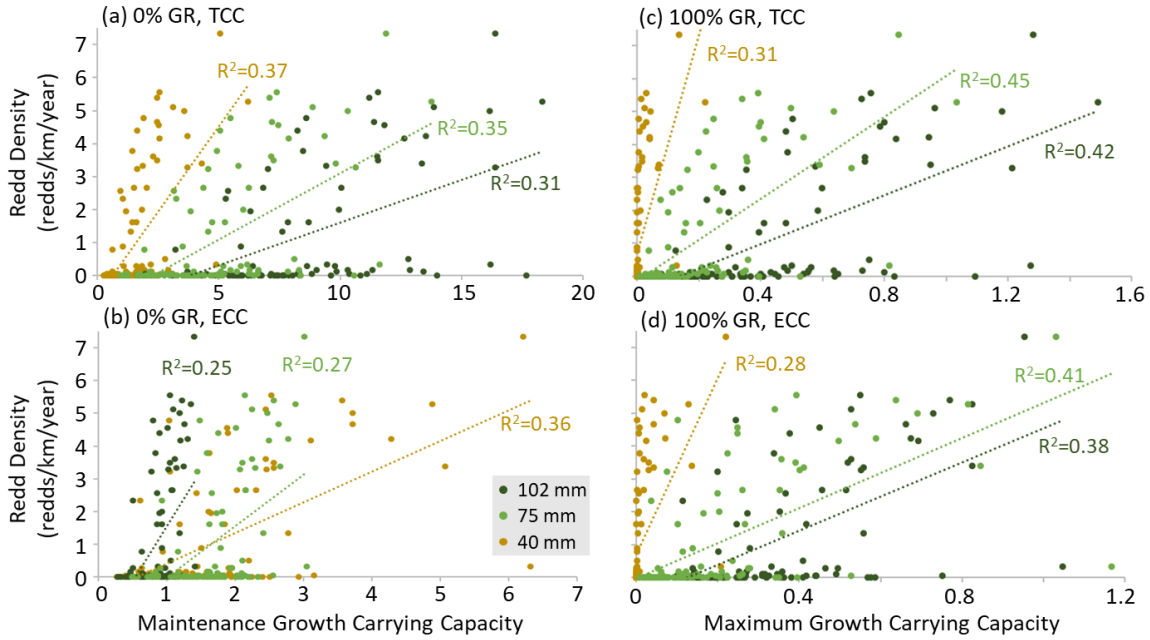

Figure 3.9: Correlations between redd density and carrying capacity for each juvenile fork length (40 mm, 75 mm, and 102 mm) for (a) 0% growth total carrying capacity, (b) 0% growth effective carrying capacity, (c) 100% growth total carrying capacity, and (d) 100% growth effective carrying capacity. Each plot is shown with linear fits and R^2 values, all correlations have p-values <0.01.

Discussion/Conclusions

Large-scale habitat modeling provided an important holistic view of the riverscape (Fausch et al., 2002). The entire length of the Lemhi River accommodated a variety of existing conditions and human impacts, from limited human impact reaches, to highly regulated and altered reaches. Based on our HSI and bioenergetics models, we found that the upper Lemhi River, with little human alteration (e.g., example reach 11, figure 3.8), had more juvenile habitat overall and more energy-profitable habitat than in the rest of the river, resulting in higher carrying capacity estimates, especially for 100% growth potential. In these reaches, altering food and temperature changed the ranges of TCC and ECC, showing potential in these areas to improve of loss habitat based on these characteristics. Whereas, the middle reaches of the Lemhi River, where the river was channelized and confined (e.g., reach 55, figure 3.8), the juvenile habitat was limited by the local hydraulics for all fork lengths and was not largely altered by changing food and temperature. This result agreed with other studies showing the limited potential for improved habitat for highly altered and confined reaches (Groll, 2017; Wohl et al., 2015; Yarnell et al., 2015). To understand how the existing conditions in the Lemhi River compare to a less altered, more pristine river, we compared the carrying capacity results to Bear Valley Creek, also in the upper Salmon River watershed. We calculated Bear Valley Creek carrying capacity for median length juvenile fish (75 mm, based on

Lemhi River data), August flows (depths and velocities from a 2D hydraulic model, see Appendix C for more information) and stream temperatures (from NorWeST, Isaak et al., 2017), but with average Lemhi River drift concentration data. We compared the Lemhi River TCC and ECC values to average TCC and ECC values for 13 km of Bear Valley Creek because carrying capacity values along Bear Valley Creek did not greatly vary. We found parts of the upper Lemhi River had similar TCC and ECC as Bear Valley Creek (Figure 3.4), but some upper reaches and the entire lower Lemhi River had lower TCC and ECC than in Bear Valley Creek, highlighting the effects of human alteration on the carrying capacity of the river for juvenile salmonids. The differences in TCC and ECC between the rivers reflect the differences in the hydraulics and temperatures, but not the drift concentrations, if accounted for, there could be larger differences assuming there is more food availability in the more natural river.

The four drift concentration scenarios we used to model food availability were within the range of values in the literature (Keeley et al., 2016; Leung et al., 2009; Macneale et al., 2010). Many energy-based juvenile growth models use spatially uniform drift densities (e.g., Booker et al., 2004; Carmichael et al., 2020), specifically focused on the central tendency of the data. However for ecology studies, using the most limiting estimate of a variable to calculate carrying capacity is suggested (Lancaster & Belyea, 2006). Drift also varies spatially and temporally (Hayes et al., 2007; Piccolo et al., 2014; Stark et al., 2002) and can be very difficult to constrain without more complex invertebrate drift models (e.g., Anderson et al., 2013), thus we opted to model a range of potential carrying capacities based on a range of food availabilities. For simplicity many of our results are shown for average drift but considering how those results could be negatively affected by limiting the food availability is important. If drift concentration was low throughout the river, the estimates of 0% and 80% TCC and ECC for all fork lengths would be reduced and the variability of carrying capacity throughout the river would be lower as we showed with the 75 mm fork length (Figure 3.4). Low drift concentration could also result in essentially no 100% growth potential for all fork lengths because DC was already very limited.

Using correct estimates of drift concentration is critical because they greatly affect carrying capacity estimates (Dodrill et al., 2016; Piccolo et al., 2014). However, we found that when carrying capacity was capped by territory size, increasing drift does not result in higher carrying capacity, but when drift was low ECC was negatively affected. This agreed with Jenkins & Keeley (2010), who found food reduction significantly reduced juvenile salmonid habitat quality, while food abundance did not have a strong effect on juvenile habitat quality. Studies have shown that drift concentration is not only

a function of benthic invertebrate density, but also depends on velocity and discharge (Gibbins et al., 2010; Kennedy et al., 2014). Based on the available drift concentration for the Lemhi River, we found that drift concentration decreased with increasing velocity. Many studies have found that drift concentration increased with increasing velocities (Gibbins et al., 2010; Hayes et al., 2016) and with rapid changes in the discharge that dislodge invertebrate from the substrate (Corrarino & Brusven, 1983; Poff & Ward, 1991), but discrepancy and variability around velocity effects on drift still exists, with some studies finding no relation (Leung et al., 2009). When modeling the effect of hydrodynamics on drift and accounting for dispersal and population dynamics of invertebrates, drift was shown to be inversely related to spatial differences in flow velocity (Anderson et al., 2013). Using a series of potential uniform drift concentration values provided a useful range of potential carrying capacities, but better constraints on the effects of velocity on drift concentration are still needed.

Temperature is an important aspect of salmonid habitat quality at all life stages, with each life stage having its own individual temperature needs (Richter & Kolmes, 2005). This is particularly important for juvenile salmonids, where higher temperatures can provide high growth rates (Connor & Burge, 2003; Reeder et al., 2021), but this effect is density dependent and, at higher fish densities, there is a negative relation between temperature and growth (Crozier et al., 2010). We found that juvenile carrying capacity was adversely impacted by increased temperature. The BioenergeticHSC software calculates NEI at instantaneous timescales, and although temperature is accounted for in variables such as swimming cost and in energy assimilation with the Wisconsin-model option, the effect of temperature on NEI is limited. Most of the variation in carrying capacity with temperature in our model is from the calculation of growth rations to estimate the energy needed to support different growth potential. The growth rations we used in out model were positively correlated with temperature to account for the increased consumption at higher temperatures (Myrick & Cech, 2000), resulting in less energy available for multiple fish at higher temperatures, but potentially greater growth for individuals (Reeder et al., 2021). If the density of juveniles was less than our reported ECC, there would be more potential for higher growth rations at higher temperatures, but as the juvenile density approached the ECC, temperature may play negative role (Crozier et al., 2010), which could greatly limit juvenile habitat.

Climate change is increasing stream temperatures (Isaak et al., 2018) and changing the hydrology (Luce et al., 2013; Mantua et al., 2010) in Pacific Northwest rivers, which emphasizes the importance of modeling the habitat impacts of temperature. Our models showed that increasing temperature in the

currently cooler reaches of the Lemhi River could greatly decrease the available habitat for 100% growth potential. This, coupled with potential decreased juvenile survival from hydraulic changes due to climate change (Walters et al., 2013), could potentially result in a large decrease in carrying capacity for all fork lengths. However, our model also highlighted the opportunities to improve habitat through temperature alteration. Specifically, for 100% growth potential, areas along the Lemhi River with large differences between the minimum and maximum temperature models represented reaches where temperature had the greatest effects. Therefore, while the potential to lose carrying capacity is large in the upper reaches of the Lemhi River, the potential to increase carrying capacity in the lower reaches of the river through temperature reduction measures such as riparian plantings (Justice et al. 2017) was also large.

For all juvenile life stages, as represented by fork lengths, 80% and 100% growth habitat is critical to ensure long-term success. Fish size affects competitive habitat selection (Fausch, 1984), migration timing (Beckman et al., 1998), overall survival (Ebersole et al., 2006), and fecundity (Healey & Heard, 1984). Based on the potential number of annual juvenile fish in the Lemhi River calculated from the redds, there was enough 80% growth habitat to support all the fry and parr/pre-smolts, but not enough 100% growth habitat to support all fry. Based on the cumulative ECC for 40 mm fork length juveniles, we back calculated (carrying capacity as number of juvenile fish, converted to number of eggs needed to be laid based on egg-fry survival rates, converted to the number of redds need to lay the eggs) to that the river could support only the juveniles produced by 3.3 redds annually at 100% growth, but up to 4,260 annual redds at 80% growth ration of fry compared to current average of ~109 redds per year in the Lemhi River. For the 102 mm fork length, the river could support 100% growth of parr/pre-smolts from 1,746 redds annually and 4,440 redds at 80% growth. As with all our carrying capacity estimates, these values only account for one size class at a time, therefore the total carrying capacity estimates for the river would be smaller when all size classes were accounted for at once because much of the suitable habitat overlaps. The smaller fry would actually be most common in the spring and early summer rather than the base flows we assessed. The higher spring and summer flows may limit the fry habitat more than we show because of their reliance on low velocities.

Studies have shown that because of the density dependence of salmonids, attempts to increase populations through stocking may not be productive (Ayllón et al., 2012); consequently, instead of focusing on creating very productive habitat in a few reaches, increasing access to more suitable habitat along an entire river would be more successful. This was highlighted by our comparisons

between TCC and ECC for each model, showing that altering different variables may not increase carrying capacity when accounting for the territorial nature of salmonids. The results of this study were for fall flow conditions, which is important for spawning fish and juveniles, but juvenile carrying capacity results will vary based on the flows discharge. Studies have found that higher stream discharges resulted in lower juvenile productivity (Neuswanger et al., 2015) and a reduction in suitable habitat (Carmichael et al., 2020); thus, the juvenile carrying capacity results we presented may be lower in periods of higher flows, such as in spring and early summer, unless lateral habitats are available with slow and deep flows.

We found suitable fall spawning habitat throughout entire Lemhi River and redds were not more likely than randomly chosen locations to be in areas with higher spawning HHS. This suggested that redd site selection was dependent on other factors besides spawning habitat suitability. Redds were more likely than randomly selected locations to be in areas of higher juvenile HHS and higher TCC and ECC based on the bioenergetics. This interesting result suggested that there were feedbacks among life stages. Success of juvenile salmonids depends on the success and growth of early juvenile stages, but also the selection of spawning locations may depend on the habitat quality and potential success and growth of juveniles.

Bioenergetics modeling of juvenile habitat improved upon HSI modeling by providing information on the processes and variables (changes in drift concentration, temperature, and juvenile life stage) affecting habitat and, therefore, provides practitioners information on the limits and opportunities to enhance juvenile habitat. Large-scale HSI and bioenergetic modeling of habitat provided a riverscape view of juvenile habitat and could help better constrain the limiting processes along the entire length of a river. Similar to HSI modeling, large-scale bioenergetic modeling could also provide micro- and meso-scale patch-based habitat information by mapping areas of different growth potential (Figure 3.1). Through bioenergetic modeling, we highlighted how changing temperature, drift concentration, and juvenile life stage affected the TCC and ECC throughout the Lemhi River. Changes to one of these variables could negatively affect carrying capacity regardless of the other variables, expect where flow hydraulics was limiting carrying capacity. Reducing food availability or increasing temperature could reduce the carrying capacity for all life stages and reduce the variability in carrying capacity throughout the river, subsequently reducing the opportunities for juveniles to find high-quality habitat in other reaches. Although, due to fish behavior limiting carrying capacity, increasing drift concentration or decreasing temperature did not have a positive effect on 0% and 80% growth habitat, but still could positively impact availability of 100% growth habitat. Riverscape-based

bioenergetics modeling could provide another layer of information for managers to assess habitat for multiple life stages under a variety of different conditions and allow for improved decision making to ensure the success of salmonids.

References

Allen, R. G. C., & Robison, C. W. (2017). Evapotranspiration and consumptive irrigation water requirements for Idaho: Supplement updating the time series through December 2016. *Research Technical Completion Report, Kimberly Research and Extension Center, University of Idaho, Moscow, ID*.

An, C., Hassan, M. A., Ferrer-Boix, C., & Fu, X. (2021). Effect of stress history on sediment transport and channel adjustment in graded gravel-bed rivers. *Earth Surface Dynamics*, *9*(2), 333–350. https://doi.org/10.5194/ESURF-9-333-2021

Anderson, K. E., Harrison, L. R., Nisbet, R. M., & Kolpas, A. (2013). Modeling the influence of flow on invertebrate drift across spatial scales using a 2D hydraulic model and a 1D population model. *Ecological Modelling*, *265*, 207–220. https://doi.org/10.1016/J.ECOLMODEL.2013.06.011

Andrews, E. D. (1994). Marginal bed load transport in a gravel bed stream, Sagehen Creek, California. *Water Resources Research*, *30*(7), 2241–2250. https://doi.org/10.1029/94WR00553

Ayllón, D., Almodóvar, A., Nicola, G. G., Parra, I., & Elvira, B. (2012). Modelling carrying capacity dynamics for the conservation and management of territorial salmonids. *Fisheries Research*, *134*, 95–103. https://doi.org/10.1016/J.FISHRES.2012.08.004

Bartley, R., & Rutherfurd, I. (2005). Measuring the reach-scale geomorphic diversity of streams: application to a stream disturbed by a sediment slug. *River Research and Applications*, *21*(1), 39–59. https://doi.org/10.1002/rra.813

Beckman, B. R., Larsen, D. A., Lee-Pawlak, B., & Dickhoff, W. W. (1998). Relation of fish size and growth rate to migration of spring Chinook salmon smolts. *North American Journal of Fisheries Management*, *18*, 537–546. https://doi.org/10.1577/1548-8675(1998)018<0537:ROFSAG>2.0.CO;2

Beechie, T., Pess, G., Roni, P., & Giannico, G. (2008). Setting river restoration priorities: a review of approaches and a general protocol for identifying and prioritizing actions. *North American Journal of Fisheries Management*, *28*(3), 891–905. https://doi.org/10.1577/m06-174.1

Benjamin, J. R., Connolly, P. J., Romine, J. G., & Perry, R. W. (2012). Potential effects of changes in temperature and food resources on life history trajectories of juvenile Oncorhynchus mykiss.

Transactions of the American Fisheries Society, *142*(1), 208–220. https://doi.org/10.1080/00028487.2012.728162

Benjankar, R., Tonina, D., Marzadri, A., McKean, J., & Isaak, D. (2016). Effects of habitat quality and ambient hyporheic flows on salmon spawning site selection. *Journal of Geophysical Research: Biogeosciences*, *121*(5), 1222–1235. https://doi.org/10.1002/2015JG003079

Bennett, J. P. (1995). Algorithm for resistance to flow and transport in sand-bed channels. *Journal of Hydraulic Engineering*, *121*(8), 578–590. https://doi.org/10.1061/(asce)0733-9429(1995)121:8(578)

Bjornn, T. C., & Reiser, D. W. (1991). Habitat requirements of Salmonids in streams. *American Fisheries Society Special Publication*, *19*(837).

Booker, D. J., Dunbar, M., & Ibbotson, A. (2004). Predicting juvenile salmonid drift-feeding habitat quality using a three-dimensional hydraulic-bioenergetic model. *Ecological Modelling*, *177*, 157–177.

Bouwes, N., Moberg, J., Weber, N., Bouwes, B., Beasley, C., Bennett, S., et al. (2011). Scientific protocol for salmonid habitat surveys within the Columbia Habitat Monitoring Program. *Prepared by the Integrated Status and Effectiveness Monitoring Program and Published by Terraqua, Inc., Wauconda, Washington.*

Bovee, K. (1982). A guide to stream habitat analysis using the instream flow incremental methodology. *Western Energy and Land Use Team, Office of Biological Services, Fish and Wildlife Service, US Department of the Interior*.

Bovee, K. D., Lamb, B. L., Bartholow, J. M., Stalnaker, C. B., & Taylor, J. (1998). *Stream habitat analysis using the instream flow incremental methodology*. *Biological Resources Division Information and Technology Report, USGS*.

Bradford, M. J. (1995). Comparative review of Pacific salmon survival rates. *Canadian Journal of Fisheries and Aquatic Sciences*, *52*(6), 1327–1338. https://doi.org/10.1139/F95-129

Bradshaw, G. A., & Spies, T. A. (1992). Characterizing canopy gap structure in forests using wavelet analysis. *The Journal of Ecology*, *80*(2), 205. https://doi.org/10.2307/2261007

Brandt, S. A. (2000). Classification of geomorphological effects downstream of dams. *CATENA*, *40*(4), 375–401. https://doi.org/10.1016/S0341-8162(00)00093-X

Brierley, G. J., & Fryirs, K. (2000). River styles, a geomorphic approach to catchment characterization: Implications for river rehabilitation in Bega Catchment, New South Wales, Australia. *Environmental Management*, *25*(6), 661–679. https://doi.org/10.1007/s002670010052

Brooks, A. P., Howell, T., Abbe, T. B., & Arthington, A. H. (2006). Confronting hysteresis: Wood based river rehabilitation in highly altered riverine landscapes of south-eastern Australia. *Geomorphology*, *79*(3–4), 395–422. https://doi.org/10.1016/j.geomorph.2006.06.035

Brown, R. A., & Pasternack, G. B. (2014). Hydrologic and topographic variability modulate channel change in mountain rivers. *Journal of Hydrology*, (510), 551–564.

Brown, R. S., Hubert, W. A., & Daly, S. F. (2011). A primer on winter, ice, and fish: What fisheries biologists should know about winter ice processes and stream-dwelling fish. *Fisheries*, *36*(1), 8–26. https://doi.org/10.1577/03632415.2011.10389052

Buffington, J. M., Lisle, T. E., Woodsmith, R. D., & Hilton, S. (2002). Controls on the size and occurrence of pools in coarse-grained forest rivers. *River Research and Applications*, *18*(6), 507–531. https://doi.org/10.1002/rra.693

Bunn, S. E., & Arthington, A. H. (2002). Basic principles and ecological consequences of altered flow regimes for aquatic biodiversity 1. *Environmental Management*, *30*(4), 492–507. https://doi.org/10.1007/s00267-002-2737-0

Carling, P. A., & Orr, H. G. (2000). Morphology of riffle-pool sequences in the River Severn, England. *Earth Surface Processes and Landforms*, *25*(4), 369–384. https://doi.org/10.1002/(SICI)1096-9837(200004)25:4<369::AID-ESP60>3.0.CO;2-M

Carmichael, R. A., Tonina, D., Keeley, E. R., Benjankar, R. M., & See, K. E. (2020). Some like it slow: A bioenergetic evaluation of habitat quality for juvenile chinook salmon in the Lemhi River, Idaho. *Canadian Journal of Fisheries and Aquatic Sciences*, *77*(7), 1221–1232. https://doi.org/10.1139/cjfas-2019-0136

Carnie, R., Tonina, D., McKean, J. A., & Isaak, D. (2016). Habitat connectivity as a metric for aquatic microhabitat quality: application to Chinook salmon spawning habitat. *Ecohydrology*, *9*(6), 982–994. https://doi.org/10.1002/ECO.1696

CHaMP. (2014). Scientific protocol for salmonid habitat surveys within the Columbia Habitat Monitoring Program. *Prepared by the Integrated Status and Effectiveness Monitoring Program*

and Published by Terraqua, Inc., Wauconda, Wash.

Chapman, D. W. (1966). Food and space as regulators of salmonid populations in streams. *The American Naturalist*, *100*(913), 345–357.

Chipps, S. R., & Wahl, D. H. (2008). Bioenergetics modeling in the 21st century: Reviewing new insights and revisiting old constraints. *Transactions of the American Fisheries Society*, *137*(1), 298–313. https://doi.org/10.1577/T05-236.1

Church, M. (1995). Geomorphic response to river flow regulation: Case studies and time-scales. *Regulated Rivers: Research & Management*, *11*(1), 3–22. https://doi.org/10.1002/rrr.3450110103

Colombini, M., Seminara, G., & Tubino, M. (1987). Finite-amplitude alternate bars. *Journal of Fluid Mechanics*, *181*, 213–232. https://doi.org/10.1017/S0022112087002064

Connor, W. P., & Burge, H. L. (2003). Growth of wild subyearling fall Chinook salmon in the Snake River. *North American Journal of Fisheries Management*, *23*, 594–599. https://doi.org/10.1577/1548-8675

Copeland, T., Venditti, D. A., & Barnett, B. R. (2014). The importance of juvenile migration tactics to adult recruitment in stream-type Chinook salmon populations. *Transactions of the American Fisheries Society*, *143*(6), 1460–1475. https://doi.org/10.1080/00028487.2014.949011

Corrarino, C. A., & Brusven, M. A. (1983). The effects of reduced stream discharge on insect drift and stranding of near shore insects. *Freshwater Invertebrate Biology*, *2*(2), 88–98. https://doi.org/10.2307/1467113

Cram, J. M., Torgersen, C. E., Klett, R. S., Pess, G. R., May, D., Pearsons, T. N., & Dittman, A. H. (2017). Spatial variability of Chinook salmon spawning distribution and habitat preferences. *Transactions of the American Fisheries Society*, *146*(2), 206–221. https://doi.org/10.1080/00028487.2016.1254112

Crozier, L. G., Zabel, R. W., Hockersmith, E. E., & Achord, S. (2010). Interacting effects of density and temperature on body size in multiple populations of Chinook salmon. *Journal of Animal Ecology*, *79*(2), 342–349. https://doi.org/10.1111/J.1365-2656.2009.01641.X

Csillag, F., & Kabos, S. (2002). Wavelets, boundaries, and the spatial analysis of landscape pattern. *Ecoscience*, *9*(2), 177–190. https://doi.org/10.1080/11956860.2002.11682704

DHI. (2003). Evaluation of diversion operations plans to meet negotiated flow targets for salmon and steelhead in the Lemhi River basin using the MIKE BASIN model. *Prepared for U.S. Bureau of Reclamation and Idaho Department of Water Resource by DHI Water and Environment, Inc.*, 41.

DHI. (2006). The Lemhi River MIKE BASIN model: A tool for evaluating stream flows, diversion operations and surface water – ground water relationships in the Lemhi River. *DHI Water and Environment, Inc. Report Prepared for Idaho Department of Water Resources*, 32.

Dietrich, J. T. (2017). Bathymetric structure-from-motion: extracting shallow stream bathymetry from multi-view stereo photogrammetry. *Earth Surface Processes and Landforms*, *42*(2), 355–364. https://doi.org/10.1002/esp.4060

Dodrill, M. J., Yackulic, C. B., Kennedy, T. A., & Hayes, J. W. (2016). Prey size and availability limits maximum size of rainbow trout in a large tailwater: insights from a drift-foraging bioenergetics model. *Canadian Journal of Fisheries and Aquatic Sciences*, *73*(5), 759–772. https://doi.org/10.1139/CJFAS-2015-0268

Duffin, J., Carmichael, R. A., Yager, E. M., Benjankar, R., & Tonina, D. (2021). Detecting multi-scale riverine topographic variability and its influence on Chinook salmon habitat selection. *Earth Surface Processes and Landforms*. https://doi.org/10.1002/esp.5077

Durafour, M., Jarno, A., Bot, S. Le, Lafite, R., & Marin, F. (2014). Bedload transport for heterogeneous sediments. *Environmental Fluid Mechanics 2014 15:4*, *15*(4), 731–751. https://doi.org/10.1007/S10652-014-9380-1

Ebersole, J. L., Wigington, P. J., Baker, J. P., Cairns, M. A., Church, M. R., Hansen, B. P., et al. (2006). Juvenile coho salmon growth and survival across stream network seasonal habitats. *Transactions of the American Fisheries Society*, *135*, 1681–1697. https://doi.org/10.1577/T05-144.1

Elliott, J. M. (1976). The energetics of feeding, metabolism and growth of brown trout (Salmo trutta L.) in relation to body weight, water temperature and ration size. *The Journal of Animal Ecology*, *45*(3), 923. https://doi.org/10.2307/3590

Elliott, J. M. (1982). The effects of temperature and ration size on the growth and energetics of salmonids in captivity. *Comparative Biochemistry and Physiology Part B: Comparative Biochemistry*, *73*(1), 81–91. https://doi.org/10.1016/0305-0491(82)90202-4

Enders, E. C., Boisclair, D., & Roy, A. G. (2003). The effect of turbulence on the cost of swimming for juvenile Atlantic salmon (Salmo salar). *Canadian Journal of Fisheries and Aquatic Sciences*, *60*(9), 1149–1160. https://doi.org/10.1139/F03-101

Escobar-Arias, M. I., & Pasternack, G. B. (2010). A hydrogeomorphic dynamics approach to assess in-stream ecological functionality using the functional flows model, part 1-model characterstics. *River Research and Applications*, *26*, 1103–1128.

Fausch, K. D. (1984). Profitable stream positions for salmonids: relating specific growth rate to net energy gain. *Canadian Journal of Zoology*, *62*, 441–451.

Fausch, K. D., Torgersen, C. E., Baxter, C. V., & Li, H. W. (2002). Landscapes to riverscapes: bridging the gap between research and conservation of stream fishes. *BioScience*, *52*(6), 483–498. https://doi.org/10.1641/0006-3568

Favrot, S. D., Jonasson, B. C., & Peterson, J. T. (2018). Fall and winter microhabitat use and suitability for spring Chinook salmon parr in a U.S. Pacific northwest river. *Transactions of the American Fisheries Society*, *147*(1), 151–170. https://doi.org/10.1002/tafs.10011

Flitcroft, R. L., Burnett, K. M., Reeves, G. H., & Ganio, L. M. (2012). Do network relationships matter? Comparing network and instream habitat variables to explain densities of juvenile coho salmon (Oncorhynchus kisutch) in mid-coastal Oregon, USA. *Aquatic Conservation: Marine and Freshwater Ecosystems*, *22*(3), 288–302. https://doi.org/10.1002/AQC.2228

Fonstad, M. A., & Marcus, W. A. (2010). High resolution, basin extent observations and implications for understanding river form and process. *Earth Surface Processes and Landforms*, n/a-n/a. https://doi.org/10.1002/esp.1969

Frissell, C. A., Liss, W. J., Warren, C. E., & Hurley, M. D. (1986). A hierarchical framework for stream habitat classification: Viewing streams in a watershed context. *Environmental Management*, *10*(2), 199–214. https://doi.org/10.1007/BF01867358

Fukushima, M. (2001). Salmonid habitat–geomorphology relationships in low-gradient streams. *Ecology*, *82*(5), 1238–1246. https://doi.org/10.1890/0012-9658(2001)082[1238:SHGRIL]2.0.CO;2

García, A., Jorde, K., Habit, E., Caamaño, D., & Parra, O. (2011). Downstream environmental effects of dam operations: Changes in habitat quality for native fish species. *River Research and*

Applications, *27*(3), 312–327. https://doi.org/10.1002/rra.1358

Garshelis, D. L. (2000). Delusions in habitat evaluation: Measuring use, selection, and importance. *Research Techniques in Animal Ecology: Controversies and Consequences*, 111–154.

Geist, D. R., & Dauble, D. D. (1998). Redd site selection and spawning habitat use by fall Chinook salmon: The importance of geomorphic features in large rivers. *Environmental Management*, *22*(5), 655–669.

Geist, J., & Hawkins, S. J. (2016, October 1). Habitat recovery and restoration in aquatic ecosystems: current progress and future challenges. *Aquatic Conservation: Marine and Freshwater Ecosystems*. John Wiley and Sons Ltd. https://doi.org/10.1002/aqc.2702

Gibbins, C. N., Vericat, D., & Batalla, R. J. (2010). Relations between invertebrate drift and flow velocity in sand-bed and riffle habitats and the limits imposed by substrate stability and benthic density. *Journal of the North American Benthological Society* , *29*(3), 945–958. https://doi.org/10.1899/09-096.1

Gibson, S., Osorio, A., Creech, C., Amorim, R., Dircksen, M., Dahl, T., & Koohafkan, M. (2019). Two pool-to-pool spacing periods on large sand-bed rivers: Mega-pools on the Madeira and Mississippi. *Geomorphology*, *328*, 196–210. https://doi.org/10.1016/j.geomorph.2018.12.021

Graf, W. L. (2006). Downstream hydrologic and geomorphic effects of large dams on American rivers. *Geomorphology*, *79*(3–4), 336–360. https://doi.org/10.1016/j.geomorph.2006.06.022

Grant, G., Schmidt, J., & Lewis, S. (2003). A geological framework for interpreting downstream effects of dams on rivers. *A Peculiar River*. *American Geophysical Union, Water Science and Applications*, (7), 203–219.

Grant, J. W., & Kramer, D. L. (1990). Territory size as a predictor of the upper limit to population density of juvenile salmonids in streams. *Canadian Journal of Fisheries and Aquatic Sciences*, *47*, 1724–1737.

Gregory, S. V., & Bisson, P. A. (1997). Degradation and loss of anadromous salmonid habitat in the Pacific northwest. *Pacific Salmon & Their Ecosystems*, 277–314. https://doi.org/10.1007/978-1-4615-6375-4_17

Groll, M. (2017). The passive river restoration approach as an efficient tool to improve the hydromorphological diversity of rivers – Case study from two river restoration projects in the

German lower mountain range. *Geomorphology*, *293*, 69–83. https://doi.org/10.1016/j.geomorph.2017.05.004

Gustafson, R. G., Waples, R. S., Myers, J. M., Weitkamp, L. A., Bryant, G. J., Johnson, O. W., & Hard, J. J. (2007). Pacific salmon extinctions: Quantifying lost and remaining diversity. *Conservation Biology*, *21*(4), 1009–1020. Retrieved from https://pubmed.ncbi.nlm.nih.gov/17650251/

Gutierrez, R. R., Abad, J. D., Parsons, D. R., & Best, J. L. (2013). Discrimination of bed form scales using robust spline filters and wavelet transforms: Methods and application to synthetic signals and bed forms of the Río Paraná, Argentina. *Journal of Geophysical Research: Earth Surface*, *118*(3), 1400–1418. https://doi.org/10.1002/jgrf.20102

Hamann, E. J., Kennedy, B. P., Whited, D. C., & Stanford, J. A. (2014). Spatial variability in spawning habitat selection by chinook salmon (oncorhynchus tshawytscha) in a wilderness river. *River Research and Applications*, *30*(9), 1099–1109. https://doi.org/10.1002/rra.2704

Hanrahan, T. P. (2007). Bedform morphology of salmon spawning areas in a large gravel-bed river. *Geomorphology*, *86*(3–4), 529–536. https://doi.org/10.1016/j.geomorph.2006.09.017

Harvey, B. C., & Railsback, S. F. (2013). Feeding modes in stream salmonid population models: is drift feeding the whole story? *Environmental Biology of Fishes*, *97*(5), 615–625. https://doi.org/10.1007/S10641-013-0186-7

Hassan, M. A., Egozi, R., & Parker, G. (2006). Experiments on the effect of hydrograph characteristics on vertical grain sorting in gravel bed rivers. *Water Resources Research*, *42*(9), 9408. https://doi.org/10.1029/2005WR004707

Hatten, J. R., Batt, T. R., Skalicky, J. J., Engle, R., Barton, G. J., Fosness, R. L., & Warren, J. (2016). Effects of dam removal on Tule Fall Chinook salmon spawning habitat in the White Salmon River, Washington. *River Research and Applications*, *32*(7), 1481–1492. https://doi.org/10.1002/rra.2982

Hauer, C., Unfer, G., Holzmann, H., Schmutz, S., & Habersack, H. (2012). The impact of discharge change on physical instream habitats and its response to river morphology. *Climatic Change 2012 116:3*, *116*(3), 827–850. https://doi.org/10.1007/S10584-012-0507-4

Hayes, J. W., Hughes, N. F., & Kelly, L. H. (2007). Process-based modelling of invertebrate drift

transport, net energy intake and reach carrying capacity for drift-feeding salmonids. *Ecological Modelling*, *207*(2–4), 171–188. https://doi.org/10.1016/J.ECOLMODEL.2007.04.032

Hayes, J. W., Goodwin, E., Shearer, K. A., Hay, J., & Kelly, L. (2016). Can weighted useable area predict flow requirements of drift-feeding salmonids? Comparison with a net rate of energy intake model incorporating drift–flow processes. *Transactions of the American Fisheries Society*, *145*(3), 589–609. https://doi.org/10.1080/00028487.2015.1121923

Healey, M. C., & Heard, W. R. (1984). Inter- and intra-population variation in the fecundity of Chinook salmon (Oncorhynchus tshawytscha) and its relevance to life history theory. *Canadian Journal of Fisheries and Aquatic Sciences*, *41*(3), 476–483. https://doi.org/10.1139/F84-057

Honea, J. M., McClure, M. M., Jorgensen, J. C., & Scheuerell, M. D. (2016). Assessing freshwater life-stage vulnerability of an endangered Chinook salmon population to climate change influences on stream habitat. *Climate Research*, *71*(2), 127–137. https://doi.org/10.3354/CR01434

Huthoff, F., Van Vuren, S., Barneveld, H. J., & Scheel, F. (2010). On the importance of discharge variability in the morphodynamic modeling of rivers. In *River Flow 2010* (pp. 985–992). Retrieved from https://hdl.handle.net/20.500.11970/99743

Huusko, A., Greenberg, L., Stickler, M., Linnansaari, T., Nykänen, M., Vehanen, T., et al. (2007). Life in the ice lane: the winter ecology of stream salmonids. *River Research and Applications*, *23*(5), 469–491. https://doi.org/10.1002/RRA.999

Isaak, D., Wenger, S., … E. P.-W. R., & 2017, undefined. (2017). The NorWeST summer stream temperature model and scenarios for the western US: A crowd-sourced database and new geospatial tools foster a user community. *Wiley Online Library*, *53*(11), 9181–9205. https://doi.org/10.1002/2017WR020969

Isaak, D J, Wollrab, S., Horan, D., & Chandler, G. (2012). Climate change effects on stream and river temperatures across the northwest U.S. from 1980-2009 and implications for salmonid fishes. *Climatic Change*, *113*, 499–524. https://doi.org/10.1007/s10584-011-0326-z

Isaak, Daniel J., Thurow, R. F., Rieman, B. E., & Dunham, J. B. (2007). Chinook salmon use of spawning patches: Relative roles of habitat quality, size, and connectivity. *Ecological Applications*, *17*(2), 352–364. https://doi.org/10.1890/05-1949

Isaak, Daniel J., Young, M. K., Nagel, D. E., Horan, D. L., & Groce, M. C. (2015). The cold-water climate shield: delineating refugia for preserving salmonid fishes through the 21st century. *Global Change Biology*, *21*(7), 2540–2553. https://doi.org/10.1111/gcb.12879

Isaak, Daniel J., Wenger, S. J., Peterson, E. E., Ver Hoef, J. M., Nagel, D. E., Luce, C. H., et al. (2017). The NorWeST summer stream temperature model and scenarios for the western U.S.: A crowd-sourced database and new geospatial tools foster a user community and predict broad climate warming of rivers and streams. *Water Resources Research*, *53*(11), 9181–9205. https://doi.org/10.1002/2017WR020969

Isaak, Daniel J., Luce, C. H., Horan, D. L., Chandler, G. L., Wollrab, S. P., & Nagel, D. E. (2018). Global warming of salmon and trout rivers in the northwestern U.S.: Road to ruin or path through purgatory? *Transactions of the American Fisheries Society*, *147*(3), 566–587. https://doi.org/10.1002/TAFS.10059

Jenkins, A. R., & Keeley, E. R. (2010). Bioenergetic assessment of habitat quality for stream-dwelling cutthroat trout (Oncorhynchus clarkii bouvieri) with implications for climate change and nutrient supplementation. *Canadian Journal of Fisheries and Aquatic Sciences*, *67*(2), 371–385. https://doi.org/10.1139/F09-193

Jungwirth, M., Moog, O., & Muhar, S. (1993). Effects of river bed restructuring on fish and benthos of a fifth order stream, melk, Austria. *Regulated Rivers: Research & Management*, *8*(1–2), 195–204. https://doi.org/10.1002/rrr.3450080122

Justice, C., White, S. M., McCullough, D. A., Graves, D. S., & Blanchard, M. R. (2017). Can stream and riparian restoration offset climate change impacts to salmon populations? *Journal of Environmental Management*, *188*, 212–227. https://doi.org/10.1016/j.jenvman.2016.12.005

Kail, J., Brabec, K., Poppe, M., & Januschke, K. (2015, June 26). The effect of river restoration on fish, macroinvertebrates and aquatic macrophytes: A meta-analysis. *Ecological Indicators*. Elsevier B.V. https://doi.org/10.1016/j.ecolind.2015.06.011

Kammel, L. E., Pasternack, G. B., Massa, D. A., & Bratovich, P. M. (2016). Near-census ecohydraulics bioverification of *Oncorhynchus mykiss* spawning microhabitat preferences. *Journal of Ecohydraulics*, *1*(1–2), 62–78. https://doi.org/10.1080/24705357.2016.1237264

Keeley, E. R., Campbell, S. O., & Kohler, A. E. (2016). Bioenergetic calculations evaluate changes to habitat quality for salmonid fishes in streams treated with salmon carcass analog. *Canadian*

Journal of Fisheries and Aquatic Sciences, *73*(5), 819–831. https://doi.org/10.1139/CJFAS-2015-0265

Keller, E. A., & Melhorn, W. N. (1978). Rhythmic spacing and origin of pools and riffles. *GSA Bulletin*, *89*(5), 723–730. https://doi.org/10.1130/0016-7606(1978)89<723:rsaoop>2.0.co;2

Kennedy, T. A., Yackulic, C. B., Cross, W. F., Grams, P. E., Yard, M. D., & Copp, A. J. (2014). The relation between invertebrate drift and two primary controls, discharge and benthic densities, in a large regulated river. *Freshwater Biology*, *59*(3), 557–572. https://doi.org/10.1111/FWB.12285

Knighton, D. (2014). *Fluvial forms and processes: a new perspective*. Routledge.

Kondolf, G. M., & Wolman, M. G. (1993). The sizes of salmonid spawning gravels. *Water Resources Research*, *29*(7), 2275–2285. https://doi.org/10.1029/93WR00402

Kruskal, W. H., & Wallis, W. A. (1952). Use of ranks in one-criterion variance analysis. *Journal of the American Statistical Association*, *47*(260), 583. https://doi.org/10.2307/2280779

Labat, D. (2008). Wavelet analysis of the annual discharge records of the world's largest rivers. *Advances in Water Resources*, *31*(1), 109–117. https://doi.org/10.1016/j.advwatres.2007.07.004

Lancaster, J., & Belyea, L. R. (2006). Defining the limits to local density: alternative views of abundance–environment relationships. *Freshwater Biology*, *51*(4), 783–796. https://doi.org/10.1111/J.1365-2427.2006.01518.X

Lane, B. A., Pasternack, G. B., Dahlke, H. E., & Sandoval-Solis, S. (2017). The role of topographic variability in river channel classification. *Progress in Physical Geography: Earth and Environment*, *41*(5), 570–600. https://doi.org/10.1177/0309133317718133

Lane, S. N. (2007). Assessment of rainfall-runoff models based upon wavelet analysis. *Hydrological Processes*, *21*(5), 586–607. https://doi.org/10.1002/hyp.6249

Leopold, L. B., Wolman, M. G., & Miller, J. P. (1964). *Fluvial Processes in Geomorphology*. New York: W. H. Freeman.

Leung, E. S., Rosenfeld, J. S., & Bernhardt, J. R. (2009). Habitat effects on invertebrate drift in a small trout stream: implications for prey availability to drift-feeding fish. *Hydrobiologia*, *623*(1), 113–125. https://doi.org/10.1007/s10750-008-9652-1

Ligon, F. K., Dietrich, W. E., & Trush, W. J. (1995). Downstream ecological effects of dams - A geomorphic perspective. *BioScience*, *45*(3), 183–192. https://doi.org/10.2307/1312557

Lofthouse, C., & Robert, A. (2008). Riffle-pool sequences and meander morphology. *Geomorphology*, *99*(1–4), 214–223. https://doi.org/10.1016/j.geomorph.2007.11.002

Luce, C. H., Abatzoglou, J. T., & Holden, Z. A. (2013). The missing mountain water: Slower westerlies decrease orographic enhancement in the Pacific northwest USA. *Science*, *342*(6164), 1360–1364. https://doi.org/10.1126/SCIENCE.1242335

Macneale, K. H., Sanderson, B. L., Courbois, J.-Y. P., & Kiffney, P. M. (2010). Effects of non-native brook trout (Salvelinus fontinalis) on threatened juvenile Chinook salmon (Oncorhynchus tshawytscha) in an Idaho stream. *Ecology of Freshwater Fish*, *19*(1), 139–152. https://doi.org/10.1111/J.1600-0633.2009.00398.X

MacWilliams, M. L., Wheaton, J. M., Pasternack, G. B., Street, R. L., & Kitanidis, P. K. (2006). Flow convergence routing hypothesis for pool-riffle maintenance in alluvial rivers. *Water Resources Research*, *42*(10), 10427. https://doi.org/10.1029/2005WR004391

Malcolm, I. A., Hannah, D. M., Donaghy, M. J., Soulsby, C., & Youngson, A. F. (2004). The influence of riparian woodland on the spatial and temporal variability of stream water temperatures in an upland salmon stream. *European Geosciences Union*, *8*(3), 449–459. Retrieved from https://hal.archives-ouvertes.fr/hal-00304936

Mantua, N., Tohver, I., & Hamlet, A. (2010). Climate change impacts on streamflow extremes and summertime stream temperature and their possible consequences for freshwater salmon habitat in Washington State. *Climatic Change 2010 102:1*, *102*(1), 187–223. https://doi.org/10.1007/S10584-010-9845-2

Mao, L. (2012). The effect of hydrographs on bed load transport and bed sediment spatial arrangement. *Journal of Geophysical Research: Earth Surface*, *117*(F3), 3024. https://doi.org/10.1029/2012JF002428

Marcus, W. A., & Fonstad, M. A. (2008). Optical remote mapping of rivers at sub-meter resolutions and watershed extents. *Earth Surface Processes and Landforms*, *33*(1), 4–24. https://doi.org/10.1002/esp.1637

Maret, T. R., Hortness, J. E., & Ott, D. S. (2005). Instream flow characterization of upper Salmon

River basin streams, central Idaho, 2004, 5212.

Masteller, C. C., Finnegan, N. J., Turowski, J. M., Yager, E. M., & Rickenmann, D. (2019). History-dependent threshold for motion revealed by continuous bedload transport measurements in a steep mountain stream. *Geophysical Research Letters*, *46*(5), 2583–2591. https://doi.org/10.1029/2018GL081325

Maturana, O., Tonina, D., Mckean, J. A., Buffington, J. M., Luce, C. H., & Caamaño, D. (2014). Modeling the effects of pulsed versus chronic sand inputs on salmonid spawning habitat in a low-gradient gravel-bed river. *Earth Surface Processes and Landforms*, *39*(7), 877–889. https://doi.org/10.1002/esp.3491

McDonald, R., Nelson, J., Paragamian, V., & Barton, G. (2010). Modeling the effect of flow and sediment transport on white sturgeon spawning habitat in the Kootenai River, Idaho. *Journal of Hydraulic Engineering*, *136*(12), 1077–1092. https://doi.org/10.1061/(asce)hy.1943-7900.0000283

McKean, J., & Tonina, D. (2013). Bed stability in unconfined gravel bed mountain streams: With implications for salmon spawning viability in future climates. *Journal of Geophysical Research: Earth Surface*, *118*(3), 1227–1240. https://doi.org/10.1002/jgrf.20092

McKean, J., Nagel, D., Tonina, D., Bailey, P., Wright, C. W., Bohn, C., & Nayegandhi, A. (2009). Remote sensing of channels and riparian zones with a narrow-beam aquatic-terrestrial LiDAR. *Remote Sensing*, *1*(4), 1065–1096. https://doi.org/10.3390/rs1041065

McKean, J. A., Isaak, D. J., & Wright, C. W. (2008). Geomorphic controls on salmon nesting patterns described by a new, narrow-beam terrestrial–aquatic lidar. *Frontiers in Ecology and the Environment*, *6*(3), 125–130. https://doi.org/10.1890/070109

McMichael, G. A., Rakowski, C. L., James, B. B., & Lukas, J. A. (2005). Estimated fall Chinook salmon survival to emergence in dewatered redds in a shallow side channel of the Columbia River. *North American Journal of Fisheries Management*, *25*(3), 876–884. https://doi.org/10.1577/M04-168.1

Meitzen, K. M., Doyle, M. W., Thoms, M. C., & Burns, C. E. (2013). Geomorphology within the interdisciplinary science of environmental flows. *Geomorphology*, *200*, 143–154. https://doi.org/10.1016/J.GEOMORPH.2013.03.013

Mi, X., Ren, H., Ouyang, Z., Wei, W., & Ma, K. (2005). The use of the Mexican Hat and the Morlet wavelets for detection of ecological patterns. *Plant Ecology*, *179*(1), 1–19. https://doi.org/10.1007/s11258-004-5089-4

Milhous, R. T. (1973, May 3). Sediment transport in a gravel-bottomed stream. *PhD Dissertation, Oregon State University, Corvallis, OR*. Retrieved from https://ir.library.oregonstate.edu/concern/graduate_thesis_or_dissertations/bv73c272r?locale=en

Milhous, R. T. (1998). Modelling of instream flow needs: the link between sediment and aquatic habitat. *Regulated Rivers: Research & Management*, *14*, 79–94. https://doi.org/10.1002/(SICI)1099-1646(199801/02)14:1

Misiti, M., Misiti, Y., Oppenheim, G., & Poggi, J.-M. (1997). *Wavelet Toolbox™ Getting Started Guide*. Retrieved from www.mathworks.com

Mohan, M., Silva, C. A., Klauberg, C., Jat, P., Catts, G., Cardil, A., et al. (2017). Individual tree detection from unmanned aerial vehicle (UAV) derived canopy height model in an open canopy mixed conifer forest. *Forests*, *8*(9), 340. https://doi.org/10.3390/f8090340

Monsalve, A., Yager, E. M., Turowski, J. M., & Rickenmann, D. (2016). A probabilistic formulation of bed load transport to include spatial variability of flow and surface grain size distributions. *Water Resources Research*, *52*(5), 3579–3598. https://doi.org/10.1002/2015WR017694

Montgomery, D. R., Buffington, J. M., Smith, R. D., Schmidt, K. M., & Pess, G. (1995). Pool spacing in forest channels. *Water Resources Research*, *31*(4), 1097–1105. https://doi.org/10.1029/94WR03285

Montgomery, D. R., Beamer, E. M., Pess, G. R., & Quinn, T. P. (1999). Channel type and salmonid spawning distribution and abundance. *Canadian Journal of Fisheries and Aquatic Sciences*, *56*(3), 377–387. https://doi.org/10.1139/f98-181

Myrick, C. A., & Cech, J. J. (2000). Temperature influences on California rainbow trout physiological performance. *Fish Physiology and Biochemistry*, *22*, 245–254.

Myrvold, K. M., & Kennedy, B. P. (2018). Increasing water temperatures exacerbate the potential for density dependence in juvenile steelhead. *Canadian Journal of Fisheries and Aquatic Sciences*, *75*, 897–907. https://doi.org/10.1139/cjfas-2016-0497

Naman, S. M., Rosenfeld, J. S., Neuswanger, J. R., Enders, E. C., & Eaton, B. C. (2019). Comparing

correlative and bioenergetics-based habitat suitability models for drift-feeding fishes. *Freshwater Biology*, *64*(9), 1613–1626. https://doi.org/10.1111/FWB.13358

Naman, S. M., Rosenfeld, J. S., Neuswanger, J. R., Enders, E. C., Hayes, J. W., Jowett, I. G., & Eaton, B. C. (2020). Bioenergetic habitat suitability curves for instream flow modeling: Introducing user-friendly software and its potential applications. *Fisheries*, *45*(11), 605–613. https://doi.org/10.1002/fsh.10489

Nelson, J. M., Logan, B. L., Kinzel, P. J., Shimizu, Y., Giri, S., Shreve, R. L., & McLean, S. R. (2011). Bedform response to flow variability. *Earth Surface Processes and Landforms*, *36*(14), 1938–1947. https://doi.org/10.1002/ESP.2212

Nelson, Jonathan M., McLean, S. R., & Wolfe, S. R. (1993). Mean flow and turbulence fields over two-dimensional bed forms. *Water Resources Research*, *29*(12), 3935–3953. https://doi.org/10.1029/93WR01932

Nelson, Jonathan M., Bennett, J. P., & Wiele, S. M. (2003). Flow and sediment-transport modeling. In *Tools in Fluvial Geomorphology* (pp. 539–576). https://doi.org/10.1002/0470868333.ch18

Nelson, Jonathan M, Shimizu, Y., Abe, T., Asahi, K., Gamou, M., Inoue, T., et al. (2016). The international river interface cooperative: Public domain flow and morphodynamics software for education and applications. *Advances in Water Resources*, *93*(Part A), 62–74.

Nelson, P. A., & Morgan, J. A. (2018). Flume experiments on flow and sediment supply controls on gravel bedform dynamics. *Geomorphology*, *323*, 98–105. https://doi.org/10.1016/J.GEOMORPH.2018.09.011

Nelson, P. A., McDonald, R. R., Nelson, J. M., & Dietrich, W. E. (2015). Coevolution of bed surface patchiness and channel morphology: 2. Numerical experiments. *Journal of Geophysical Research F: Earth Surface*, *120*(9), 1708–1723. https://doi.org/10.1002/2014JF003429

Nelson, P. A., Brew, A. K., & Morgan, J. A. (2015). Morphodynamic response of a variable-width channel to changes in sediment supply. *Water Resources Research*, *51*(7), 5717–5734. https://doi.org/10.1002/2014WR016806

Neuswanger, J. R., Wipfli, M. S., Evenson, M. J., Hughes, N. F., & Rosenberger, A. E. (2015). Low productivity of Chinook salmon strongly correlates with high summer stream discharge in two Alaskan rivers in the Yukon drainage. *Canadian Journal of Fisheries and Aquatic Sciences*,

72(8), 1125–1137. https://doi.org/10.1139/CJFAS-2014-0498

Newson, M. D., & Newson, C. L. (2000). Geomorphology, ecology and river channel habitat: mesoscale approaches to basin-scale challenges. *Progress in Physical Geography: Earth and Environment*, *24*(2), 195–217. https://doi.org/10.1177/030913330002400203

NMFS. (2019). Endangered Species Act (ESA) section 7 (a)(2) biological opinion and Magnuson-Stevens Fishery Conservation and management act essential fish habitat (EFH) consultation. *NMFS Consultation Number: WCRO-2018-00152*.

O'Neill, M. P., & Abrahams, A. D. (1984). Objective identification of pools and riffles. *Water Resources Research*, *20*(7), 921–926. https://doi.org/10.1029/WR020i007p00921

Parker, G., & Klingeman, P. C. (1982). On why gravel bed streams are paved. *Water Resources Research*, *18*(5), 1409–1423. https://doi.org/10.1029/WR018i005p01409

Parker, G., Toro-Escobar, C. M., Ramey, M., & Beck, S. (2003). Effect of floodwater extraction on mountain stream morphology. *Journal of Hydraulic Engineering*, *129*(11), 885–895. https://doi.org/10.1061/(ASCE)0733-9429(2003)129:11(885))

Pasternack, G. B., & Brown, R. A. (2013). Ecohydraulic design of riffle-pool relief and morphological unit geometry in support of regulated gravel-bed river rehabilitation. *Ecohydraulics: An Integrated Approach*, 337–355.

Phillips, C. B., Hill, K. M., Paola, C., Singer, M. B., & Jerolmack, D. J. (2018). Effect of flood hydrograph duration, magnitude, and shape on bed load transport dynamics. *Geophysical Research Letters*, *45*(16), 8264–8271. https://doi.org/10.1029/2018GL078976

Piccolo, J. J., Frank, B. M., & Hayes, J. W. (2014). Food and space revisited: The role of drift-feeding theory in predicting the distribution, growth, and abundance of stream salmonids. *Environmental Biology of Fishes 2014 97:5*, *97*(5), 475–488. https://doi.org/10.1007/S10641-014-0222-2

Le Pichon, C., Gorges, G., Boët, P., Baudry, J., Goreaud, F., & Faure, T. (2006). A spatial explicit resource-based approach for managing stream fishes in riverscapes. *Environmental Management*, *37*(3), 322–335.

Le Pichon, C., Gorges, G., Baudry, J., Goreaud, F., & Boët, P. (2009). Spatial metrics and methods for riverscapes: quantifying variability in riverine fish habitat patterns. *Environmetrics*, *20*(5),

512–526. https://doi.org/10.1002/ENV.948

Plumb, B. D., Juez, C., Annable, W. K., McKie, C. W., & Franca, M. J. (2020). The impact of hydrograph variability and frequency on sediment transport dynamics in a gravel-bed flume. *Earth Surface Processes and Landforms*, *45*(4), 816–830. https://doi.org/10.1002/ESP.4770

Poff, L. N., & Zimmermann, J. K. H. (2010). Ecological responses to altered flow regimes: a literature review to 987 inform the science and management of environmental flows. *Freshwater Biology*, *55*, 194–205.

Poff, N. L., & Huryn, A. D. (1998). Multi-scale determinants of secondary production in Atlantic salmon (Salmo salar) streams. *Canadian Journal of Fisheries and Aquatic Sciences*, *55*(1), 201–217. https://doi.org/10.1139/D98-013

Poff, N. L., & Ward, J. V. (1991). Drift responses of benthic invertebrates to experimental streamflow variation in a hydrologically stable stream. *Canadian Journal of Fisheries and Aquatic Sciences*, *48*(10), 1926–1936. https://doi.org/10.1139/F91-229

Poff, N. L., Allan, J. D., Bain, M. B., Karr, J. R., Prestegaard, K. L., Richter, B. D., et al. (1997). The natural flow regime. *BioScience*, *47*(11), 769–784. https://doi.org/10.2307/1313099

Polvi, L. E., Nilsson, C., & Hasselquist, E. M. (2014). Potential and actual geomorphic complexity of restored headwater streams in northern Sweden. *Geomorphology*, *210*, 98–118. https://doi.org/10.1016/j.geomorph.2013.12.025

Quinn, T. P. (2018). *The behavior and ecology of Pacific salmon & trout* (2nd ed.). University of Washington Press in association with American Fisheries Society.

Railsback, S. F. (2016). Why it is time to put PHABSIM out to pasture. *Fisheries*, *41*(12), 720–725. https://doi.org/10.1080/03632415.2016.1245991

Rayburg, S. C., & Neave, M. (2008). Assessing morphologic complexity and diversity in river systems using three-dimensional asymmetry indices for bed elements, bedforms and bar units. *River Research and Applications*, *24*(10), 1343–1361. https://doi.org/10.1002/rra.1096

Raymond, P. A., Zappa, C. J., Butman, D., Bott, T. L., Potter, J., Mulholland, P., et al. (2012). Scaling the gas transfer velocity and hydraulic geometry in streams and small rivers. *Limnology and Oceanography: Fluids and Environments*, *2*(1), 41–53. https://doi.org/10.1215/21573689-1597669

Redolfi, M., Bertoldi, W., Tubino, M., & Welber, M. (2018). Bed load variability and morphology of gravel bed rivers subject to unsteady flow: A laboratory investigation. *Water Resources Research*, *54*(2), 842–862. https://doi.org/10.1002/2017WR021143

Reeder, W. J., Gariglio, F., Carnie, R., Tang, C., Isaak, D., Chen, Q., et al. (2021). Some (fish might) like it hot: Habitat quality and fish growth from past to future climates. *Science of The Total Environment*, *787*, 147532. https://doi.org/10.1016/J.SCITOTENV.2021.147532

Reich, P., & Lake, P. S. (2015). Extreme hydrological events and the ecological restoration of flowing waters. *Freshwater Biology*, *60*(12), 2639–2652. https://doi.org/10.1111/fwb.12508

Reid, I., Frostick, L. E., & Layman, J. T. (1985). The incidence and nature of bedload transport during flood flows in coarse-grained alluvial channels. *Earth Surface Processes and Landforms*, *10*(1), 33–44. https://doi.org/10.1002/ESP.3290100107

Reiser, D. W., Ramey, M. P., Beck, S., Lambert, T. R., & Geary, R. E. (1989). Flushing flow recommendations for maintenance of salmonid spawning gravels in a steep, regulated stream. *Regulated Rivers: Research & Management*, *3*(1), 267–275. https://doi.org/10.1002/rrr.3450030126

Richter, A., & Kolmes, S. A. (2005). Maximum temperature limits for Chinook, coho, and chum salmon, and steelhead trout in the Pacific northwest. *Reviews in Fisheries Science*, *13*(1), 23–49.

Richter, B. D., Mathews, R., Harrison, D. L., & Wigington, R. (2003). Ecologically Sustainable Water Management: Managing River Flows for Ecological Integrity. *Ecological Applications*, *13*(1), 206–224. https://doi.org/10.1890/1051-0761(2003)013

Riegl. (2016). VQ-880-G data sheet. Retrieved from http://www.riegl.com/uploads/tx_pxpriegldownloads/Infosheet_VQ-880-G_2016-05-23.pdf

Roloff, G. J., & Kernohan, B. J. (1999). Evaluating reliability of habitat suitability index models. *Wildlife Society Bulletin*, *27*(4), 973–985.

Roni, P., Hanson, K., & Beechie, T. (2008). Global review of the physical and biological effectiveness of stream habitat rehabilitation techniques. *North American Journal of Fisheries Management*, *28*(3), 856–890. https://doi.org/10.1577/m06-169.1

Ryan, S. E., Porth, L. S., & Troendle, C. A. (2005). Coarse sediment transport in mountain streams in Colorado and Wyoming, USA. *Earth Surface Processes and Landforms*, *30*(3), 269–288.

https://doi.org/10.1002/esp.1128

Sawyer, A. M., Pasternack, G. B., Moir, H. J., & Fulton, A. A. (2010). Riffle-pool maintenance and flow convergence routing observed on a large gravel-bed river. *Geomorphology*, *114*(3), 143–160. https://doi.org/10.1016/J.GEOMORPH.2009.06.021

Serinaldi, F., & Grimaldi, S. (2011). Synthetic design hydrographs based on distribution functions with finite support. *Journal of Hydrologic Engineering*, *16*(5), 434–446. https://doi.org/10.1061/(ASCE)HE.1943-5584.0000339

Shirvell, C. S. (1989). Ability of phabsim to predict chinook salmon spawning habitat. *Regulated Rivers: Research & Management*, *3*(1), 277–289. https://doi.org/10.1002/RRR.3450030127

Sinokrot, B., & Gulliver, J. (2000). In-stream flow impact on river water temperatures. *Journal of Hydraulic Research*, *38*(5), 339–349.

Smith, J. D., & McLean, S. R. (1977). Spatially averaged flow over a wavy surface. *Journal of Geophysical Research*, *82*(12), 1735–1746. https://doi.org/10.1029/JC082i012p01735

Sokolova, M., Japkowicz, N., & Szpakowicz, S. (2006). *Beyond Accuracy, F-score, and ROC: A Family of Discriminant Measures for Performance Evaluation*. Retrieved from www.aaai.org

Stark, J. D., Shearer, K. A., & Hayes, J. W. (2002). Are aquatic invertebrate drift densities uniform? Implications for salmonid foraging models. *Internationale Vereinigung Für Theoretische Und Angewandte Limnologie: Verhandlungen*, *28*(2), 988–991. https://doi.org/10.1080/03680770.2001.11901865

Stewart, D. J., & Lbarra, M. (1991). Predation and production by salmonine fishes in Lake Michigan, 1978-88. *Canadian Journal of Fisheries and Aquatic Sciences*, *48*, 909–922.

Tamminga, A., Hugenholtz, C., Eaton, B., & Lapointe, M. (2015). Hyperspatial remote sensing of channel reach morphology and hydraulic fish habitat using an unmanned aerial vehicle (UAV): A first assessment in the context of river research and management. *River Research and Applications*, *31*(3), 379–391. https://doi.org/10.1002/rra.2743

Tews, J., Brose, U., Grimm, V., Tielbörger, K., Wichmann, M. C., Schwager, M., & Jeltsch, F. (2004). Animal species diversity driven by habitat heterogeneity/diversity: the importance of keystone structures. *Journal of Biogeography*, *31*(1), 79–92. https://doi.org/10.1046/j.0305-0270.2003.00994.x

Thompson, A. (1986). Secondary flows and the pool-riffle unit: A case study of the processes of meander development. *Earth Surface Processes and Landforms*, *11*(6), 631–641. https://doi.org/10.1002/esp.3290110606

Thompson, D. M., Wohl, E. E., & Jarrett, R. D. (1996). A revised velocity-reversal and sediment-sorting model for a high-gradient, pool-riffle stream. *Physical Geography*, *17*(2), 142–156. https://doi.org/10.1080/02723646.1996.10642578

Thompson, D M, & Wohl, E. E. (2009). The linkage between velocity patterns and sediment entrainment in a forced-pool and riffle unit Linkage between velocity sediment entrainment in a pool and riffle. *Earth Surface Processes and Landforms*, *34*(2), 197–9337. https://doi.org/10.1002/esp.1698

Thompson, Douglas M. (2001). Random controls on semi-rhythmic spacing of pools and riffles in constriction-dominated rivers. *Earth Surface Processes and Landforms*, *26*(11), 1195–1212. https://doi.org/10.1002/esp.265

Thompson, Douglas M., Nelson, J. M., & Wohl, E. E. (1998). Interactions between pool geometry and hydraulics. *Water Resources Research*, *34*(12), 3673–3681. https://doi.org/10.1029/1998WR900004

Tonina, D, & Jorde, K. (2013). Hydraulic modeling approaches for ecohydraulic studies: 3D, 2D, 1D and non-numerical models. *Ecohydraulics: An Integrated Approach*, 31–66.

Tonina, Daniele, McKean, J. A., Benjankar, R. M., Wright, C. W., Goode, J. R., Chen, Q., et al. (2019). Mapping river bathymetries: Evaluating topobathymetric LiDAR survey. *Earth Surface Processes and Landforms*, *44*(2), 507–520. https://doi.org/10.1002/esp.4513

Tonina, Daniele, McKean, J. A., Benjankar, R. M., Yager, E., Carmichael, R. A., Chen, Q., et al. (2020). Evaluating the performance of topobathymetric LiDAR to support multi-dimensional flow modelling in a gravel-bed mountain stream. *Earth Surface Processes and Landforms*, *45*(12), 2850–2868. https://doi.org/10.1002/esp.4934

Torgersen, C. E., Gresswell, R. E., & Bateman, D. S. (2004). Pattern detection in stream networks: quantifying spatial variability in fish distribution. *GIS/Spatial Analyses in Fishery and Aquatic Sciences*, 405–420.

Torgersen, C. E., Baxter, C. V, Li, H. W., & Mcintosh, B. A. (2006). Landscape influences on

longitudinal patterns of river fishes: Spatially continuous analysis of fish-habitat relationships. *American Fisheries Society Symposium*, *48*, 473–492.

Torrence, C., & Compo, G. P. (1998). A practical guide to wavelet analysis. *Bulletin of the American Meteorological Society*, *79*(1), 61–78. https://doi.org/10.1175/1520-0477(1998)079<0061:APGTWA>2.0.CO;2

Torrence, C., & Webster, P. J. (1999). Interdecadal changes in the ENSO-monsoon system. *Journal of Climate*, *12*(8), 2679–2690. https://doi.org/10.1175/1520-0442(1999)012<2679:icitem>2.0.co;2

Trudel, M., & Welch, D. W. (2005). Modeling the oxygen consumption rates in Pacific salmon and steelhead: model development. *Transactions of the American Fisheries Society*, *134*, 1542–1561. https://doi.org/10.1577/T04-156.1

Turowski, J. M., Badoux, A., Rickenmann, D., Turowski, C. :, Badoux, A., & Rickenmann, D. (2011). Start and end of bedload transport in gravel-bed streams. *Geophysical Research Letters*, *38*(4). https://doi.org/10.1029/2010GL046558

Urabe, H., Nakajima, M., Torao, M., & Aoyama, T. (2010). Evaluation of habitat quality for stream salmonids based on a bioenergetics model. *Transactions of the American Fisheries Society*, *139*(6), 1665–1676. https://doi.org/10.1577/T09-210.1

Vargas-Luna, A., Crosato, P., & Byishimo & Wim, S. J. (2019). Impact of flow variability and sediment characteristics on channel width evolution in laboratory streams. *Journal of Hydraulic Research*, *57*(1), 51–61. https://doi.org/10.1080/00221686.2018.1434836

Vericat, D., Batalla, R. J., & Garcia, C. (2006). Breakup and reestablishment of the armour layer in a large gravel-bed river below dams: The lower Ebro. *Geomorphology*, *76*(1–2), 122–136. https://doi.org/10.1016/J.GEOMORPH.2005.10.005

Wall, C. E., Bouwes, N., Wheaton, J. M., Saunders, W. C., & Bennett, S. N. (2016). Net rate of energy intake predicts reach-level steelhead (Oncorhynchus mykiss) densities in diverse basins from a large monitoring program. *Canadian Journal of Fisheries and Aquatic Sciences*, *73*(7), 1081–1091. https://doi.org/10.1139/CJFAS-2015-0290

Walters, A. W., Bartz, K. K., & Mcclure, M. M. (2013). Interactive effects of water diversion and climate change for juvenile Chinook salmon in the Lemhi River Basin (U.S.A.). *Conservation*

Biology, *27*(6), 1179–1189. Retrieved from https://pubmed.ncbi.nlm.nih.gov/24299084/

Waters, K. A., & Curran, J. C. (2015). Linking bed morphology changes of two sediment mixtures to sediment transport predictions in unsteady flows. *Water Resources Research*, *51*(4), 2724–2741. https://doi.org/10.1002/2014WR016083

Wheaton, J. M., Brasington, J., Darby, S. E., Merz, J., Pasternack, G. B., Sear, D., & Vericat, D. (2009). Linking geomorphic changes to salmonid habitat at a scale relevant to fish. *River Research and Applications*, *26*(4), 469–486. https://doi.org/10.1002/rra.1305

White, J. Q., Pasternack, G. B., & Moir, H. J. (2010). Valley width variation influences riffle-pool location and persistence on a rapidly incising gravel-bed river. *Geomorphology*, *121*(3–4), 206–221. https://doi.org/10.1016/j.geomorph.2010.04.012

Whiting, P. J., & Dietrich, W. E. (1991). Convective accelerations and boundary shear stress over a Channel Bar. *Water Resources Research*, *27*(5), 783–796. https://doi.org/10.1029/91WR00083

Williams, G. P., & Wolman, M. G. (1984). Downstream effects of dams on alluvial rivers. *U.S. Geol. Surv. Prof. Pap.*, (1286).

Wohl, E. (2012). Identifying and mitigating dam-induced declines in river health: Three case studies from the western United States. *International Journal of Sediment Research*, *27*(3), 271–287. https://doi.org/10.1016/S1001-6279(12)60035-3

Wohl, E., Bledsoe, B. P., Jacobson, R. B., Poff, N. L., Rathburn, S. L., Walters, D. M., & Wilcox, A. C. (2015). The Natural Sediment Regime in Rivers: Broadening the Foundation for Ecosystem Management. *BioScience*, *65*(4), 358–371. https://doi.org/10.1093/biosci/biv002

Wolman, M. G. (1954). A method of sampling coarse river-bed material. *Transactions, American Geophysical Union*, *35*(6), 951. https://doi.org/10.1029/TR035i006p00951

Wong, M., & Parker, G. (2006). One-dimensional modeling of bed evolution in a gravel bed river subject to a cycled flood hydrograph. *Journal of Geophysical Research: Earth Surface*, *111*(F3), 3018. https://doi.org/10.1029/2006JF000478

Woodget, A. S., Carbonneau, P. E., Visser, F., & Maddock, I. P. (2015). Quantifying submerged fluvial topography using hyperspatial resolution UAS imagery and structure from motion photogrammetry. *Earth Surface Processes and Landforms*, *40*(1), 47–64. https://doi.org/10.1002/esp.3613

Woodget, Amy S., Austrums, R., Maddock, I. P., & Habit, E. (2017). Drones and digital photogrammetry: from classifications to continuums for monitoring river habitat and hydromorphology. *Wiley Interdisciplinary Reviews: Water*, *4*(4), e1222. https://doi.org/10.1002/wat2.1222

Yager, E. M., Kenworthy, M., & Monsalve, A. (2015). Taking the river inside: Fundamental advances from laboratory experiments in measuring and understanding bedload transport processes. *Geomorphology*, *244*, 21–32. https://doi.org/10.1016/J.GEOMORPH.2015.04.002

Yalin, M. S. (1963). An expression for bed-load transportation. *Journal of the Hydraulics Division*, *89*(3), 221–250. https://doi.org/10.1061/jyceaj.0000874

Yarnell, S. M., Petts, G. E., Schmidt, J. C., Whipple, A. A., Beller, E. E., Dahm, C. N., et al. (2015). Functional flows in modified riverscapes: Hydrographs, habitats and opportunities. *BioScience*. Oxford University Press. https://doi.org/10.1093/biosci/biv102

Zhang, C., Xu, M., Hassan, M. A., Chartrand, S. M., Wang, Z., & Ma, Z. (2020). Experiment on morphological and hydraulic adjustments of step-pool unit to flow increase. *Earth Surface Processes and Landforms*, *45*(2), 280–294. https://doi.org/10.1002/ESP.4722

Zhou, Z., Hua, D., Wang, Y., Yan, Q., Li, S., Li, Y., & Wang, H. (2013). Improvement of the signal to noise ratio of Lidar echo signal based on wavelet de-noising technique. *Optics and Lasers in Engineering*, *51*(8), 961–966. https://doi.org/10.1016/j.optlaseng.2013.02.011

Zimmerman, M. S., Kinsel, C., Beamer, E., Connor, E. J., & Pflug, D. E. (2015). Abundance, survival, and life history strategies of juvenile Chinook salmon in the Skagit River, Washington. *Transactions of the American Fisheries Society*, *144*(3), 627–641. https://doi.org/10.1080/00028487.2015.1017658

Zolezzi, G., & Güneralp, I. (2015). Continuous wavelet characterization of the wavelengths and regularity of meandering rivers. *Geomorphology*, *252*, 98–111.

Appendix A: Supporting Information for Chapter 1

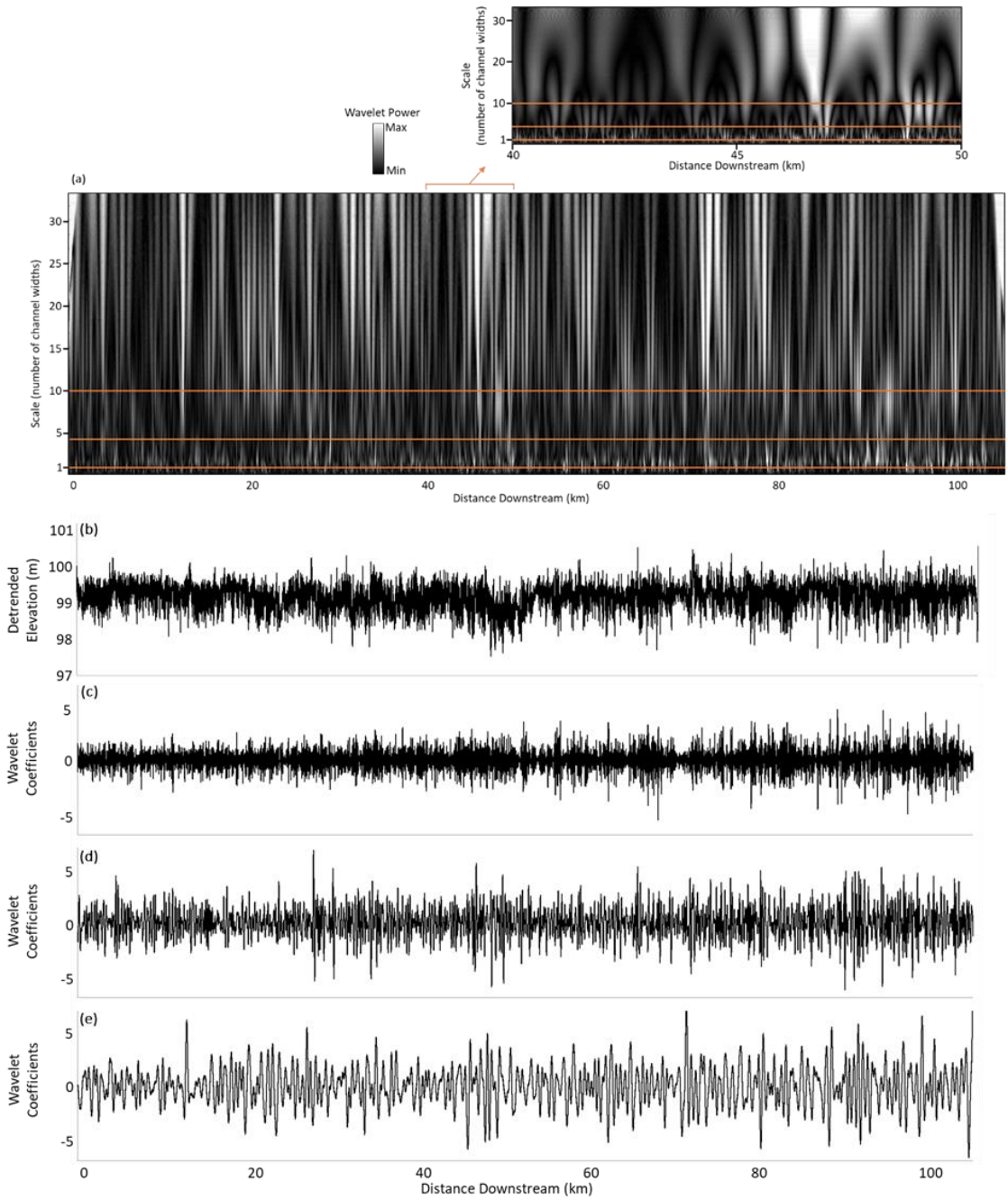

Figure A.1: Wavelet analysis with the Mexican hat wavelet form for 106 km of the Lemhi River. (a) The heat map of all wavelet power with wavelet scales of interest shown with orange lines. (b) Detrended longitudinal thalweg profile, (c) small-scale variability (1 channel width, 15 m) wavelet coefficients, (d) mid-scale variability (4 channel widths, 60 m) wavelet coefficients, and (e) large-scale variability (10 channel widths, 150 m) wavelet coefficients

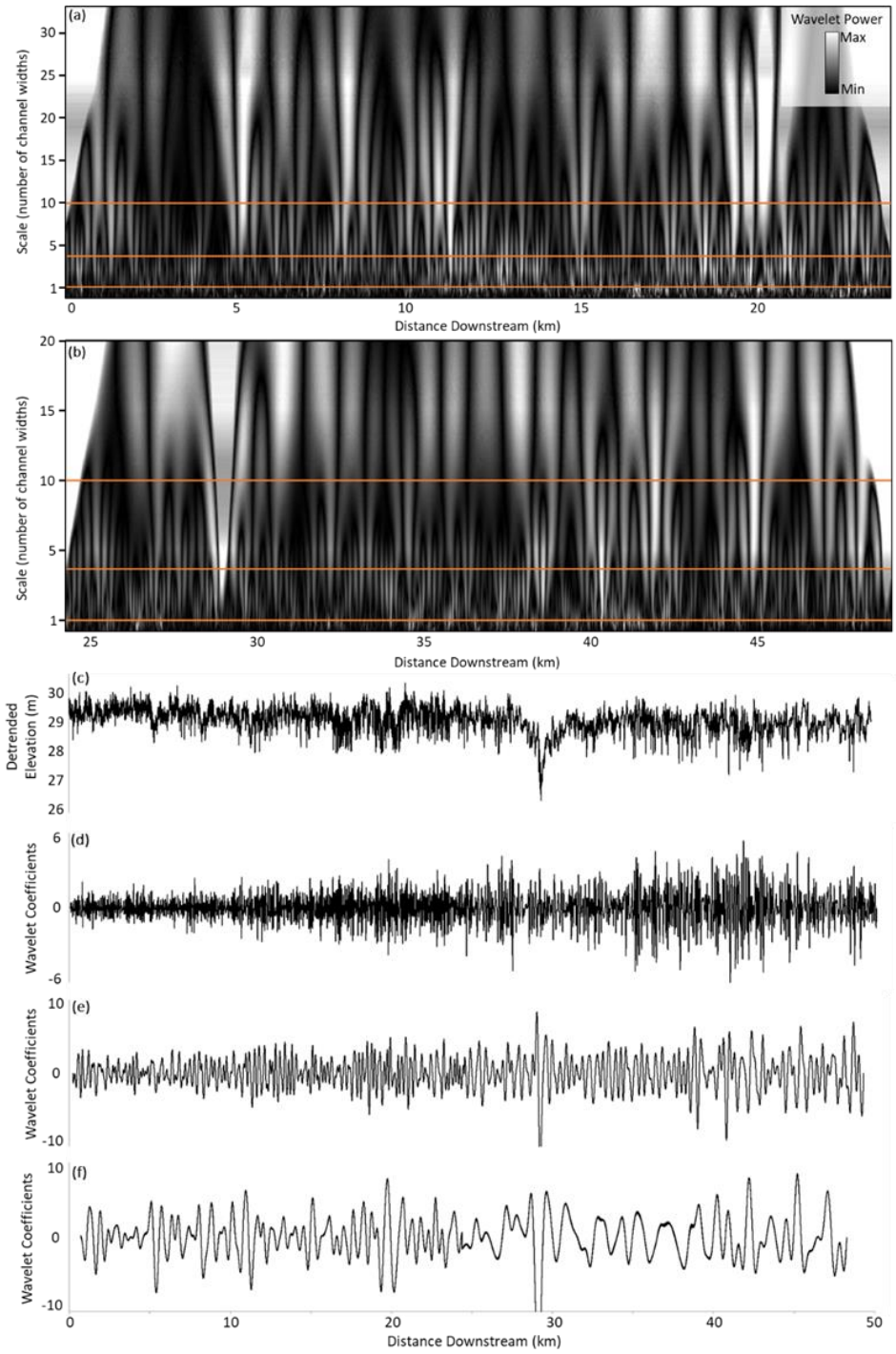

Figure A.2: Wavelet analysis with the Mexican hat wavelet form for 49 km of the Upper Salmon River. (a) Heat map for the first 24 km of the Upper Salmon River and (b) the heat map for the lower 25 km of the river. The scales of interest in this paper are shown by the orange lines. The white areas along the figure sides are edge effects from the moving window that increase as the scale of analysis increases. (c) Detrended longitudinal thalweg profile, (d) small-scale variability wavelet coefficients, (e) mid-scale variability wavelet coefficients, and (f) large-scale wavelet coefficients for the Upper Salmon River.

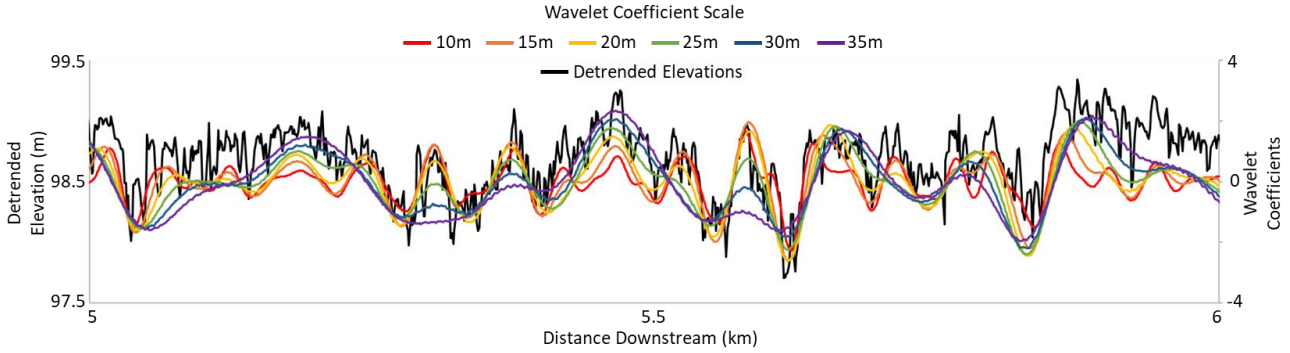

Figure A.3: 1 km of Bear Valley Creek showing how multiple wavelet scales fit the topography and that a range of scales highlight the same general topographic patterns.

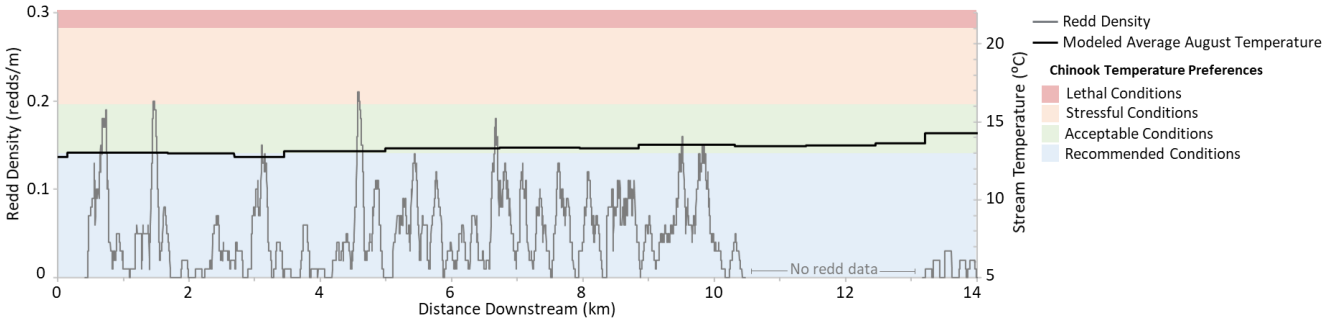

Figure A.4: Redd density (grey line) variation with distance downstream on the Bear Valley Creek. The modeled average daily August stream temperatures (from NorWeST, Isaak et al., 2017) are shown by the black line.

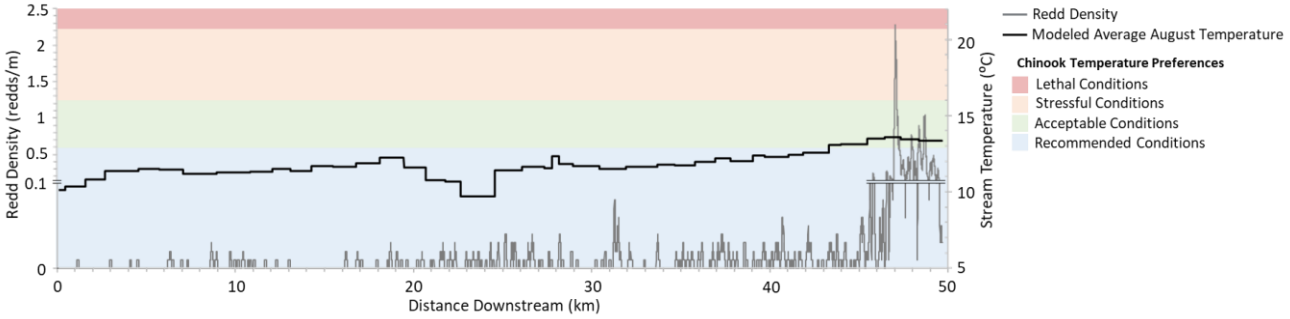

Figure A.5: Redd density (grey line) variation with distance downstream on the Upper Salmon River, note the y-axis scale break for redd density at 0.1 redds/m. The modeled average daily August stream temperatures (from NorWeST, Isaak et al., 2017) are shown by the black line.

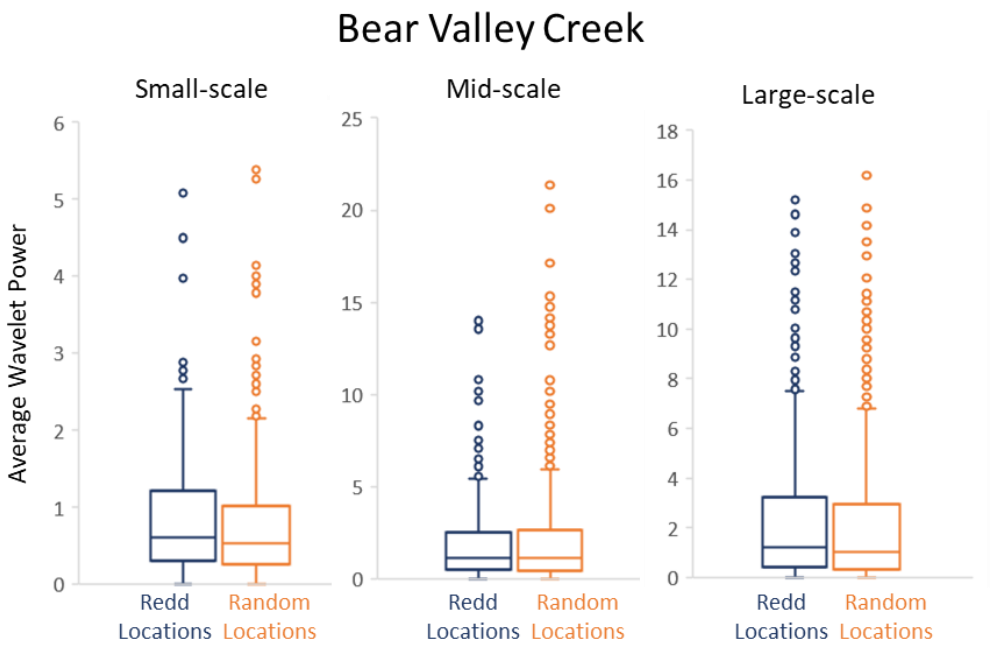

Figure A.6: Boxplots showing the distribution of small-scale, mid-scale, and large-scale average wavelet power for redd locations and random locations along Bear Valley Creek.

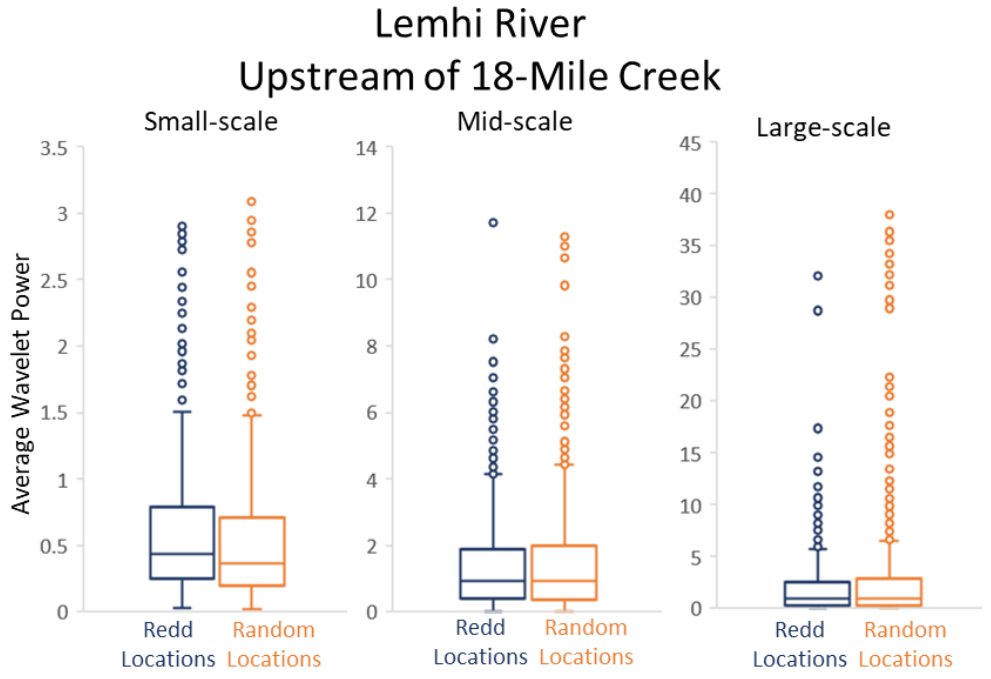

Figure A.7: Boxplots showing the distribution of small-scale, mid-scale, and large-scale average wavelet power for redd locations and random locations along the Lemhi River upstream of 18-Mile Creek.

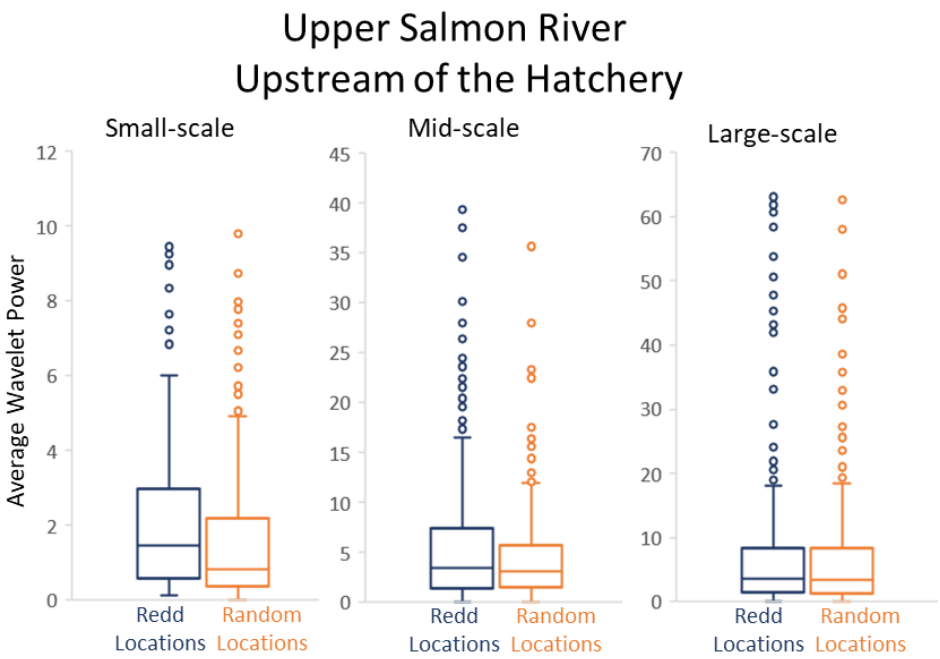

Figure A.8: Boxplots showing the distribution of small-scale, mid-scale, and large-scale average wavelet power for redd locations and random locations along the Upper Salmon River upstream of the hatchery.

Appendix B: Supporting Information for Chapter 2

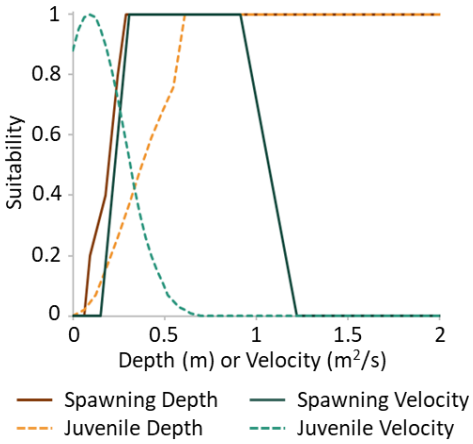

Figure B.1: Suitability curves (Maret, 2005) for Chinook salmon spawning and juvenile habitat.

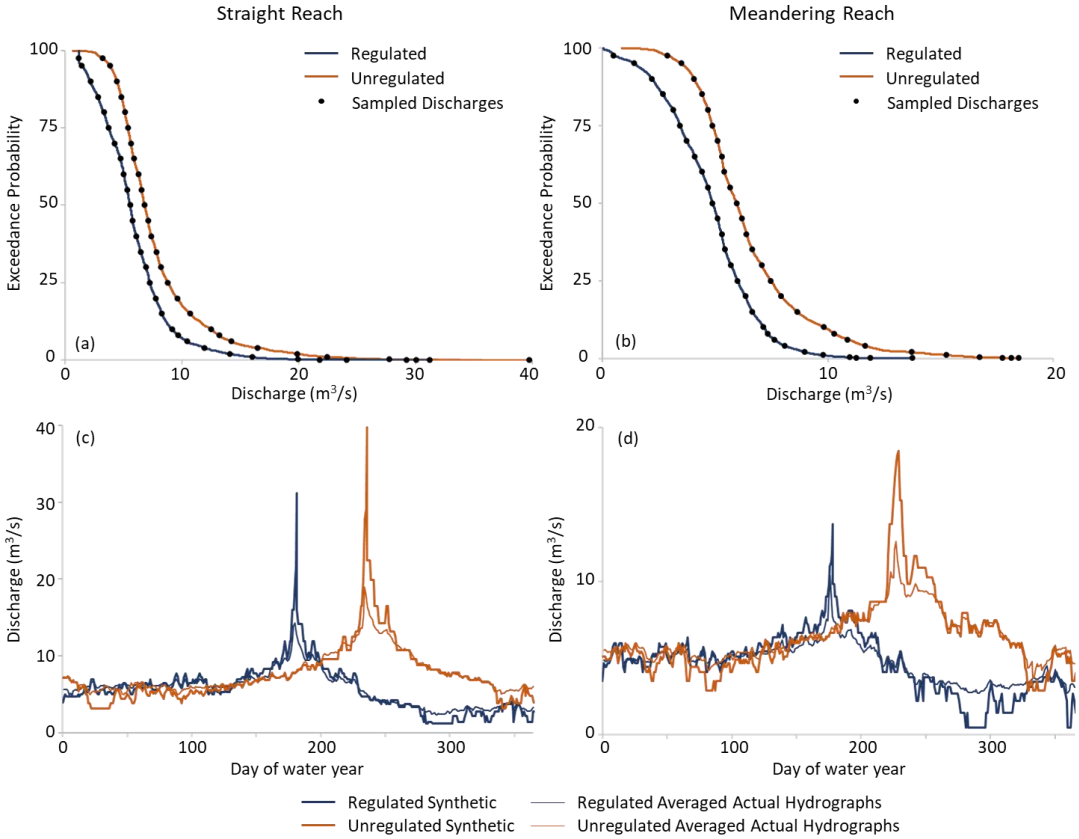

Figure B.2: Exceedance probabilities for all the regulated and unregulated flows in the 10 years of actual hydrographs for (a) the straight reach and (b) the meandering reach. The black points show the selected sampled discharges used to create the annual synthetic hydrographs. The synthetic hydrographs (thick lines) for the (c) straight reach and (d) meandering reach, were created by ordering the sampled discharges in the same order as the average of the 10 years of actual registered (by the annual high flow) hydrographs (fine line) by magnitude of flows.

Table B.1: The regulated and unregulated discharges for the straight and meandering reaches calculated at each selected exceedance probability. The number of days each exceedance probability represented is also shown.

Exceedance Probability	Number Days Exceeding the Sampled Discharge	Straight Reach Sampled Regulated Discharge	Straight Reach Sampled Unregulated Discharge	Meandering Reach Sampled Regulated Discharge	Meandering Reach Sampled Unregulated Discharge
100	365	1.19	0.71	0.03	0.85
95	346.75	1.44	3.87	1.40	3.49
90	328.5	2.18	4.47	2.18	4.06
85	310.25	2.82	4.84	2.67	4.41
80	292	3.34	5.14	3.12	4.67
75	273.75	3.76	5.40	3.43	4.87
70	255.5	4.28	5.65	3.73	5.10
65	237.25	4.75	5.90	4.09	5.28
60	219	5.05	6.30	4.40	5.40
55	200.75	5.33	6.57	4.67	5.66
50	182.5	5.59	6.83	4.88	5.94
45	164.25	5.8	7.12	5.10	6.18
40	146	6.13	7.39	5.28	6.39
35	127.75	6.5	7.82	5.42	6.64
30	109.5	6.92	8.21	5.69	7.05
25	91.25	7.29	8.82	5.97	7.46
20	73	7.77	9.62	6.33	7.92
15	54.75	8.3	10.75	6.64	8.65
10	36.5	9.18	12.49	7.14	9.82
8	29.2	9.67	13.19	7.31	10.27
6	21.9	10.47	14.26	7.62	10.86
4	14.6	11.95	16.47	8.09	11.64
2	7.3	14.13	19.89	8.97	13.70
1	3.65	16.05	22.44	9.80	15.25
0.27	0.99	19.93	27.77	10.96	16.73
0.14	0.51	21.78	29.25	11.24	17.76
0.082	0.30	24.07	30.06	11.88	18.15
0.027	0.1	31.2	39.71	13.73	18.48

Appendix C: Supporting Information for Chapter 3

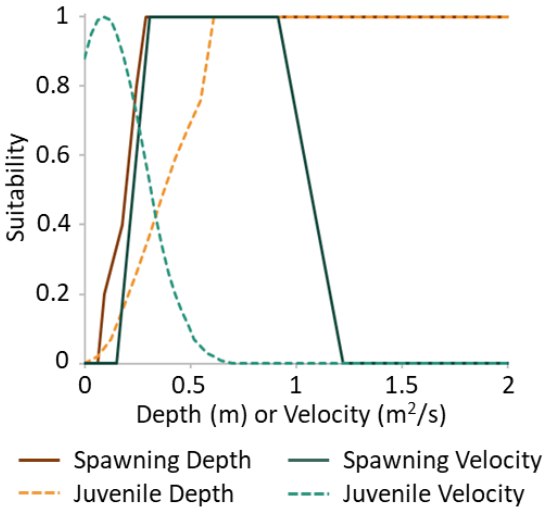

Figure C.1: Habitat suitability curves for depth and velocity suitability for spawning and juvenile Chinook salmon (Maret et al., 2005).

Table C.1: Constants for the growth ration equation to estimate the food requirements for different growth rations (Elliott, 1975, 1976)

Growth Ration	a	b_1	b_2
100% Growth (Maximum)	15.018	0.759	0.171
80% Growth	3.446	0.780	0.130
0% Growth (Maintenance)	2.711	0.737	0.105

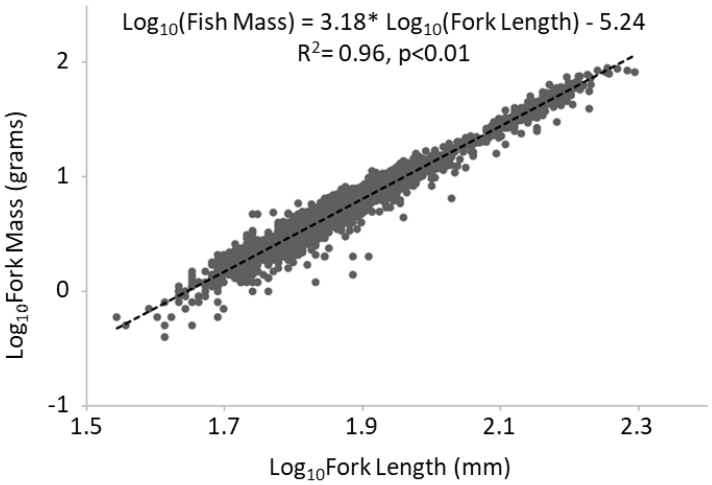

Figure C.2: Distribution of the fork length (mm) and fish mass (grams) of all available Chinook juvenile captures from the Integrated Status Effectiveness Monitoring Program. These data were used to create the regression model: Log10(Fish Mass) = 3.18* Log10(Fork Length) - 5.24.

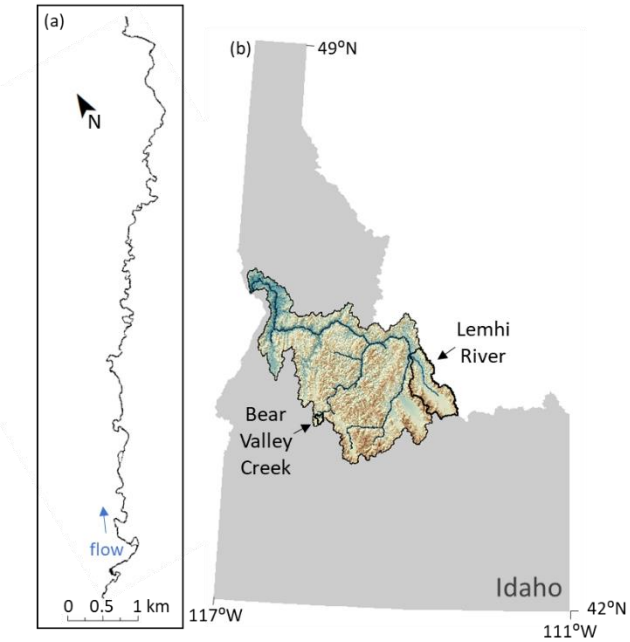

Figure C.3: (a) The centerline extent of the 14 km long Bear Valley Creek 2D hydraulic model and (b) its location within the Salmon River basin, Idaho. The 2D hydraulic model was created in MIKE 21 using 1-meter resolution bathymetric LiDAR data collected by the Experimental Advanced Airborne Research LiDAR (EAARL) in October 2007. The model roughness was calibrated to reduce the errors between the modeled and field collected depth and velocity measurements during a low fall flow.